Adaptive Spectral Inversion for Inverse Medium Problems

Inauguraldissertation

zur
Erlangung der Würde eines Doktors der Philosophie
vorgelegt der
Philosophisch-Naturwissenschaftlichen Fakultät
der Universität Basel

von

Yannik Gerald Gleichmann

Basel, 2023

Genehmigt von der Philosophisch-Naturwissenschaftlichen Fakultät

auf Antrag von

Erstbetreuer:	Prof. Dr. Marcus J. Grote
Zweitbetreuer:	Prof. Dr. Helmut Harbrecht
externer Experte:	Prof. Dr. Otmar Scherzer

Basel, den 19. September 2023

Prof. Dr. Marcel Mayor
Dekan

Abstract

Inverse medium problems are typically dedicated to finding the cause behind measured behaviors. Examples include exploring the Earth's interior through seismic or geophysical imaging, using ultrasounds or X-rays for medical imaging, or investigating materials in material science. In each case, our goal is to determine the unknown, also referred to as the medium, responsible for these measured observations by solving a constraint minimization problem for the data misfit. The constraints arise from the physical state, which is modeled and mathematically expressed by a partial differential equation.

In this Thesis, we propose a nonlinear iterative optimization method to solve inverse medium problems. Instead of using a grid based optimization approach, which leads to challenging large scale problems, we iteratively minimize the data misfit within a small finite dimensional subspace spanned by the first few eigenfunctions of a carefully chosen elliptic operator. As the operator depends on the minimizer in the previous search space, so do its eigenfunctions, and consequently the subsequent search space. This approach allows us to incorporate regularization inherently at each iteration without the need for additional penalization, such as Total Variation or Tikhonov regularization.

By introducing a key *angle condition*, we can prove the convergence of the resulting *Adaptive Spectral Inversion* (ASI) method and demonstrate its regularizing effect. Through numerical experiments, we illustrate the remarkable accuracy of the ASI, even detecting the smallest inclusions where previous methods failed. Furthermore, we demonstrate that the ASI performs favorably compared to standard grid based inversion using Tikhonov regularization when applied to an elliptic inverse problem.

The choice of the elliptic operator for obtaining the subsequent search space is crucial for achieving accurate reconstructed media. For known piecewise constant media, consisting of a few interior inclusions, we prove that the first few eigenfunctions of the operator, that depend on the medium, effectively approximate the medium and its discontinuities. Then, we validate these analytically proven properties of the operator through various numerical experiments.

Acknowledgments

I want to express my sincere thanks to my supervisor, Prof. Dr. Marcus J. Grote, for giving me the opportunity to do my PhD under his guidance, advising and supporting me throughout our insightful meetings and discussions, closing open questions but revealing new ones. Additionally, I extend my thanks to Prof. Dr. Helmut Harbrecht for serving as my co-supervisor and to Prof. Dr. Otmar Scherzer for kindly agreeing to act as an external expert for my thesis.

I also want to offer my thanks to the former and current members of the research groups Numerical Analysis and Computational Mathematics of the University of Basel, especially to Dr. Jet Hoe Tang who taught me a lot about (efficient) programming, and to Dr. Daniel H. Baffet with his helping discussions.

Many thanks go to all my friends from youth and colleagues, that accompanied me through my Bachelor's, Master's, and PhD studies, who where not only colleagues but became also friends.

Special thanks go to Emily Gajendran and Dr. Johannes Jehn for proofreading my thesis.

I am truly thankfully to my family – my mother Liesgret, brother Axel, and aunt and uncle Annette and Hans-Peter – who were always there for me when needed, not only guiding me throughout my childhood, but also supporting me throughout adulthood.

This thesis was written at the Department of Mathematics and Computer Science at the University of Basel and was partly supported by the Swiss National Science Foundation.

Contents

List of Figures

List of Tables

Chapter 1

Introduction

Since it may not always be clear what we mean when talking about *inverse problems*, we follow the definition of Keller [69]:

We call two problems inverse to one another, if the formulations of each involves all or part of the solution of the other. From this definition, it is arbitrary which one of the two problems we call the direct and which one the inverse problem. However, for historical – or other – reasons, one of the two problems has been studied extensively for some time and is better understood than the other. This one we would call the direct problem.

An illustration of an inverse problem is the following:

What is the question, to which the answer is "42"? [1]

Clearly, this simple demonstration shows that there may not be a unique answer to this question and that some answers may be favored over others. Some examples in mathematics are the following [69]:

(i) Find a polynomial $p(x)$ of degree n with roots $x_1, \ldots, x_n$. This task is inverse to the direct problem of finding the roots $x_1, \ldots, x_n$ of a given polynomial $p(x)$ of degree n. In this case, the inverse problem is easier, having the solution $p(x) = c(x - x_1) \ldots (x - x_n)$, which is not unique as $c \neq 0$ is an arbitrary constant.

(ii) Find a polynomial $p(x)$ of degree n with given values $y_1, \ldots, y_n$ at $x_1, \ldots, x_n$. The corresponding direct problem is to find the values $y_1, \ldots, y_n$ of a given

[1] There are many theories why *the Answer to the Ultimate Question of Life, the Universe, and Everything is 42* from the comic science fiction series *The Hitchhiker's Guide to the Galaxy* by *Douglas Adams*. However, Adams gave this answer: The answer to this is very simple. It was a joke. It had to be a number, an ordinary, smallish number, and I chose that one. Binary representations, base thirteen, Tibetan monks are all complete nonsense. I sat at my desk, stared into the garden and thought "42 will do" I typed it out. End of story.

polynomial $p(x)$ at $x_1, \ldots, x_n$. The inverse problem is called the Lagrange interpolation problem, while the direct problem is the evaluation of the polynomial.

(iii) Given a real symmetric matrix $\mathbf{A}$ of order n and n real numbers $\lambda_1, \ldots, \lambda_n$, find a diagonal matrix $\mathbf{D}$ such that $\mathbf{A} + \mathbf{D}$ has the eigenvalues $\lambda_1, \ldots, \lambda_n$. This is inverse to the direct problem of finding the eigenvalues $\lambda_1, \ldots, \lambda_n$ of a given real symmetric matrix $\mathbf{A} + \mathbf{D}$.

A common problem used in intelligence tests is:

(iv) Given the first few members a_1, a_2, a_3, a_4 of a sequence, find the law of formation of the sequence, i.e. find a_n for all positive integers n. Usually, only the next few members a_5, a_6, a_7 are asked for as evidence that the law of formation has been found. The direct problem is to evaluate the first few members of a sequence a_n, given the law of formation. A well known instance of this inverse problem is to find the next few members of the sequence, which begins with 4, 14, 34, 42. The solution is 59, 125, 145, since the sequence consists of the express stops on the 8^{th} Avenue subway in New York [111]. It is clear that such inverse problems have many solutions and for this reason, their use in intelligence tests has been criticized.

Therefore, we will give the abstract definition of the *direct* and *inverse problem* for a given operator F:

Direct problem: Given u, evaluate $F(u) = y$.

Inverse problem: Given y, find u satisfying $F(u) = y$.

Throughout this Thesis, we refer to F as the *forward operator*, to y as the *state* variable, and to u as the *medium* or sometimes the *control* variable.

1.1 Inverse Medium Problems

Inverse medium problems occur in a wide range of real life applications [105, 118], such as medical imaging [4, 81, 105, 127], geophysical or seismic imaging [52, 114, 122–124], and non-destructive testing [32, 79, 93]. In these applications, a known incident wave will be sent into an unknown medium, such as the human body for medical imaging, the earth's surface for geophysical imaging, or an object for non-destructive testing. These waves will then be reflected or scattered by the unknown medium as shown in Figure 1.1. These reflected waves can be measured using devices typically located at the boundary of the unknown medium.

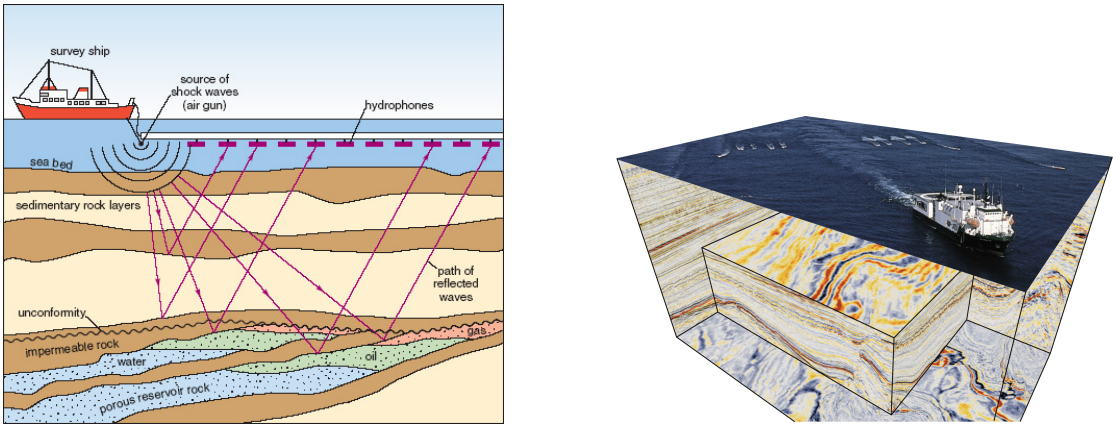

Fig. 1.1: Seismic inverse problem: A survey ship sends a (point) source of waves into the sea. Those waves illuminate the medium, usually consisting of gas and oil reservoirs and different sediment layers, and get reflected by those scatterers. These scattered, or reflected waves, are measured at sea level. The reflected waves can then be used to reveal the different layers of the earth [2, 3].

With these measured observations, usually perturbed or noisy due to measurement errors of the device, one tries to reconstruct the medium to determine the scatterers, e.g. cancer, oil reservoirs as in Figure 1.1, or cracks inside an object.

To mathematically formulate the inverse problem to be able to reconstruct the (unknown) medium, we consider two Hilbert spaces H_1, H_2 and the forward operator F,

$$F : H_1 \to H_2, \qquad F(u) = y.$$

This is the mapping of the (unknown) medium $u \in H_1$ to the known data $y \in H_2$, e.g. the measured waves as shown in Figure 1.1, where u consists of the different layers. Let us denote by $u^\dagger$ the exact, but unknown, medium. Usually, the exact data $y^\dagger = F(u^\dagger)$ is perturbed due to measurement errors, and hence only noised data $y^\delta \in H_2$ is available, satisfying

$$\|y^\dagger - y^\delta\|_{H_2} \leqslant \delta,$$

where the noise $\delta \geqslant 0$ is known. Thus, we wish to solve the inverse problem

$$F(u) = y^\delta. \tag{1.1}$$

This may be done by reformulating it as a least squares minimization problem: Find $u^{\dagger,\delta}$ satisfying

$$\min_{u \in H_1} J^\delta(u) = \min_{u \in H_1} \frac{1}{2} \|F(u) - y^\delta\|^2_{H_2}, \tag{1.2}$$

with the misfit $J^\delta : H_1 \to \mathbb{R}$. To find such $u^{\dagger,\delta}$, we may use standard minimization methods to solve this optimization problem, as we will explain in Section 2.4.

1.2 Model Problems

As mentioned above, inverse medium problems typically consist of finding a minimizer $u^{\dagger,\delta}$ of the misfit J^δ satisfying (1.2), where y itself satisfies a partial differential equation (PDE) $A[u]y = f$, the so called forward problem, where the source $f : \Omega \to \mathbb{R}$ is known. Thus, our aim is to solve

$$\begin{aligned} \min_{u,y} \quad & \frac{1}{2}\|y - y^\delta\|_{H_2}^2 \\ \text{s.t.} \quad & A[u]y - f = 0. \end{aligned} \tag{1.3}$$

In this Thesis, we will focus on two distinct models representing the forward problem:.

1.2.1 Elliptic Inverse Problem

As the first model problem, we consider the forward problem $A[u]y = f$ corresponding to the elliptic PDE

$$\begin{aligned} -\nabla \cdot (u(\mathbf{x})\nabla y(\mathbf{x})) &= f(\mathbf{x}), && \mathbf{x} \in \Omega, \\ y(\mathbf{x}) &= 0, && \mathbf{x} \in \partial\Omega, \end{aligned} \tag{1.4}$$

for a bounded domain $\Omega \subset \mathbb{R}^d$, $d \geqslant 1$. It is known from the theory of PDEs [38] that (1.4) admits a unique (weak) solution y. The inverse problem to (1.4) is now to find a solution $u^{\dagger,\delta}$ to (1.3) with given noisy data y^δ. This model problem, for example, occurs in groundwater filtration and inverse conductivity problems [7, 23, 80, 112].

1.2.2 Inverse Scattering Problem for the Wave Equation

Next, as a second model problem, we consider the forward problem to be the wave equation in time-domain

$$\begin{aligned} \frac{\partial^2}{\partial t^2} y(\mathbf{x},t) - \nabla \cdot (u(\mathbf{x})\nabla y(\mathbf{x},t)) &= f(\mathbf{x},t), && \mathbf{x} \in \Omega,\ t \in (0,T), \\ y(\mathbf{x},0) = \tfrac{\partial}{\partial t} y(\mathbf{x},0) &= 0, && \mathbf{x} \in \Omega, \\ \tfrac{\partial}{\partial t} y(\mathbf{x},t) + \sqrt{u(\mathbf{x})}\tfrac{\partial}{\partial n} y(\mathbf{x},t) &= 0, && \mathbf{x} \in \partial\Omega,\ t \in (0,T), \end{aligned} \tag{1.5}$$

for a bounded spatial domain $\Omega \subset \mathbb{R}^d$, $d \geqslant 1$, and time-domain $(0, T)$, $T > 0$, where we impose zero initial conditions and absorbing boundary conditions [36, 47]. Here, u denotes the squared wave speed and f the known source which illuminates the medium, as illustrated in Figure 1.1.

In the context of seismic inversion where one is interested to probe the Earth as shown in Figure 1.1 and only data at the boundary of Ω can be measured, this method is known as the full waveform inversion (FWI). Thus, we wish to solve

$$\begin{aligned} \min_{u,y} \quad & \frac{1}{2} \int_0^T \int_{\partial\Omega} |y(\mathbf{x}, t) - y^\delta(\mathbf{x}, t)| \, d\mathbf{x} \, dt. \\ \text{s.t.} \quad & (1.5). \end{aligned} \tag{1.6}$$

Using an iterative minimization algorithm to solve (1.6). This was originally studied by Bamberger, Chavent, and Lailly [14] as well as Tarantola [114, 115]. Instead of considering the time dependent model problem (1.6), one can also assume that the corresponding forward problem to solve the FWI is given in the frequency domain, see Pratt *et al.* [95–97], which is obtained by using a Fourier transform on (1.5). Thus, this eliminates the time-dependency, resulting in a stationary PDE which now depends on the frequency.

1.3 Outline and Main Contribution

De Buhan and Osses [29, Section 5.4], as well as De Buhan and Kray [28], recently introduced an iterative adaptive method to solve inverse problems. Instead of minimizing (1.2) within the entire space H_1, they employ a sequence of subspaces $\{\Psi^m\}_m \subset H_1$, adaptively chosen after each iteration. These subspaces consist of the first few eigenfunctions of a well chosen judicious elliptic differential operator $L_\varepsilon[u^m]$, $\varepsilon > 0$, where u^m denotes the previous solution to the inverse problem in the search space Ψ^m.

Since $L_\varepsilon[u^m]$ depends on the previous solution u^m, the eigenfunctions, and consequently the new search space, also depend on u^m. As a result, (good) information from u^m is successively transported to the new search space, leading to a better reconstruction u^{m+1} in the subsequent iteration.

This choice of search spaces has proven to be highly effective in solving inverse medium problems whenever the exact yet unknown medium is assumed to be piecewise constant. It has been used for various model problems, such as acoustic [44, 50], electromagnetic [27], and, combined with frequency stepping, for seismic inverse scattering problems [39, 48], as well as in optimal control [104]. However, the choice of the dimension of the search space was arbitrary until Baffet, Grote, and Tang [11] introduced a strategy to choose its dimension adaptively. In this work, they also made the first progress in developing mathematical theory to

study the approximation of piecewise constant functions v by the eigenfunctions of the elliptic operator $L_\varepsilon[v]$. This led to rigorous L^2-error estimates proven by Baffet, Gleichmann, and Grote [10]. Recently, Gleichmann and Grote [43] established convergence and regularization theory for the adaptive inversion method, introducing a new criterion to select the eigenfunctions incorporated into the new search space. This has proven crucial in reconstructing small inclusions inside the medium, where the previous methods have failed to detect these.

The structure of this Thesis is as follows. In Chapter I, we delve into the theory concerning inverse problems, discuss their solvability, realization, and numerical methods to practically solve inverse medium problems. Chapter II introduces the *Adaptive Spectral (AS) decomposition*, establish its approximation properties based on [10, 11], and validate these theoretical results numerically. In Section 6 of Chapter III, we present the general iterative *Adaptive Inversion* method for solving inverse problems. This method involves solving (1.2) in a sequence of finite dimensional subspaces $\Psi^m \subset H_1$, which may not be known beforehand. We identify a crucial *angle condition* that ensures the convergence of the Adaptive Inversion method and also prove its effectiveness as a regularization technique. To further enhance the approach, we combine the Adaptive Inversion method with the AS decomposition, resulting in the *Adaptive Spectral Inversion (ASI)* Algorithm presented in Section 7. This algorithm incorporates the angle condition introduced in Section 6. Finally, in Section 8, we present various numerical experiments to illustrate the performance of the ASI method and validate the theory presented in Section 6.

Part I

Preliminaries

Chapter 2

Numerical Methods

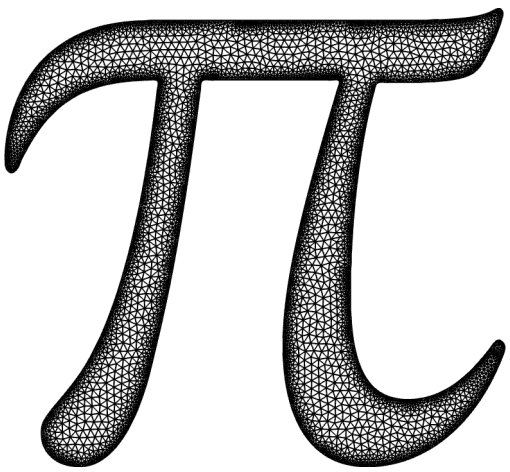

In general, it is not possible to obtain closed or explicit forms for the solution of inverse problems or even the forward problem. However, using numerical methods we are able to approximate the solution to the forward and inverse problem numerically. To do so, there are mainly two methods: Finite Differences (FD) and Finite Elements (FE).

Finite Difference Methods rely on approximating derivatives with finite differences. Therefore, one has to discretize the domain of interest into discrete grid points and apply an appropriate finite difference scheme, usually resulting in a system of linear equations. This system can then be solved with appropriate matrix algebra techniques. However, the drawback of the FD method is that one is limited to simple geometric shapes of the domain, such as rectangles or disks. The Finite Element Method (FEM), which we will solely use in this Thesis, on the other hand, discretizes the domain of interest in small, finitely many elements – usually triangles or rectangles in two dimensions – which is called a mesh. This method of discretizing the domain introduces more freedom to mesh domains and admits more complex geometries such as the π-shaped domain shown above. Another huge advantage is that the elements in the mesh do not have to admit the same size, thus this allows us to have a finer mesh size and therefore have a better resolution where edges or small features are located in the domain. Before introducing the FEM we first need some theory from functional analysis.

2.1 A Brief Survey of Functional Analysis

This chapter briefly outlines the basic concepts of functional analysis needed throughout this Thesis. For more details we refer to the standard literature [6, 100, 128, 129] and the references therein.

2.1.1 Derivative of Functionals

Consider a Hilbert space H and a *functional* J that maps each element of H to a real number,

$$J : H \to \mathbb{R},$$

equipped with the norm

$$\|J\|_{H\to\mathbb{R}} = \sup_{\|u\|_H \neq 0} \frac{|J(u)|}{\|u\|_H} = \sup_{\|u\|_H = 1} |J(u)|.$$

The functional J is Gateaux differentiable in $u \in H$ in the direction $v \in H$, $\|v\|_H = 1$, if the limit

$$J'(u; v) = \lim_{\varepsilon \to 0} \frac{J(u + \varepsilon v) - J(u)}{\varepsilon} = \frac{\partial}{\partial \varepsilon} J(u + \varepsilon v)|_{\varepsilon=0}$$

exists. If it exists for all directions v, we say that J is Gateaux differentiable at u. Note that the functional $J'(u; \cdot) : H \to \mathbb{R}$ may not be linear. However, the *Fréchet* derivative $J'(u) : H \to \mathbb{R}$ of J in u is the unique *linear* operator defined by

$$J(u + v) = J(u) + J'(u)v + o(\|v\|_H)$$

or, equivalently,

$$\lim_{\|v\|_H \to 0} \frac{J(u + v) - J(u) - J'(u)v}{\|v\|_H}.$$

Note that if J is Fréchet differentiable it is also Gateaux differentiable with Gateaux derivative

$$F'(u; v) = F'(u)v,$$

thus the Gateaux derivative is linear for each direction v. However, the converse does not hold.

Up to now, we have not used that H is a Banach space. Hence the concepts introduced also hold true for any normed space. Exploiting that H is equipped with a scalar product $(\cdot, \cdot)_H$, we know from the Riesz representation theorem that there exists a uniquely determined element $\nabla J(u) \in H$, such that

$$J'(u)v = (\nabla J(u), v)_H, \quad \forall v \in H, \qquad \text{with} \quad \|J'(u)\|_{H\to\mathbb{R}} = \|\nabla J(u)\|_H. \tag{2.1}$$

2.1.2 Lebesgue and Sobolev Spaces

To analyze PDEs the usual spaces of p-times differentiable function $C^p(\Omega)$, for $\Omega \subset \mathbb{R}^d$ bounded, are not sufficient anymore and we have to extend them to the so-called *Lebesgue* and *Sobolev* spaces that are no longer defined pointwise on Ω. Thus we identify two functions u, v with each other if $u(\mathbf{x}) = v(\mathbf{x})$ for $\mathbf{x} \in \Omega$ except on a null set. We may simply denote this by $u(\mathbf{x}) = v(\mathbf{x})$ a.e. or $u = v$.

Now, we define the Lebesgue space $L^p(\Omega)$ for $1 \leqslant p < \infty$ via

$$L^p(\Omega) = \left\{ u : \Omega \to \mathbb{R} : \int_\Omega |u(\mathbf{x})|^p \, d\mathbf{x} < \infty \right\},$$

with corresponding norm

$$\|u\|_{L^p(\Omega)} = \left(\int_\Omega |u(\mathbf{x})|^p \, d\mathbf{x} \right)^{1/p}$$

and for $p = \infty$ via

$$\begin{aligned} L^\infty(\Omega) &= \left\{ u : \Omega \to \mathbb{R} : \|u\|_{L^\infty(\Omega)} < \infty \right\}, \\ \|u\|_{L^\infty(\Omega)} &= \operatorname{ess\,sup}_{\mathbf{x} \in \Omega} |u(\mathbf{x})|. \end{aligned}$$

One can show that for $1 \leqslant p < q \leqslant \infty$ we obtain the embedding $L^q(\Omega) \subset L^p(\Omega)$ for the Lebesgue spaces. For $p = 2$ it is easy to see that the space of square integrable functions $L^2(\Omega)$ is a Hilbert space, equipped with the underlying scalar product and induced norm

$$\begin{aligned} (u, v)_{L^2(\Omega)} &= \int_\Omega u(\mathbf{x}) v(\mathbf{x}) \, d\mathbf{x}, \\ \|u\|_{L^2(\Omega)} &= \int_\Omega |u(\mathbf{x})|^2 \, d\mathbf{x}. \end{aligned}$$

Note that there exists an analogy to the spaces of sequences: Consider a sequence $\mathbf{x} = (x_1, x_2, x_3, \ldots)$. We say that $\mathbf{x} \in \ell^p$ if $\|\mathbf{x}\|_{\ell^p} < \infty$, with

$$\begin{aligned} \|\mathbf{x}\|_{\ell^p} &= \left(\sum_k |x_k| \right)^{1/p}, \qquad 1 \leqslant p < \infty, \\ \|\mathbf{x}\|_{\ell^\infty} &= \sup_k |x_k|. \end{aligned}$$

As with $L^2(\Omega)$, ℓ^2 is also a Hilbert space with a corresponding underlying scalar product.

Since PDEs involve derivatives, see both model problems (1.4) and (1.5), we now extend the concept of a derivative to the *weak derivative* for Lebesgue spaces.

For a multi index $\alpha = (\alpha_1, \ldots, \alpha_n) \in \mathbb{N}^n$, we define the α^{th} weak derivative v of u if

$$\int_\Omega u D^\alpha \varphi = (-1)^{|\alpha|} \int_\Omega v\varphi$$

holds for all $\varphi \in C_c^\infty(\Omega)$ with

$$D^\alpha \varphi(\mathbf{x}) = \frac{\partial^{|\alpha|}\varphi(\mathbf{x})}{\partial x_1^{\alpha_1} \cdots \partial x_n^{\alpha_n}}.$$

We then denote the weak derivative of u by $v = D^\alpha u$. With this, we can define the Sobolev space $W^{k,p}(\Omega)$ via

$$W^{k,p}(\Omega) = \left\{ u \in L^p(\Omega) : \; D^\alpha u \in L^p(\Omega), \; \forall |\alpha| \leqslant k \right\},$$

with its corresponding norm

$$W^{k,p}(\Omega) = \begin{cases} \left(\sum\limits_{|\alpha| \leqslant k} \|D^\alpha u\|_{L^p(\Omega)}^p \right)^{1/p}, & 1 \leqslant p < \infty, \\ \max\limits_{|\alpha| \leqslant k} \|D^\alpha u\|_{L^\infty(\Omega)}, & p = \infty. \end{cases} \tag{2.2}$$

If we define the seminorm by

$$|u|_{W^{k,p}(\Omega)} = \left(\sum_{|\alpha| = k} \|D^\alpha u\|_{L^p(\Omega)}^p \right)^{1/p},$$

(2.2) simply reads as

$$\|u\|_{W^{k,p}(\Omega)} = \left(\sum_{j=0}^{k} |u|_{W^{j,p}(\Omega)}^p \right)^{1/p}.$$

For $p = 2$ the Sobolev space $W^{k,2}(\Omega)$ is also a Hilbert space, commonly denoted by $H^k(\Omega)$, with underlying scalar product

$$(u, v)_{H^k(\Omega)} = \sum_{|\alpha| \leqslant k} (D^\alpha u, D^\alpha v)_{L^2(\Omega)},$$

and is often needed for the analysis of PDEs. Next, we denote the function space $H_0^k(\Omega) \subset H^k(\Omega)$ by all functions that simply correspond to all functions in $H^k(\Omega)$ with zero boundary. An important space, especially in the context of PDEs and the FEM, is $H^1(\Omega)$ with scalar product, seminorm, and norm given by

$$\begin{aligned} (u, v)_{H^1(\Omega)} &= (u, v)_{L^2(\Omega)} + (\nabla u, \nabla v)_{L^2(\Omega)}, \\ |u|_{H^1(\Omega)} &= \|\nabla u\|_{L^2(\Omega)}, \\ \|u\|_{H^1(\Omega)} &= \sqrt{\|u\|_{L^2(\Omega)}^2 + |u|_{H^1(\Omega)}^2}. \end{aligned}$$

With this, we can now introduce the Galerkin and the Finite Element Method.

2.2 The Ritz-Galerkin and Finite Element Method

Before we discuss methods to solve inverse problems we first have to study solving the forward problem given by a PDE. Since, in general, it is not possible to obtain explicit forms for the solution of PDEs, we will introduce the FEM to obtain a numerical solution, an approximation to the exact solution. Since this chapter only covers the numerical aspect of solving PDEs, we refer to the standard literature [38, 54] for the theoretical aspects. Also, this chapter is not meant to cover all the details about the FEM and we refer to [9, 38, 54, 98] for a more in-depth reading, as well as [73] for a good guide regarding implementation.

Let us consider the elliptic PDE as given in the test example (1.4),

$$\begin{aligned} -\nabla \cdot (u \nabla y) &= f \qquad && \text{in } \Omega, \\ y &= 0 && \text{on } \partial\Omega, \end{aligned} \tag{2.3}$$

for a bounded domain $\Omega \subset \mathbb{R}^d$, known source f, and unknown solution y. Hence, classical or strong solutions to (2.3) have to be in $C^2(\Omega)$. However, if we consider its variational or weak form, we allow solutions in a wider class of function spaces. To obtain the weak formulation of (2.3) we formally integrate (2.3) over Ω, use Green's theorem, and incorporate the boundary conditions on $\partial\Omega$. Thus, the weak problem corresponding to (2.3) is: Find $y \in H_0^1(\Omega)$ such that

$$a(y, z) = (f, z)_{L^2(\Omega)}, \qquad \forall\, z \in H_0^1(\Omega), \tag{2.4}$$

for the given bilinear form $a(y, z) = (u\nabla y, \nabla z)_{L^2(\Omega)}$.

2.2.1 The Ritz-Galerkin Method

To solve (2.4) numerically, a natural approach would be to consider (2.4) not in in $H^1(\Omega)$ or $H_0^1(\Omega)$, but in a finite dimensional subspace $V^h \subset H^1(\Omega)$ or $V_0^h = V^h \cap H_0^1(\Omega)$, as introduced by Ritz [101] and Galerkin [40]. The parameter $h > 0$ acts as a discretization parameter and suggest that for $h \to 0$ the solution obtained in V^h should converge to the exact solution in $H^1(\Omega)$. Thus, the Galerkin formulation to (2.4) is: Find $y_h \in V^h$ such that

$$a(y_h, z_h) = (f, z_h)_{L^2(\Omega)} \qquad \forall\, z_h \in V^h. \tag{2.5}$$

If we choose a basis $\{\varphi_1, \ldots, \varphi_N\}$ of V^h we can expand y_h in V^h satisfying

$$y_h = \sum_{k=1}^{N} y_k \varphi_k.$$

Since (2.5) holds for all $z_h \in V^h$, it also holds for all basis functions φ_j. Hence, this Ansatz leads to the linear system of equations

$$\sum_{k=1}^{N} a(\varphi_k, \varphi_j) y_k = (f, \varphi_j)_{L^2(\Omega)}, \qquad j = 1, \dots, N,$$

which we write in matrix-vector-notation as

$$\mathbf{A}\mathbf{y} = \mathbf{f}, \tag{2.6}$$

where $\mathbf{y} = [y_1, \dots, y_N]^\top$ is the solution vector and

$$\mathbf{A}_{j,k} = a(\varphi_k, \varphi_j), \qquad \mathbf{f}_j = (f, \varphi_j)_{L^2(\Omega)},$$

the stiffness matrix and load vector, respectively. Additionally, we will define the mass matrix $\mathbf{M}$, which we will need later, via

$$\mathbf{M}_{j,k} = (\varphi_k, \varphi_j)_{L^2(\Omega)}. \tag{2.7}$$

The last piece necessary to solve (2.5) numerically, is the choice of the underlying discrete space V^h.

2.2.2 The Finite Element Method

The first step to specify a finite element space V^h is to partition the domain Ω into elements, i.e. as shown in Figure 2.1. Common elements in two dimensions are triangles or rectangles and in three dimensions tetrahedrons, prisms, or hexahedrons. In the following, we will restrict ourselves to triangles in $\mathbb{R}^2$. A triangulation $\mathcal{T}_h = \{T_1, \dots, T_M\}$ is an admissible triangulation for Ω if

(i) $\overline{\Omega} = \cup_{j=1}^{M} T_j$

(ii) and for $k \neq j$, $T_k \cap T_j$ is either empty, consists of exactly one common vertex of T_k and T_j, or is a common edge of T_k and T_j.

Let H_T be the radius of the circumscribed circle of a triangle T and h_T the radius of its inscribed circle. We call a family of triangulations $\{\mathcal{T}_h\}_{h>0}$

(i) *shape-regular*, if there exists $\kappa > 0$ such that

$$\max_{T \in \mathcal{T}} \frac{H_T}{h_T} \leqslant \kappa \qquad \forall\, \mathcal{T} \in \{\mathcal{T}_h\}_{h>0}$$

(ii) and *quasi-uniform*, if there exists $c > 0$ such that

$$\frac{\max_{T \in \mathcal{T}} H_T}{\min_{T \in \mathcal{T}} H_T} \leqslant c \qquad \forall\, \mathcal{T} \in \{\mathcal{T}_h\}_{h>0}.$$

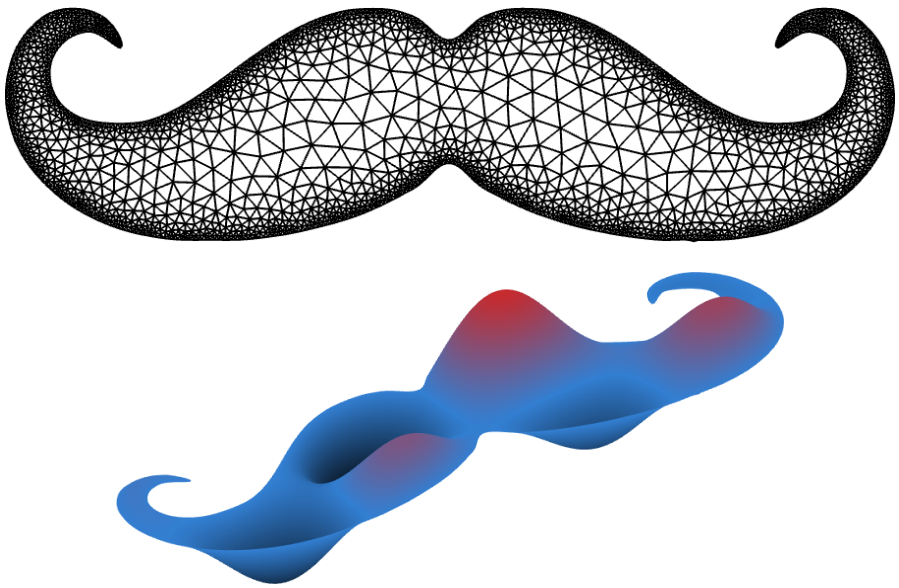

Fig. 2.1: Elliptic forward problem: Finite element solution (bottom) for the elliptic problem (2.3) with corresponding triangulation of a moustache shaped domain (top).

Next, we are going to employ the finite element space V^h. Since there are a lot of different finite elements [1], some of them fulfilling only a special purpose, we will restrict ourselves to the space of piecewise polynomials of degree $r \geqslant 1$,

$$\mathcal{P}^r = \{z \in L^2(\Omega) : \ z|_T \in \mathbb{P}^r(T) \quad \forall\, T \in \mathcal{T}_h\},$$

where $\mathbb{P}^r(T)$ denotes the polynomials of degree r on the triangle T. Thus, a natural choice of basis functions $\{\varphi_k\}_{k=1}^N$ are the functions satisfying

$$\varphi_k(\mathbf{x}_j) = \delta_{k,j}, \qquad 1 \leqslant k, j \leqslant N,$$

on each node $\mathbf{x}_k$ of the underlying mesh. In practice, the calculation of the mass matrix, stiffness matrix, and load vector will first be done over each element $T \in \mathcal{T}_h$ and then take the sum over all elements. Computing the integrals over each element T is simply done by transforming T to a reference element $\hat{T}$, where we then need the local basis functions $\hat{\varphi}_k$, $k = 1, \dots \hat{N}$ satisfying $\hat{\varphi}_j(\hat{\mathbf{x}}_k) = \delta_{j,k}$ on the local nodes $\hat{\mathbf{x}}_k$ of $\hat{T}$, where $\hat{N}$ is the number of local basis functions and thus the number of nodes on the reference element. The computation of these integrals over $\hat{T}$ can then be done explicitly or with an appropriate quadrature rule. In Figure 2.2 (a) the reference element $\hat{T}$ being the unit triangle, together with its nodes $\hat{\mathbf{x}}_k$, is shown for $\mathcal{P}^1, \mathcal{P}^2$, and $\mathcal{P}^3$ finite elements.

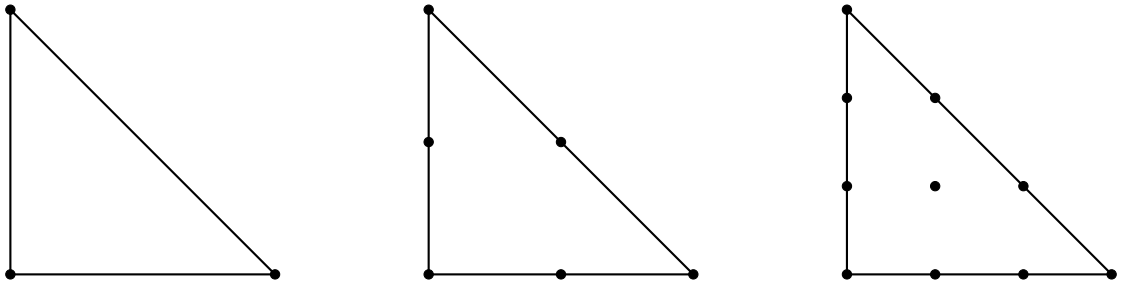

(a) From left to right: Each node $\hat{\mathbf{x}}_k$ on the unit triangle $\hat{T}$ for $\mathcal{P}^1$, $\mathcal{P}^2$, and $\mathcal{P}^3$ finite elements.

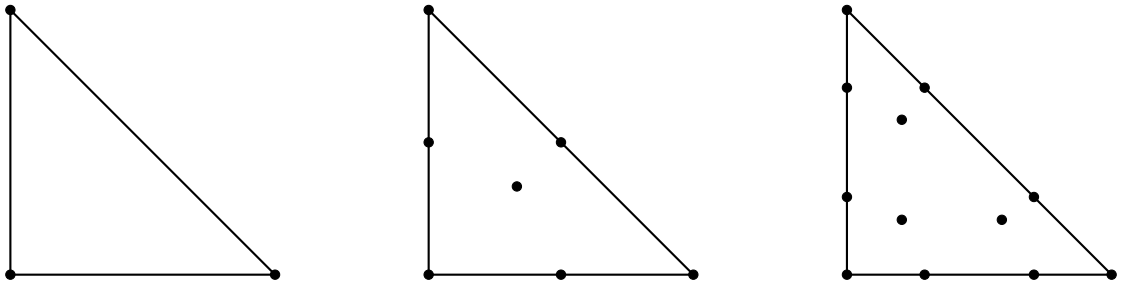

(b) From left to right: Each node $\hat{\mathbf{x}}_k$ on the unit triangle $\hat{T}$ for $\mathcal{P}_b^1$, $\mathcal{P}_b^2$, and $\mathcal{P}_b^3$ finite elements.

Fig. 2.2: Reference element $\hat{T}$: Nodes $\hat{\mathbf{x}}_k$ for standard finite elements $\mathcal{P}^r$ (top) and $\mathcal{P}_b^r$-FE with bubble function $b \in \mathbb{P}$ (bottom).

In the next section we will see that, for time dependent problems, we usually have to use a numerical scheme in time after applying the FEM in space to obtain numerical solutions. Even if we do this with an explicit method, e.g. the leap frog method, the mass matrix has to be inverted in each time-iteration, see Section 2.3. To avoid this, we use the *mass lumping* technique [24, 84], where we approximate the mass matrix $\mathbf{M}$ with a diagonal mass matrix $\tilde{\mathbf{M}}$, also called the lumped mass matrix, without losing any accuracy in the numerical solution. Since the lumped mass matrix is diagonal, its inverse is also diagonal and cheap to compute. To obtain $\tilde{\mathbf{M}}$ for $\mathcal{P}^1$ elements we have to choose the trapezoidal quadrature rule to calculate the integrals that make up the the mass matrix (2.7) numerically. For higher order elements, only choosing an appropriate quadrature rule is no longer sufficient. We also have to consider additional basis functions b_j, so called *bubble* functions, together with the standard basis functions $\hat{\varphi}_k$, equipped with an appropriate quadrature rule, see [84, Table 1]. We will denote this space by $\mathcal{P}_b^r = \mathcal{P}^r \oplus [b]$. For $\mathcal{P}_b^r$ elements, with $r \geqslant 2$, each bubble function is a polynomial of degree $r+1$. Thus $\mathcal{P}^r \subset \mathcal{P}_b^r \subset \mathcal{P}^{r+1}$ holds. With this, $\mathcal{P}_b^r$ yields the same accuracy as $\mathcal{P}^r$ however, only by adding the basis function of one degree higher. A comparison of the

basis functions and nodes for $\mathcal{P}^r$ and $\mathcal{P}_b^r$ elements is illustrated in Figure 2.2 and 2.3.

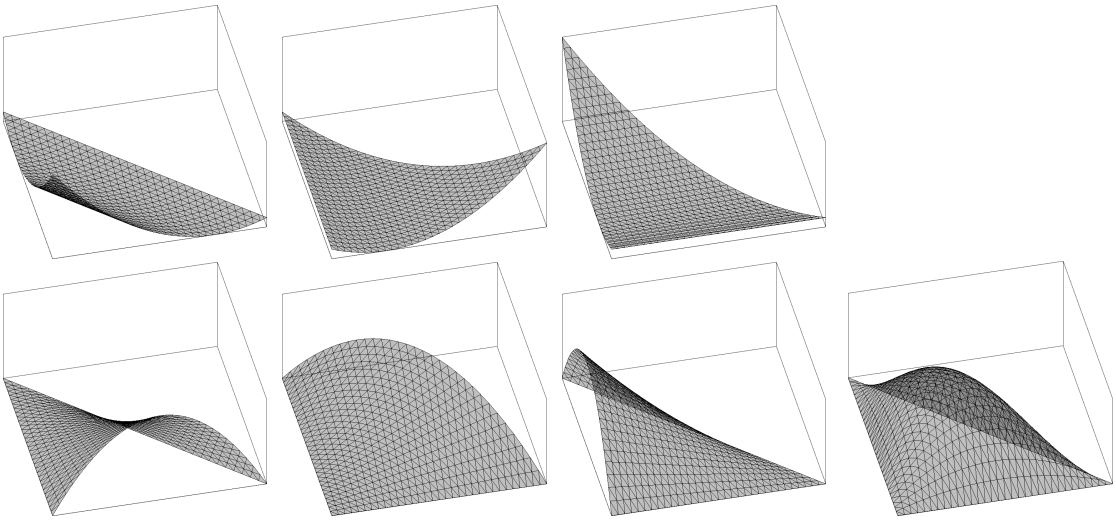

(a) $\hat{\varphi}_k$ **(b)** b_1

Fig. 2.3: Standard FE basis functions: $\hat{\varphi}_k$, $k = 1, \ldots, 6$, for $\mathcal{P}^2$ FE (left), as well as the bubble function $b_1 \in \mathbb{P}^3$ (right) to obtain the finite element space $\mathcal{P}_b^2$ and ensure mass lumping.

As an example we consider problem (1.4),

$$\begin{aligned} -\nabla \cdot (u \nabla y) &= f \qquad \text{in } \Omega, \\ y &= 0 \qquad \text{on } \partial\Omega, \end{aligned}$$

for a bounded domain $\Omega \in \mathbb{R}^d$. As seen above, its weak form is given by (2.4)

$$a(y, z) = (f, z)_{L^2(\Omega)}, \qquad \forall\, z \in H_0^1(\Omega)$$

and its Galerkin formulation by (2.5)

$$a(y_h, z_h) = (f, z_h)_{L^2(\Omega)}, \qquad \forall\, z_h \in V_0^h. \tag{2.8}$$

As the domain Ω, we consider a moustache-shaped domain and use the triangulation as shown in Figure 2.1. Next, we choose $V^h = \mathcal{P}^1$ elements as the underlying finite element space, thus (2.8) translates to the linear system $\mathbf{Ay} = \mathbf{f}$, c.f. (2.6). The numerical finite element solution obtained by (2.8) can be seen in Figure 2.1

2.3 The Leap Frog Method

Before we introduce the *leap frog* method we take a glimpse at the wave equation (1.5), considering homogeneous boundary data and zero initial conditions

$$\begin{aligned} \frac{\partial^2}{\partial t^2} y(\mathbf{x},t) - \nabla \cdot (u(\mathbf{x}) \nabla y(\mathbf{x},t)) &= f(\mathbf{x},t), && \mathbf{x} \in \Omega,\ t \in (0,T), \\ y(\mathbf{x},0) = \tfrac{\partial}{\partial t} y(\mathbf{x},0) &= 0, && \mathbf{x} \in \Omega, \\ y(\mathbf{x},t) &= 0, && \mathbf{x} \in \partial\Omega,\ t \in (0,T). \end{aligned} \tag{2.9}$$

Similarly as above, we can derive the (semi-discrete) Galerkin formulation for (2.9). Find $y_h \in C^2((0,T), V^h)$ such that

$$\begin{aligned} \frac{\partial^2}{\partial t^2}(y_h(t), z_h) + a(y_h(t), z_h) &= (f(\cdot,t), z_h) \qquad \forall\ z_h \in V_0^h,\ t \in (0,T) \\ y_h(t) = \tfrac{\partial}{\partial t} y_h(t) &= 0. \end{aligned}$$

Thus, if we choose a basis $\{\varphi_1, \ldots, \varphi_N\}$ of V^h, we can expand y_h via

$$y_h(t) = \sum_{k=1}^{N} y_k(t) \varphi_k$$

which leads to the finite element formulation

$$\mathbf{M} \frac{\partial^2}{\partial t^2} \mathbf{y}(t) + \mathbf{A}\mathbf{y}(t) = \mathbf{f}(t), \qquad \mathbf{y}(t)|_{t=0} = \frac{\partial}{\partial t} \mathbf{y}(t)|_{t=0} = 0, \tag{2.10}$$

where

$$\begin{aligned} \mathbf{y}(t) &= [y_1(t), \ldots, y_N(t)]^\top, \\ \mathbf{f}(t) &= [f_1(t), \ldots, f_N(t)]^\top, \qquad \text{with} \quad f_k = (f(t), \varphi_k)_{L^2(\Omega)}. \end{aligned}$$

The resulting semi discrete finite element formulation (2.10) corresponds to an ordinary differential equation (ODE) in time. To solve this ODE we will use the *leap frog* method [89], see also [56, Chapter I.1.4 and the following], which approximates the second time-derivative with central finite differences. For this, we discretize the time domain $(0,T)$ via $0 = t_0 < t_1 < \ldots < t_{N_T} = T$, $t_n = n\Delta t$ for the time step size[1] $\Delta t > 0$, denote by $\mathbf{y}^n \approx \mathbf{y}(t_n)$ the fully discrete solution at

[1] Note that we can not choose an arbitrarily (large) time step size $\Delta t > 0$. The step size has to satisfy a CFL-condition [26] that couples the spatial discretization with the time discretization, where usually a finer mesh size results in a finer time step. Thus, if only a few elements in the mesh are small in contrast to the others, the time step size is depicted only with respect to the smallest elements, resulting in a huge computational effort without gaining any significant accuracy on larger elements. The leap frog based local time stepping method [31, 49] solves this problem by only considering small time steps whenever the element size is small but allows larger time steps on coarser elements without losing any accuracy, thus keeping the computational costs low.

time t_n, and set $\mathbf{f}^n = \mathbf{f}(t_n)$. Then, the fully discrete wave equation obtained with the leap frog method is given by

$$\mathbf{M}\frac{\mathbf{y}^{n+1} - 2\mathbf{y}^n + \mathbf{y}^{n-1}}{\Delta t^2} + \mathbf{A}\mathbf{y}^n = \mathbf{f}^n, \qquad n = 1, 2, 3, \dots$$

or equivalently

$$\mathbf{M}\mathbf{y}^{n+1} = (2\mathbf{M} - \Delta t^2 \mathbf{A})\mathbf{y}^n - \mathbf{M}\mathbf{y}^{n-1} + \Delta t^2 \mathbf{f}^n. \tag{2.11}$$

Even though the leap frog method is fully explicit, we still have to solve a system of equations in (2.11) for each time step n. To circumvent this, we use the mass lumping technique as explained in Section 2.2.2. Thus, we formally replace the mass matrix $\mathbf{M}$ by the lumped mass matrix $\tilde{\mathbf{M}}$, which is diagonal and its inverse is easy and cheap to compute. To obtain the solution to (2.11), we first need the initial conditions $\mathbf{y}^n$ for $n = 0, 1$. Since the exact solution satisfies $y(\mathbf{x}, 0) = 0$ for all $\mathbf{x}$, c.f. (2.9), we set $\mathbf{y}^0 = 0$. To obtain $\mathbf{y}^1$ we simply use a Taylor expansion

$$\mathbf{y}(\Delta t) = \mathbf{y}(0) + \frac{\partial}{\partial t}\mathbf{y}(0) + \frac{\Delta t^2}{2}\frac{\partial^2}{\partial t^2}\mathbf{y}(0) + \mathcal{O}(\Delta t^3)$$

and together with (2.10) we obtain the initial condition for $n = 1$ by

$$\tilde{\mathbf{M}}\mathbf{y}^1 = \frac{\Delta t^2}{2}\mathbf{f}^0. \tag{2.12}$$

Note that if we do not have homogeneous initial conditions or different boundary conditions for y, (2.12) would admit a slightly different form.

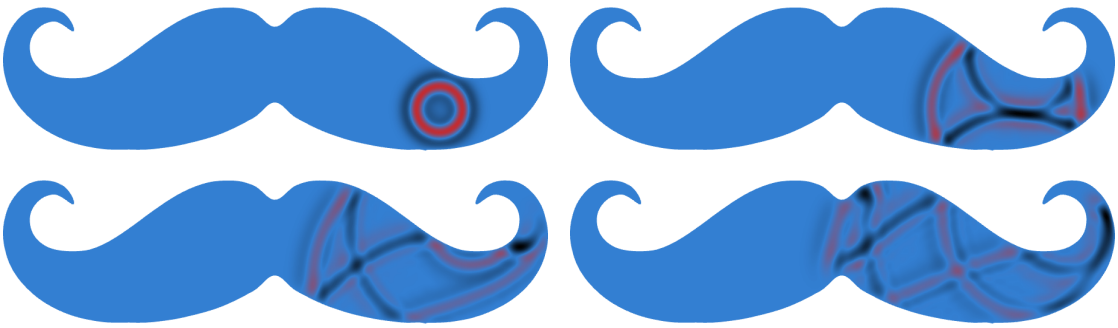

Fig. 2.4: Wave equation: Numerical solution to (2.9) for different times.

A solution to the wave equation (2.9) for different times t_n is illustrated in Figure 2.4, where we used $\mathcal{P}_b^2$ finite elements for the space discretization and the leap frog method for time integration.

2.4 Optimization Methods

This section follows [19, 90] and introduces the two main methods we will use to numerically solve the optimization problem

$$\min_{\mathbf{u}\in\mathbb{R}^d} J(\mathbf{u}), \tag{2.13}$$

where $J : \mathbb{R}^d \to \mathbb{R}$. Even though there exist various algorithms to solve (2.13), such as the gradient free Nelder-Mead method [19, Section 1.8.2], the Conjugate Gradient (CG) method [19, Section 1.6] and [90, Chapter 5], and the Trust-Region method [90, Chapter 4], here we only consider descent directional methods.

Descent-directional methods are intuitive and easy to explain: Consider being lost on top of a mountain, with no map at hand, and wanting to go back to civilization. Your approach is to go downhill, usually in a direction of descent, but only for a few steps. After you made these few steps you reorient yourself and try to find a better direction of descent and take a few more steps in that direction. This is a generic descent directional method and immediately raises two main questions. How many steps should you go? Is one enough, or should you go a thousand before searching for a new direction of descent? What happens if you land on a plateau where you can no longer find a direction of descent? Mathematically we can formulate this as follows. We start at a given point $\mathbf{u}^0 \in \mathbb{R}^d$ and determine the search direction $\mathbf{d}^0$ and a step length $\alpha_0 \geqslant 0$. Thus, the next point is given via $\mathbf{u}^1 = \mathbf{u}^0 + \alpha_0\mathbf{d}^0$, where we determine the descent direction $\mathbf{d}^0$ such that $J(\mathbf{u}^0 + \mathbf{d}^0) < J(\mathbf{u}^0)$ holds, and the step length α_0 as the minimizer of $J(\mathbf{u}^0 + \alpha\mathbf{d}^0)$. After doing this, we proceed to obtain the next iterate $\mathbf{u}^{m+1}$ via $\mathbf{u}^{m+1} = \mathbf{u}^m + \alpha_m\mathbf{d}^m$, where α_m is a minimizer of $J(\mathbf{u}^m + \alpha\mathbf{d}^m)$. If J is differentiable, a natural choice for $\mathbf{d}^m$ would be the steepest descent $-\nabla J(\mathbf{u}^m)$, which leads to the *steepest descent* method.

Another selection of a descent direction $\mathbf{d}^m$ is characterized by $\nabla J(\mathbf{u}^m)^\top \mathbf{d}^m < 0$. If $\nabla J(\mathbf{u}^m) \neq 0$, we can pick any $\mathbf{d}^m = -\mathbf{B}_m \nabla J(\mathbf{u}^m)$, for $\mathbf{B}_m$ positiv definit, to obtain a descent direction. If J is two times differentiable, the choice $\mathbf{B}_m = (\nabla^2 J(\mathbf{u}^m))^{-1}$ yields *Newton's* method. Since we do not compute the inverse explicitly, we have to solve the system

$$\nabla^2 J(\mathbf{u}^m)\mathbf{d}^m = -\nabla J(\mathbf{u}^m). \tag{2.14}$$

Since the Hessian $\nabla^2 J$ is usually not sparse, solving (2.14) is a major drawback of Newton's method.

This issue may be solved by allowing descent directions $\mathbf{d}^m$ that satisfy (2.14) only up to a small tolerance $\eta_m > 0$ satisfying

$$\|\nabla J(\mathbf{u}^m) + \nabla^2 J(\mathbf{u}^m)\mathbf{d}^m\| \leqslant \eta_m \|\nabla J(\mathbf{u}^m)\|, \tag{2.15}$$

resulting in the *inexact Newton's* method [30]. To obtain $\mathbf{d}^m$ that satisfies (2.15) may be done by using the (iterative) CG-method to solve (2.14) and stop after the first few iterations until the tolerance (2.15) is reached.

The last class of directional descent algorithms we wish to mention are *quasi Newton* methods. Quasi Newton methods do not use the exact Hessian $\nabla^2 J$ or its inverse explicitly but try to approximate it in every step. Then, to obtain the next approximated Hessian, the old approximation gets updated by the use of the iterates $\mathbf{u}^m, \mathbf{u}^{m+1}$ and gradients $\nabla J(\mathbf{u}^m), \nabla J(\mathbf{u}^{m+1})$ but not the exact Hessian itself, and is thus cheap to compute. Hence, the benefit of quasi Newton methods is given by completely omitting the calculation of the true Hessian which may not be available, hard to derive, or expensive to compute. The most prominent methods are the Davidon-Fletcher-Powell (DFP) and the Broyden-Fletcher-Goldfarb-Shanno (BFGS) method. There exist two variants of the BFGS method, where we only focus on the latter method. The first one is to approximate the Hessian $\mathbf{H}_m \approx \nabla^2 J(\mathbf{u}^m)$ and then obtain the new search direction by solving $\mathbf{H}_m \mathbf{d}^m = -\nabla J(\mathbf{u}^m)$. The second one is to approximate the inverse of the Hessian $\mathbf{B}_m \approx (\nabla^2 J(\mathbf{u}^m))^{-1}$ and thus obtain the new search direction by simply calculating $\mathbf{d}^m = -\mathbf{B}_m \nabla J(\mathbf{d}^m)$. However, one can show that $\mathbf{B}_m = \mathbf{H}_m^{-1}$ and therefore we prefer to approximate the inverse Hessian since this only requires a matrix vector multiplication, avoiding to solve a system of equations.

Comparing the methods above, we see that the steepest descent method only requires the computation of the gradient at each iteration, whereas the Newton-type methods require either the exact Hessian (Newton's and inexact Newton's method), or an approximation of it (DFP and BFGS method). Since the exact Hessian might not always be available, hard to derive, or expensive to compute, we rely on the BFGS method, where we approximate the inverse of the Hessian in each step. Thus, the BFGS algorithm is given by

Algorithm 1 BFGS Algorithm

Input:

initial guess $\mathbf{u}^0$, approximated inverse Hessian $\mathbf{B}_0$

set $m = 0$, $\varepsilon > 0$

1. **while** $\|\nabla J(\mathbf{u}^m)\|/\|\nabla J(\mathbf{u}^0)\| \geqslant \varepsilon$ **do**
2. Compute search direction $\mathbf{d}^m = -\mathbf{B}_m \nabla J(\mathbf{u}^m)$.
3. Compute step size $\alpha_m > 0$.
4. Set

$$\mathbf{u}^{m+1} = \mathbf{u}^m + \alpha_m \mathbf{d}^m$$

5. Compute

$$\begin{aligned} \mathbf{s}^m &= \mathbf{u}^{m+1} - \mathbf{u}^m, & \mathbf{y}^m &= \nabla J(\mathbf{u}^{m+1}) - \nabla J(\mathbf{u}^m), \\ \rho_m &= \frac{1}{\mathbf{y}^{m^\top} \mathbf{s}^m}, & \mathbf{V}_m &= \mathbf{I} - \rho_m \mathbf{y}^m \mathbf{s}^{m^\top}. \end{aligned} \tag{2.16}$$

6. Update the approximate inverse Hessian

$$\mathbf{B}_{m+1} = \mathbf{V}_m^\top \mathbf{B}_m \mathbf{V}_m + \frac{\mathbf{s}^m \mathbf{s}^{m^\top}}{\mathbf{y}^{m^\top} \mathbf{s}^m}$$

7. $m \leftarrow m + 1$

The downside of all Newton-type methods is that the Hessian, or its approximation, is, in general, dense. Thus, these methods are not well suited for large scale optimization problems. To solve such large scale problems, we make use of the limited memory BFGS (L-BFGS) method, which does not require storing the full approximated Hessian and is easy to implement. The L-BFGS method avoids calculating the descent direction $\mathbf{d}^m = -\mathbf{B}_m \nabla J(\mathbf{u}^m)$ by an explicit matrix vector multiplication and instead, finds an approximation of $\mathbf{d}^m$ by only computing a few scalar products. Therefore, we only save the first k few vector pairs $\{\mathbf{s}^i, \mathbf{y}^i\}_{i=m-k}^{m-1}$ computed via (2.16) and use them to calculate $\mathbf{r}^m \approx \mathbf{B}_m \nabla J(\mathbf{u}^m)$. After $\mathbf{r}^m$ is computed, we discard the oldest vector pair $\{\mathbf{s}^{m-k}, \mathbf{y}^{m-k}\}$ and replace it by $\{\mathbf{u}^m, \mathbf{y}^m, \}$. The two-loop recursion to determine $\mathbf{r}^m \approx \mathbf{B}_m \nabla J(\mathbf{u}^m)$ is given by the following algorithm, where we choose $\mathbf{B}_m^0$ in Step 5 according to [90, equation (7.20)].

Algorithm 2 approximated search direction

Input: gradient $\nabla J(\mathbf{u}^m)$, vector pairs $\{\mathbf{s}^i, \mathbf{y}^i\}_{i=m-k}^{m-1}$
Output: $\mathbf{r} \approx \mathbf{B}_m \nabla J(\mathbf{u}^m)$

1. $\mathbf{q} = \nabla J(\mathbf{u}^m)$
2. **for** $j = m-1, m-2, \ldots, m-k$ **do**
3. $\quad \sigma_j = \rho_j \mathbf{s}^{j^\top} \mathbf{q}$
4. $\quad \mathbf{q} = \mathbf{q} - \alpha_j \mathbf{y}^j$
5. $\mathbf{r} \leftarrow \mathbf{B}_m^0$
6. **for** $j = m-k, m-k+1, \ldots, m-1$ **do**
7. $\quad \beta = \gamma_j \mathbf{y}^{j^\top} \mathbf{r}$
8. $\quad \mathbf{r} = \mathbf{r} + \mathbf{s}^j(\sigma_j - \beta)$

With this, we can state the L-BFGS algorithm as follows.

Algorithm 3 L-BFGS Algorithm

Input:
initial guess $\mathbf{u}^0$, approximated inverse Hessian $\mathbf{B}_0$
set $m = 0$, $\varepsilon > 0$

1. **while** $\|\nabla J(\mathbf{u}^m)\| / \|\nabla J(\mathbf{u}^0)\| \geqslant \varepsilon$ **do**
2. $\quad$ Compute search direction $\mathbf{d}^m = -\mathbf{r}$ from Algorithm 2.
3. $\quad$ Compute step size $\alpha_m > 0$.
4. $\quad$ Set

$$\mathbf{u}^{m+1} = \mathbf{u}^m + \alpha_m \mathbf{d}^m$$

5. $\quad$ **if** m > k **then**
6. $\quad\quad$ Discard the vector pair $\{\mathbf{s}^{m-k}, \mathbf{y}^{m-k}\}$.
7. $\quad\quad$ Compute the vector pair $\{\mathbf{s}^m, \mathbf{y}^m\}$ via (2.16).
8. $\quad m \leftarrow m + 1$

The last step is to determine the step size α_m. As mentioned above, α_m should be a minimizer of $l(\alpha) = J(\mathbf{u}^m + \alpha \mathbf{d}^m)$ to ensure a sufficient decrease of J. However, we do not want to spend too much time and computational effort finding such step size. Finding α_m can be done by the standard inexact line search method, which is usually realized by iteratively testing different values of α_m until we found a sufficient decrease in J. The simplest condition would be to pick (the largest) α_m satisfying $l(\alpha_m) = J(\mathbf{u}^m + \alpha_m \mathbf{d}^m) < J(\mathbf{u}^m) = l(0)$. This may be not enough to yield a sufficient decrease in $l(\alpha)$ which may leads to a local minimum that does not yield the best possible α_m.

A popular inexact line search condition is the *Armijo* condition

$$J(\mathbf{u}^m + \alpha_m \mathbf{d}^m) \leqslant J(\mathbf{u}^m) + c_1 \alpha_m \nabla J(\mathbf{u}^m)^\top \mathbf{d}^m \tag{2.17}$$

with $c_1 \in (0,1)$. Note that this is stricter than $l(\alpha_m) < l(0)$, since $J(\mathbf{u}^m)^\top \mathbf{d}^m < 0$ in the right side of (2.17). The numerical realization of the Armijo condition is simply and done via the *backtracking* algorithm.

Algorithm 4 backtracking line search

Input:

$c_1, \alpha \in (0,1)$

$\mathbf{u}^m, \mathbf{d}^m$ such that $J(\mathbf{u}^m)^\top \mathbf{d}^m < 0$

1. Choose $\alpha_m = \max\{\alpha^j : \ j = 0, 1, 2, \ldots\}$ such that (2.17) holds:

$$J(\mathbf{u}^m + \alpha_m \mathbf{d}^m) \leqslant J(\mathbf{u}^m) + c_1 \alpha_m \nabla J(\mathbf{u}^m)^\top \mathbf{d}^m.$$

We can also allow the step size to be larger than 1, which may be incorporated in Step 1 by also checking negative values for j.

Next, we wish to mention that the backtracking algorithm is a "soft line search", since it is not expensive to compute. To find α_m via Algorithm 4 to satisfy the Armijo condition, we only need evaluations of the functional J and not its gradient ∇J, which is, usually for large scale problems, expensive to compute. Using the backtracking line search to compute the search direction for the BFGS and L-BFGS algorithm, Algorithm 1 and 3 respectively, we see that we need to compute $\nabla J(\mathbf{u}^m)$ anyway, and can thus reuse it in the backtracking Algorithm 4. While the backtracking line search is appropriate for Newton's method, it is less well-suited for quasi-Newton methods, see [90, Section 3.1]. For these methods, the *Wolfe* conditions

$$\begin{aligned} J(\mathbf{u}^m + \alpha_m \mathbf{d}^m) &\leqslant J(\mathbf{u}^m) + c_1 \alpha_m \nabla J(\mathbf{u}^m)^\top \mathbf{d}^m, \\ \nabla J(\mathbf{u}^m + \alpha_m \mathbf{d}^m)^\top \mathbf{d}^m &\geqslant c_2 \nabla J(\mathbf{u}^m)^\top \mathbf{d}^m, \end{aligned}$$

$0 < c_1 < c_2 < 1$, or the *Goldstein* conditions

$$\begin{aligned} J(\mathbf{u}^m) + (1-c)\alpha_m \nabla J(\mathbf{u}^m)^\top \mathbf{d}^m &\leqslant J(\mathbf{u}^m + \alpha_m \mathbf{d}^m) \\ &\leqslant J(\mathbf{u}^m) + c\alpha_m \nabla J(\mathbf{u}^m)^\top \mathbf{d}^m, \end{aligned}$$

with $0 < c < 1/2$, are more appropriate. However, they are not easy to implement in comparison to the backtracking line search and require more expensive gradient evaluations [90, Algorithm 3.5 & 3.6]. Since our problems of interest are large

scale, where the gradient is expensive to compute, we will only use the backtracking line search to find the step length α_m combined with the BFGS or L-BFGS algorithms. Note that there exist more line search methods than those mentioned above, where an extensive discussion can be found in [91].

Chapter 3

Inverse Problems

In this chapter, we will discuss inverse problems and important techniques to solve them, namely regularization and numerical implementation. In general, when solving inverse problems, we are interested to find or reconstruct the cause for an observed effect. Usually, such inverse problems are *ill-posed* in the sense of Hadamar [55]: We will call a mathematical problem *well-posed*, if

(i) the problem has a solution for all possible data,

(ii) this solution is unique, and

(iii) this solution depends continuously on the data.

Accordingly, we will call a problem ill-posed if it violates one of these three conditions.

In the following, we will study inverse problems of the form

$$F : H_1 \to H_2, \qquad F(u) = y, \tag{3.1}$$

where y is given, u unknown, and H_1, H_2 are Hilbert spaces. Note that H_1, H_2 can also be Banach spaces, where we refer to the standard literature [63, 107, 109]. Normally we do not have access to the exact data $y^\dagger$ but know noised or perturbed data y^δ such that

$$\|y^\dagger - y^\delta\|_{H_2} \leqslant \delta, \tag{3.2}$$

with $\delta \geqslant 0$ known. Thus, if we denote the exact solution to the noise free problem of (3.1) by $u^\dagger$ satisfying $F(u^\dagger) = y^\dagger$ and the solution to the noised or perturbed problem

$$F(u) = y^\delta \tag{3.3}$$

by $u^{\dagger,\delta}$, we wish to have stability of the form $u^{\dagger,\delta} \to u^\dagger$ as $\delta \to 0$.

If the inverse problem can not satisfy condition (i) (existence) or (ii) (uniqueness) this may be treated by adding constraints to the solution u, for example that we wish to find the minimal norm solution or add more data, e.g. by invoking more measurements. However, the stability constraint (iii) needs more sophisticated methods such as regularization.

Example 3.1. *A simple example of ill-posed inverse problems is the differentiation of (noisy) functions. For given $y^\dagger \in H_2 = C([0,1])$ we wish to find its derivative $u^\dagger := (y^\dagger)' \in H_1 = C([0,1])$. Thus, the forward operator is given by*

$$F : C([0,1]) \to C([0,1]), \qquad u = y' \mapsto y.$$

Now we assume that only noisy data y^δ is given such that

$$y^\delta = y^\dagger + \eta, \qquad \eta(x) = \delta \sin(k\pi x), \quad \delta \geqslant 0.$$

Hence, if we denote by $u^{\dagger,\delta} = (y^\delta)'$ the noised derivative we obtain

$$\begin{aligned} \|y^\delta - y^\dagger\|_{C([0,1])} &= \|\eta\|_{C([0,1])} = \delta, \\ \|u^\dagger - u^{\dagger,\delta}\|_{C([0,1])} &= \|\eta'\|_{C([0,1])} = \delta k\pi, \end{aligned} \tag{3.4}$$

where the latter one can be arbitrarily large for large k, even if the error in the known data (3.4) is arbitrarily small. To overcome this ill-posedness, we may consider the image space of F to be $C^1([0,1])$ and thus know a bound for the noise and therefore for the data misfit, in the C^1-norm,

$$\|y^\dagger - y^\delta\|_{C^1([0,1])} \leqslant \delta,$$

which yields

$$\|u^\dagger - u^{\dagger,\delta}\|_{C([0,1])} \leqslant \|y^\dagger - y^\delta\|_{C^1([0,1])} \to 0, \qquad \delta \to 0.$$

This illustrates that ill-posedness also depends on the underlying space and norm. However, using $C^1([0,1])$ as the image space would also require y', which is exactly the quantity we want to reconstruct.

3.1 Regularization Methods

Next, we discuss some standard regularization strategies for linear and nonlinear ill-posed inverse problems of the form (3.3)

$$F : H_1 \to H_2, \qquad F(u) = y,$$

or its least squares representation

$$\min_{u \in H_1} J(u) = \min_{u \in H_1} \frac{1}{2} \|F(u) - y\|_{H_2}^2. \tag{3.5}$$

3.1.1 Truncated Singular Value Decomposition

First, we will discuss the *truncated singular value decomposition* (TSVD) for the linear finite dimensional case, c.f. [8, 61, 125]. For the infinite dimensional case with linear operators we refer to [35, Chapter 3 & Example 4.8]

Assume we have a linear inverse problem of the form (3.3) with $H_1 = \mathbb{R}^n$, $H_2 = \mathbb{R}^m$, $n \leqslant m$ and the corresponding matrix $\mathbf{F} \in \mathbb{R}^{m\times n}$ with full rank $\mathbf{F} = n$. Thus, there exists a singular value decomposition (SVD) of $\mathbf{F}$, given by

$$\mathbf{F} = \mathbf{W}\Sigma\mathbf{V}^\top \tag{3.6}$$

with unitary

$$\mathbf{W} = [\mathbf{w}_1|\dots|\mathbf{w}_m] \in \mathbb{R}^{m\times m},$$
$$\mathbf{V} = [\mathbf{v}_1|\dots|\mathbf{v}_n] \in \mathbb{R}^{n\times n},$$

and $\Sigma \in \mathbb{R}^{m\times n}$ where, for $1 \leqslant i \leqslant n$, $\Sigma_{i,i} = \sigma_i$ for a sequence of singular values $\sigma_1 \geqslant \sigma_2 \geqslant \dots \geqslant \sigma_n > 0$ and zero otherwise. Again, we denote by $\mathbf{u}^\dagger$ the exact solution with exact data $\mathbf{y}^\dagger$ satisfying $\mathbf{F}\mathbf{u}^\dagger = \mathbf{y}^\dagger$ and by $\mathbf{u}^{\dagger,\delta}$ the solution to the inverse problem

$$\mathbf{F}\mathbf{u} = \mathbf{y}^\delta$$

with given perturbed data

$$\mathbf{y}^\delta = \mathbf{y}^\dagger + \eta, \qquad \|\eta\|_{\ell^2} = \delta, \quad \delta \geqslant 0.$$

Now, we can use the SVD (3.6) of $\mathbf{F}$ to obtain its pseudo inverse

$$\mathbf{F}^\dagger = \mathbf{V}\Sigma^\dagger\mathbf{W}^\top$$

with $\Sigma^\dagger_{i,i} = 1/\sigma_i$, $1 \leqslant i \leqslant n$ and zero otherwise. Thus, the minimal norm solution can be expressed as

$$\mathbf{u}^{\dagger,\delta} = \mathbf{F}^\dagger\mathbf{y}^\delta = \mathbf{V}\Sigma^\dagger\mathbf{W}^\top\mathbf{y}^\delta = \sum_{i=1}^{n} \frac{1}{\sigma_i}(\mathbf{w}_i, \mathbf{y}^\delta)_{\ell^2}\mathbf{v}_i. \tag{3.7}$$

This expression easily shows that small singular values σ_i result in an amplification of errors in the noisy data $\mathbf{y}^\delta$ and thus leads to a noisy, unregularized solution. The simplest way to regularize the solution is by neglecting all singular values that are "small enough", that is, truncating all singular values that satisfy $\sigma_i^2 \leqslant \alpha$ for $\alpha \geqslant 0$. This yields the truncated singular value decomposition (TSVD) solution of (3.7)

$$\mathbf{u}^{\alpha,\delta} = \sum_{\sigma_i^2 > \alpha} \frac{1}{\sigma_i}(\mathbf{w}_i, \mathbf{y}^\delta)_{\ell^2}\mathbf{v}_i.$$

Since we can express the error $\mathbf{e}$ as

$$\mathbf{e} = \mathbf{u}^{\alpha,\delta} - \mathbf{u}^{\dagger} = \mathbf{e}^{\delta} - \mathbf{e}^{\alpha},$$

where

$$\mathbf{e}^{\delta} = \sum_{\sigma_i^2 > \alpha} \frac{1}{\sigma_i} (\mathbf{w}_i, \eta)_{\ell^2} \mathbf{v}_i,$$
$$\mathbf{e}^{\alpha} = \sum_{\sigma_i^2 \leqslant \alpha} \frac{1}{\sigma_i} (\mathbf{w}_i, \mathbf{y}^{\dagger})_{\ell^2} \mathbf{v}_i$$

with the *noise amplification error* $\mathbf{e}^{\delta}$ due to given noisy data and *solution truncation error* $\mathbf{e}^{\alpha}$ due to regularization. This immediately implies that

$$\mathbf{e}^{\alpha} \to 0, \qquad \alpha \to 0.$$

If we choose $\alpha = \alpha(\delta) = \delta^p$, $0 < p < 2$, the noise amplification error tends to zero as $\delta \to 0$

$$\|\mathbf{e}^{\delta}\|_{\ell^2} \leqslant \frac{\delta}{\sqrt{\alpha}} = \delta^{1-p/2} \to 0, \qquad \delta \to 0,$$

and for this particular choice of $\alpha = \alpha(\delta)$, the solution truncation error $\mathbf{e}^{\alpha(\delta)}$ also tends to 0 as δ approaches 0. In summary, if we set $\alpha = \alpha(\delta) = \delta^p$ for $0 < p < 2$, we obtain convergence of the form

$$\mathbf{u}^{\alpha(\delta),\delta} \to \mathbf{u}^{\dagger}, \qquad \delta \to 0.$$

This simple examination shows that the parameter $\alpha(\delta)$, $\alpha(\delta) \to 0$ for $\delta \to 0$, balances the solution truncation error and noise amplification error. Thus, α has to be chosen wisely such that the noise does not affect the reconstruction, while too much important information to reconstruct $u^{\dagger}$ won't be neglected.

3.1.2 Regularization and Parameter Choice Rules

As we have seen, the parameter α specifies how well the exact solution $u^{\dagger}$ can be approximated or regularized. Consequently, we will call α the *regularization parameter*.

Definition 3.2. A function

$$\alpha : \mathbb{R}_{\geqslant 0} \times H_2 \to \mathbb{R}_{\geqslant 0}, \qquad (\delta, y^{\delta}) \mapsto \alpha(\delta, y^{\delta}),$$
$$\alpha(\delta, y^{\delta}) \to 0, \qquad \delta \to 0,$$

is called a *parameter choice rule* and we distinguish the three cases

(i) *a priori choice rules* if $\alpha = \alpha(\delta)$ only depends on δ,

(ii) *a posteriori choice rules* if $\alpha = \alpha(\delta, y^\delta)$ depends on both, δ and y^δ,

(iii) *heuristic choice rules* if $\alpha = \alpha(y^\delta)$ only depends on y^δ.

Since we only consider the regularization parameter to be a parameter choice rule, we simply refer to a regularization parameter if it satisfies the definition of a parameter choice rule.

Definition 3.3. Consider a regularization parameter $\alpha = \alpha(\delta, y^\delta)$ depending on the *noise* $\delta \geqslant 0$ and noisy data y^δ. We will call a family $\{R_\alpha\}_{\alpha \geqslant 0}$, $R_\alpha : H_2 \to H_1$ a *regularization method* for the inverse problem $F(u) = y$, if it approximates the pseudo inverse $F^\dagger$ pointwise for every element in the domain of $F^\dagger$, i.e.

$$R_\alpha(y) \to F^\dagger y, \qquad \alpha \to 0.$$

Additionally, if $\alpha = \alpha(\delta, y^\delta)$ is a parameter choice rule satisfying Definition 3.2, $R_{\alpha(\delta, y^\delta)}$ is said to be a *(convergent) regularization method* if

$$R_{\alpha(\delta, y^\delta)} y^\delta \to F^\dagger(y^\dagger), \qquad \delta \to 0. \tag{3.8}$$

If we denote by $u^{\alpha(\delta, y^\delta), \delta} = R_{\alpha(\delta, y^\delta)} y^\delta$ the regularized solution to the noised inverse problem and by $u^\dagger = F^\dagger(y^\dagger)$ the exact solution to the (noise-free) inverse problem, (3.8) simply reads

$$u^{\alpha(\delta, y^\delta), \delta} \to u^\dagger, \qquad \delta \to 0.$$

The benefit of heuristic choice rules, especially in real life applications, is that one only needs the already given data y^δ and not the noise δ, or an approximation of it, which may not be available. However, Bakushinskii [12] showed that using a heuristic choice rule (iii) to solve ill-posed problems cannot yield a convergent regularization method. Of course, regularization parameters such as the *quasi-optimality criterion* by Tikhonov, Arsenin, and Glasko [119, 120], the *L-curve method* by Hansen and O'Leary [59, 60, 62], and the *modified discrepancy partner rule* [58] by Hanke and Raus have been studied, but it outlines that such methods have to be treated with care.

A priori parameter choice rules (i), on the other hand, only make use of the noise δ and do not take the measured data y^δ into account. Hence, the parameter $\alpha = \alpha(\delta)$ may be determined before actually solving the inverse problem. For a linear forward operator F, there always exists an a priori parameter choice rule such that the regularization $R_{\alpha(\delta)}$ is a convergent regularization method, see [35, Proposition 3.4].

Theorem 3.4. *Consider a linear forward operator F and its pseudo inverse $F^\dagger$. Let $\{R_\alpha\}_{\alpha\geqslant 0}$ be a regularization method according to Definition 3.3 which is continuous but possibly nonlinear. Then, for every element $y^\dagger$ in the domain of $F^\dagger$, there exists an a priori parameter choice rule $\alpha(\delta)$ such that $R_{\alpha(\delta)}$ is a convergent regularization method* (3.8).

Proof. Since, by assumption, R_α is a regularization method, there exists for all $\varepsilon > 0$ a monotonically decreasing function $\sigma : \mathbb{R}_{>0} \to \mathbb{R}_{>0}$, $\varepsilon \mapsto \sigma(\varepsilon)$, with $\lim_{\varepsilon\to 0} \sigma(\varepsilon) \to 0$, such that

$$\|R_{\sigma(\varepsilon)} y - T^\dagger y\|_{H_1} \leqslant \frac{\varepsilon}{2}.$$

Since $R_{\sigma(\varepsilon)}$ is, itself, continuous, for every fixed $\varepsilon > 0$ there exists $\rho(\varepsilon) > 0$ such that

$$\|R_{\sigma(\varepsilon)} z - R_{\sigma(\varepsilon)} y\|_{H_1} \leqslant \frac{\varepsilon}{2} \qquad \text{if } \|z - y\|_{H_2} \leqslant \rho(\varepsilon).$$

Without loss of generality, we can assume that $\rho : \mathbb{R}_{>0} \to \mathbb{R}_{>0}$, $\lim_{\varepsilon\to 0} \rho(\varepsilon) = 0$ is strictly increasing and thus, it admits a strictly monotone and continuous inverse ρ^{-1} with $\lim_{\delta\to 0} \rho^{-1}(\delta) = 0$. Thus, we can define the monotonic function

$$\alpha : \mathbb{R}_{>0} \to \mathbb{R}_{>0}, \qquad \delta \mapsto \alpha(\delta) = \sigma(\rho^{-1}(\delta)), \qquad \text{with } \lim_{\delta\to 0} \alpha(\delta) = 0. \tag{3.9}$$

Hence, for all $\varepsilon > 0$ there exists $\rho = \rho(\delta) > 0$ such that, for $\|y^\delta - y^\dagger\|_{H_2} \leqslant \delta$,

$$\|R_{\alpha(\delta)} y^\delta - F^\dagger y^\dagger\|_{H_1} \leqslant \|R_{\alpha(\delta)} y^\delta - R_{\alpha(\delta)} y^\dagger\|_{H_1} + \|R_{\alpha(\delta)} y^\dagger - F^\dagger y^\dagger\|_{H_1} \leqslant \varepsilon.$$

This implies that $\alpha(\delta)$, given by (3.9), is a parameter choice rule and thus, $R_{\alpha(\delta)}$ is a convergent regularization method. □

Note that in Section 3.1.1, where we studied the TSVD, we truncated all singular values σ_i satisfying $\sigma_i^2 \leqslant \alpha(\delta) = \delta^p$, $0 < p < 2$. Thus, this choice is an a priori choice rule. A common a priori choice rule is the *balancing principle* by Lepskij [75], where the propagated noise error is taken into account. For an extensive discussion and numerical comparison regarding different parameter choice rules we refer to Bauer and Lukas [15].

Even though there exist more a posteriori parameter choice rules [15], throughout this Thesis we will only discuss and use the *discrepancy principle*. This parameter choice rule was first proposed by Phillips [94] and later analyzed by Morozov [82, 83]. The motivation is simple and intuitive: The regularized solution $u^{\alpha,\delta}$ should not overfit the data misfit. Recall that we have given data y^δ and unknown data $y^\dagger = F(u^\dagger)$ with the exact but unknown solution $u^\dagger$ such that

$$\|F(u^\dagger) - y^\delta\|_{H_2} = \|y^\dagger - y^\delta\|_{H_2} \leqslant \delta, \tag{3.10}$$

with $\delta \geqslant 0$ known. Thus, it is not reasonable to obtain a smaller data misfit in (3.10) with $u^{\alpha,\delta} = R_\alpha(y^\dagger)$ than with the exact solution $u^\dagger$. Hence, we want to choose (the possibly largest) $\alpha = \alpha(\delta, y^\delta)$ such that

$$\|F(u^{\alpha,\delta}) - y^\delta\|_{H_2} \leqslant \tau\delta, \qquad \tau > 1. \tag{3.11}$$

For linear inverse problems it can be shown that the regularization method R_α, where $\alpha = \alpha(\delta, y^\delta)$ is chosen according to the discrepancy principle (3.11), is a convergent regularization method, see, for example, [35, Section 4.3 & Theorem 3.17]. Even though the discrepancy principle is easy to validate, since we only need one evaluation of the forward operator to compute the data misfit, its drawback is that it needs precise noise δ. If δ is not known exactly and only an approximated value is available, this parameter choice rule may lead to very poor solutions, see [60, Chapter 7] and also [57]. In practice we consider a monotonically decreasing null sequence $\{\alpha_n\}_{n\geqslant 1}$ and compute $u^{\alpha_n,\delta} = R_{\alpha_n} y^\delta$ until the discrepancy principle (3.11) is satisfied.

Next, we will study different types of regularization methods, where the forward operator F is not necessarily linear. For the theory of linear inverse problems we refer to the standard literature [99, Chapter 3], [63, Chapter 3], [71, Chapter 2 & 3], and [35, Chapter 4 – 8]

3.1.3 Tikhonov Regularization

Recall that we want to solve the inverse problem (3.3) with given noisy data as in (3.2). That is, for $F : H_1 \to H_2$, with H_1, H_2 Hilbert spaces, we wish to find $u^{\dagger,\delta} \in H_1$ satisfying

$$F(u^{\dagger,\delta}) = y^\delta, \qquad \text{where} \quad \|y^\dagger - y^\delta\|_{H_2} \leqslant \delta$$

for the known noise $\delta \geqslant 0$ and with exact but unknown data $y^\dagger = F(u^\dagger)$ corresponding to the exact but unknown solution $u^\dagger$. Instead of solving $F(u) = y^\delta$, for $\alpha > 0$ Tikhonov proposed to minimize the Tikhonov functional [116, 117]

$$J_\alpha^\delta : H_1 \to \mathbb{R}, \qquad J_\alpha^\delta(u) = \frac{1}{2}\|F(u) - y^\delta\|_{H_2}^2 + \frac{\alpha}{2}\|u\|_{H_1}^2. \tag{3.12}$$

Following [35, 63, 71] we will obtain the convergence results:

Theorem 3.5. *Let $F : H_1 \to H_2$ be continuous and weak sequentially closed. Then there exists a minimizer $u^{\alpha,\delta}$ of the Tikhonov functional J_α^δ.*

Proof. Since $J_\alpha^\delta(u) \geqslant 0$ for all $u \in H_1$, there exists a minimizing sequence $\{u^m\}_m$ such that

$$J_\alpha^\delta(u^m) \to n := \inf_{u\in H_1} J_\alpha^\delta(u).$$

Note that the convergence of the sequence $\{J_\alpha^\delta(u^m)\}_m$ does not imply convergence of u^m. However, since $\{J_\alpha^\delta(u^m)\}_m$ converges, it is also bounded. Thus, there exists $N > 0$ such that $J_\alpha^\delta(u^m) \leqslant N$ for all m. Since

$$\|u^m\|_{H_1}^2 \leqslant \frac{2}{\alpha} J_\alpha^\delta(u^m) \leqslant \frac{2}{\alpha} N,$$

the sequence $\{u^m\}_m$ is also bounded and thus contains a weakly convergent subsequence, for simplicity denoted by $\{u^m\}_m$, such that $u^m \rightharpoonup \bar{u}$. Analogously we deduce that the sequence $\{F(u^m)\}_m$ is bounded and therefore admits a weakly convergent subsequence, for simplicity again denoted by $\{F(u^m)\}_m$, with limit $F(u^m) \rightharpoonup y$. Since F is assumed to be weak sequentially closed we have $F(\bar{u}) = y$ and hence

$$n \leqslant J_\alpha^\delta(\bar{u}) = \lim_{m\to\infty} J_\alpha^\delta(u^m) = \inf_{u\in H_1} J_\alpha^\delta(u) = n.$$

This implies that $u^{\alpha,\delta} = \bar{u}$ is a minimizer of the Tikhonov functional J_α^δ. □

In general, a minimizer of (3.12) does not have to be unique. However, we can show stability in the sense that it is continuous with respect to given data y^δ.

Theorem 3.6. *Let $F : H_1 \to H_2$ be continuous and weak sequentially closed and $\{u^m\}_m \subset H_1$, $\{y^m\}_m \subset H_2$ be two sequences such that $y^m \to y^\dagger$ where u^m is the corresponding minimizer of J_α^δ with y^δ replaced by y^m. Then u^m has a weakly convergent subsequence and every accumulation point is a minimizer of J_α^δ. If additionally, J_α^δ admits a unique minimizer, then the whole sequence $\{u^m\}_m$ converges strongly.*

Proof. For this technical proof we refer to [35, Theorem 10.2] or [63, Theorem 4.2]. □

What remains to be shown is that $u^{\alpha,\delta}$ converges to the exact solution $u^\dagger$ for $\delta \to 0$ if we choose α in dependence of δ wisely.

Theorem 3.7. *Let $F : H_1 \to H_2$ be continuous and weak sequentially closed, assume that there exists a minimum norm solution $u^\dagger \in H_1$, i.e. $F(u^\dagger) = y^\dagger$ with minimal H_1-norm, and consider, for a null-sequence $\delta_m \to 0$, $\alpha_m = \alpha(\delta_m)$ with*

$$\alpha(\delta) \to 0, \quad \frac{\delta^2}{\alpha(\delta)} \to 0, \qquad \text{as } \delta \to 0. \tag{3.13}$$

Then every sequence $\{u^{\alpha_m,\delta_m}\}_m$, where u^{α_m,δ_m} minimizes $J_{\alpha_m}^{\delta_m}$, has a convergent subsequence and its limit is a minimum norm solution. If this minimum norm solution is unique, then

$$\lim_{\delta\to 0} u^{\alpha(\delta),\delta} \to u^\dagger.$$

Proof. Since u^{α_m,δ_m} minimizes $J^{\delta_m}_{\alpha_m}$, we obtain

$$\begin{aligned} J^{\delta_m}_{\alpha_m}(u^{\alpha_m,\delta_m}) &= \frac{1}{2}\|F(u^{\alpha_m,\delta_m}) - y^{\delta_m}\|^2_{H_2} + \frac{\alpha_m}{2}\|u^{\alpha_m,\delta_m}\|^2_{H_1} \\ &\leqslant J^{\delta_m}_{\alpha_m}(u^\dagger) \leqslant \frac{1}{2}\delta_m^2 + \frac{\alpha_m}{2}\|u^\dagger\|^2_{H_1} \end{aligned} \tag{3.14}$$

and

$$\|u^{\alpha_m,\delta_m}\|^2_{H_1} \leqslant \frac{2}{\alpha_m} J^{\delta_m}_{\alpha_m}(u^{\alpha_m,\delta_m}) \leqslant J^{\delta_m}_{\alpha_m}(u^\dagger) \leqslant 2\frac{\delta_m^2}{\alpha_m} + \|u^\dagger\|^2_{H_1}. \tag{3.15}$$

□

From (3.14) it follows that $F(u^{\alpha_m,\delta_m}) \to y^\dagger$ as $m \to \infty$ and (3.15) implies that the sequence $\{u^{\alpha_m,\delta_m}\}_m$ is bounded. Thus it admits a convergent subsequence denoted by $\{u^{\alpha_m,\delta_m}\}_m$ that converges weakly to a limit point $\bar{u}$. The weak sequentially closedness of F yields $F(\bar{u}) = y^\dagger$, and $\bar{u}$ is a minimum norm solution due to (3.15) and

$$\|\bar{u}\|^2_{H_1} \leqslant \limsup_{n\to\infty} \|u^{\alpha_m,\delta_m}\|^2_{H_1} \leqslant \limsup_{n\to\infty} 2\frac{\delta_m^2}{\alpha_m} + \|u^\dagger\|^2_{H_1} = \|u^\dagger\|^2_{H_1}.$$

What remains to be shown is that $\{u^{\alpha_m,\delta_m}\}_m$ converges strongly to $\bar{u}$. Due to the weak convergence of $\{u^{\alpha_m,\delta_m}\}_m$, we obtain strong convergence via

$$\|u^{\alpha_m,\delta_m} - \bar{u}\|^2_{H_1} = \|u^{\alpha_m,\delta_m}\|^2_{H_1} + \|\bar{u}\|^2_{H_1} - 2(u^{\alpha_m,\delta_m}, \bar{u})_{H_1} \to 0, \qquad m \to \infty. \tag{3.16}$$

Note that this only implies that u^{α_m,δ_m} converges to a minimum norm solution $\bar{u}$ which is not necessarily $u^\dagger$. However, if $u^\dagger$ is unique, every sequence $\{u^{\alpha_m,\delta_m}\}_m$ has a convergent subsequence converging to $u^\dagger$. Since $u^\dagger$ is itself a minimum norm solution, we obtain $\|\bar{u}\|_{H_1} = \|u^\dagger\|_{H_1}$ and due to the norm convergence (3.16), we obtain strong convergence to $u^\dagger$.

Generalization of Tikhonov Regularization

We are able to generalize the framework of the Tikhonov regularization by adding a *regularization* or *penalty* term R to the least square functional J from (3.5), to obtain the minimization problem

$$\min_{u\in H_1} J^\delta_\alpha = \min_{u\in H_1} J^\delta(u) + \alpha R(u) \tag{3.17}$$

with $J^\delta(u) = {}^1\!/_2\|F(u) - y^\delta\|^2_{L^2(\Omega)}$. As we have seen before, choosing the regularization term $R_{L^2}(u) = {}^1\!/_2\|u\|^2_{L^2(\Omega)}$ yields Tikhonov regularization and favors minimal

L^2-norm solutions. However, there are many other realizations of regularization terms R that are common, for example

$$\begin{aligned}
\text{sparsity} \qquad & R_0(u) = \|\mathbf{u}\|_{\ell^0} \ \#\text{ of nonzero elements of } \mathbf{u} \\
\text{(approximately) sparsity} \qquad & R_1(u) = \|\mathbf{u}\|_{\ell^1} = \sum_{k\in\mathbb{N}} |(u,\varphi_k)_{L^2(\Omega)}| \\
\text{Total Variation (TV)} \qquad & \mathrm{TV}(u) = \int_\Omega |\nabla u| = \|\nabla u\|_{L^1(\Omega)} \\
\text{regularized TV} \qquad & \mathrm{TV}_\varepsilon(u) = \int_\Omega \sqrt{|\nabla u|^2 + \varepsilon^2} \\
\text{semi } H^1 \text{ penalization} \qquad & R_{H^1}(u) = {}^1\!/_2 |u|_{H^1(\Omega)} = {}^1\!/_2 \|\nabla u\|^2_{L^2(\Omega)}
\end{aligned}$$

where $u = \sum_{k\in\mathbb{N}} u_k\varphi_k$, $u_k = (u,\varphi_k)_{L^2(\Omega)}$, $\mathbf{u} = (u_1, u_2, \ldots)$ for a basis $\{\varphi_k\}_k \subset L^2(\Omega)$. Sparsity promoting regularization techniques can be used when the unknown medium is known to have many sparse entries, e.g. deblurring a black and white picture. Instead of using $R(u) = \|\mathbf{u}\|_{\ell^0}$ as a regularization term, it is more convenient (due to an easier realization) to use $\|\cdot\|_{\ell^1}$ or even $\|\cdot\|^p_{\ell^p}$ as penalization [20, 34, 45]. Total Variation (TV) on the other hand, was first introduced by Rudin, Osher, and Fatemi [102] in image denoising and is able to accurately remove noise while preserving edges and sharp contrast [5, 33]; thus, it is a good choice if the unknown medium u is known to be piecewise constant. The downside of the TV functional is its non-differentiability. However, Vogel and Oman introduced the regularized TV function TV_ε [22, 126], which is differentiable and hence useful to solve (3.17) with gradient-type methods. Semi H^1 penalization on the other hand, is used when the medium is known to be smooth or when the noise-level δ may be large [70, 108].

3.1.4 Iterative Regularization

Another strategy to obtain regularization for (nonlinear) inverse problems of the form (3.3) are *iterative regularization* methods. Such methods rely on a good initial guess $u^{0,\delta}$ and then obtain the next iterate $u^{m+1,\delta}$ successively via

$$u^{m+1,\delta} = u^{m,\delta} + G_m(u^{m,\delta}, y^\delta) \tag{3.18}$$

for a (non)-linear operator G_m. For analysis regarding iterative methods for linear inverse problems we refer to Engl, Hanke, and Neubauer [35, Chapter 6 & 7] and for nonlinear inverse problems to Kaltenbacher, Neubauer, and Scherzer [66]. To obtain a regularization method, iteration (3.18) has to be stopped by an appropriate stopping rule to act as a (convergent) regularization method. For this we will again consider the discrepancy principle (3.11) acting on the iterative formula.

That is, we will stop the algorithm at iteration m_*, determined via

$$m_* = m_*(\delta) = \min\{m \in \mathbb{N} : \ \|F(u^{m,\delta}) - y^\delta\|_{H_2} \leqslant \tau\delta\}, \qquad \tau > 1.$$

From this, it is clear that the stop criterion depends on the noise-level δ and that the iteration number m itself acts as a regularization parameter. In the context of the previous section, the regularization parameter α corresponds to the reciprocal of m.

The most well known iterative method is the *Landweber iteration* [72], given in the context of (3.18) by

$$u^{m+1,\delta} = u^{m,\delta} - F'(u^{m,\delta})^*(y^\delta - F(u^{m,\delta}).$$

Starting from this, it is easy to see that the Landweber iteration simply corresponds to the gradient descent method to solve the least squares minimization problem (3.5) with misfit $^1/_2\|F(u) - y^\delta\|_{H_2}$. We may also combine the Landweber iteration with Tikhonov regularization, too, to obtain the scheme

$$u^{m+1,\delta} = u^{m,\delta} - [F'(u^{m,\delta})^*(y^\delta - F(u^{m,\delta})) + \alpha_m u^{m,\delta}].$$

Note that in this case, α_m is not the regularization parameter but a penalization parameter that favors to minimize the regularization term when chosen large and leads to minimization of the misfit when selected small. Usually, one wants a decreasing sequence for α_m Following [35, Section 11.2] and using (3.13), we want α_m to satisfy

$$\begin{aligned} &\alpha_m > 0, && 1 \leqslant \frac{\alpha_m}{\alpha_{m+1}} \leqslant r, && \alpha_m \to 0, && r > 1,\ m \to \infty \\ &\alpha_m(\delta) \to 0, && \frac{\delta^2}{\alpha_m(\delta)} \to 0, && \delta \to 0. \end{aligned} \tag{3.19}$$

It is easy to verify that the two parameter choices

$$\alpha_m = \alpha_0 p^m \qquad \text{or} \qquad \alpha_m = \frac{\alpha_0}{m^p} \tag{3.20}$$

for $\alpha_0 = \delta^q,\ q, p \in (0, 1)$ satisfy the conditions (3.19). Another intuitive choice proposed by Rudin, Osher, and Fatemi [102] and later used by Tang [113, Section 5.1] is the following. Consider a solution $\bar{u}$ that minimizes

$$J^\delta_\alpha(u) = J^\delta(u) + \alpha R(u).$$

Thus, it is a stationary point of J^δ_α and satisfies

$$0 = (\nabla J^\delta_\alpha(\bar{u}), \varphi)_{H_2} = (\nabla J^\delta(\bar{u}), \varphi)_{H_2} + \alpha(\nabla R(\bar{u}), \varphi)_{H_2}, \qquad \forall \varphi \in H_1.$$

Choosing $\varphi = \bar{u} = u^{m,\delta}$, we may use

$$\alpha_m = \begin{cases} \alpha_0 \dfrac{|(\nabla J^\delta(u^{m,\delta}), u^{m,\delta})_{H_2}|}{|(\nabla R(u^{m,\delta}), u^{m,\delta})_{H_2}|} & \text{if } (\nabla R(u^{m,\delta}), u^{m,\delta})_{H_2} \neq 0, \\ 0 \text{ or as in } (3.20) & \text{otherwise,} \end{cases}$$

with either $\alpha_0 = \delta^q$ or $\alpha_0 = p$, for $q, p \in (0, 1)$.

Another class is Newton-type methods, such as the *Levenberg-Marquardt* method [76, 78]

$$\begin{aligned} u^{m+1,\delta} &= u^{m,\delta} + d^{m,\delta}, \\ d^{m,\delta} &= \operatorname*{argmin}_{d \in H_1} \frac{1}{2} \|F'(u^{m,\delta})d + F(u^{m,\delta}) - y^\delta\|_{H_2}^2 + \frac{\alpha_m}{2} \|d\|_{H_1}^2 \end{aligned}$$

with explicit scheme

$$u^{m+1,\delta} = u^{m,\delta} + (F'(u^{m,\delta})^* F'(u^{m,\delta}) + \alpha_m I)^{-1} F'(u^{m,\delta})^* (y^\delta - F(u^{m,\delta})),$$

a modified version of the Levenberg-Marquardt, or *iteratively regularized Gauß-Newton*, method proposed by [13]

$$\begin{aligned} u^{m+1,\delta} &= u^{m,\delta} + d^{m,\delta}, \\ d^{m,\delta} &= \operatorname*{argmin}_{d \in H_1} \frac{1}{2} \|F'(u^{m,\delta})d + F(u^{m,\delta}) - y^\delta\|_{H_2}^2 + \frac{\alpha_m}{2} \|d + u^{m,\delta}\|_{H_1}^2, \end{aligned}$$

with explicit scheme

$$u^{m+1,\delta} = u^{m,\delta} + (F'(u^{m,\delta})^* F'(u^{m,\delta}) + \alpha_m I)^{-1} (F'(u^{m,\delta})^* (y^\delta - F(u^{m,\delta})) - \alpha_m u^{m,\delta}),$$

and Broyden's quasi-Newton method for Hilbert spaces [46, 103]

$$\begin{aligned} d^{m,\delta} &= -(B^{m,\delta})^\dagger (F(u^{m,\delta}) y^\delta), \\ u^{m+1,\delta} &= u^{m,\delta} + d^{m,\delta}, \\ B^{m+1,\delta} &= B^{m,\delta} + \frac{(d^{m,\delta}, \cdot)_{H_1}}{\|d^{m,\delta}\|_{H_1}^2} (F(u^{m+1,\delta}) - y^\delta), \end{aligned}$$

for $B^{0,\delta}$ a regular and sufficiently good approximation to $F'(u^\dagger)$, e.g. $B^{0,\delta} = F'(u^{0,\delta})$. For convergence and regularization theory, as well as different iterative regularization methods, we refer to the standard literature [66].

3.1.5 Regularization by Discretization

Since, in practice, one usually first discretizes the inverse problem and then solves it numerically, considering regularization by discretization or projection is a natural choice and was first started by Natterer [85]. To do so, there are three main discretization strategies to solve the inverse problem

$$F : H_1 \to H_2, \qquad F(u) = y. \tag{3.21}$$

(i) Projection in image space, also called the least squares method, where one considers finite dimensional spaces $H_2^m \subset H_2$,

(ii) projection in preimage space, also called the least squares method, where one considers finite dimensional spaces $H_1^m \subset H_1$,

(iii) or a combination of both.

Before we further discuss the three methods, we will consider a simple linear example where we (poorly) discretize the preimage space and do not obtain convergence. Consider the identity operator $F = \mathbf{I}$,

$$\mathbf{I} : \ell^2 \to \ell^2, \qquad \mathbf{Iu} = \mathbf{y}, \tag{3.22}$$

with given $\mathbf{y} = (y_1, y_2, \ldots)$, $y_n = 1/n$. Since $\|\mathbf{y}\|_{\ell^2}^2 = \pi^2/6$, we have $\mathbf{y} \in \ell^2$ and thus, the exact solution to (3.22) is simply $\mathbf{u}^\dagger = \mathbf{y}$. We now discretize the preimage space by $H_1^m = \operatorname{span}\{(1, 0, \ldots)\} \subset \ell^2$ for all m. Thus, the solution to the discretized equation of (3.22)

$$\mathbf{Iu}^m = \mathbf{y}, \qquad \mathbf{u}^m \in H_1^m,$$

is given by $\mathbf{u}^m = (1, 0, \ldots) \neq \mathbf{u}^\dagger$ for all m. This simple example shows that one has to pay attention to choose an appropriate discretization of the space. Note that Seidman [110] showed a more general result for the nonconvergence of the least squares problem to ill-posed inverse problems.

Projection onto image space, or also called the dual least squares for (3.21) for given noisy data $y = y^\delta$, consists of choosing finite dimensional subspaces

$$H_2^1 \subset \ldots \subset H_2^m \subset \ldots \subset H_2, \qquad \overline{\bigcup_{m \in \mathbb{N}} H_2^m} = H_2, \tag{3.23}$$

to solve

$$F(u) = y^{m,\delta}, \qquad y^{m,\delta} = \Pi_{H_2^m} y^\delta, \tag{3.24}$$

or equivalently

$$(\Pi_{H_2^m} F(u), z^m)_{H_2} = (y^{m,\delta}, z^m)_{H_2^m}, \qquad \forall\, z^m \in H_2^m,$$

successively for $m \geqslant 1$, until an appropriate stoping criterion is reached, where $\Pi_{H_2^m}$ denotes the projection into H_2^m. In [65, Theorem 2] Kaltenbacher generalized the results for liner inverse problems [71, 92, 121] to nonlinear problems, where she proved that the dual least squares method is, under additional assumptions, a regularization method whenever the discretization level m, and thus H_2^m, is determined by the discrepancy principle

$$m_* = m_*(\delta) = \min\{m \in \mathbb{N} : \ \|F(u^{m,\delta}) - y^\delta\|_{H_2} \leqslant \tau\delta\}, \qquad \tau > 1, \tag{3.25}$$

where $u^{m,\delta}$ denotes the solution to (3.24), that is,

$$u^{m_*(\delta),\delta} \to u^\dagger, \qquad \delta \to 0,$$

for the noise-free solution $u^\dagger$ to exact data $y^\dagger$.

Projection in preimage space or also called the least squares method for (3.21) consists of discretizing the preimage space H_1 by finite dimensional subspaces $H_1^m \subset H_1$ and then solve (3.21) for $u \in H_1^m$. If we choose a basis $\{\varphi_1, \ldots, \varphi_{K_m}\}$ for H_2^m we thus have to solve

$$F(\sum_{k=1}^{K_m} u_k \varphi_k) = y^\delta$$

for $\mathbf{u} = (u_1, \ldots, u_{K_m})$ and set

$$u^{m,\delta} = u^{m,\delta}[\mathbf{u}] = \sum_{k=1}^{K_m} u_k \varphi_k.$$

This may be done by solving the minimization problem

$$\min_{u \in H_1^m} \frac{1}{2}\|F(u) - y^\delta\|_{H_2}^m = \min_{\mathbf{u} \in \mathbb{R}^{K_m}} \frac{1}{2}\|F(u[\mathbf{u}]) - y^\delta\|_{H_2}^m. \tag{3.26}$$

A generalization for the results of linear problems has been carried out by Kaltenbacher and Offtermatt [68, Theorem 3.4], where the discrepancy principle (3.25) is again used as the a priori parameter choice rule. Note that here, compared to (3.23), we only need

$$\|(I - \Pi_{H_1^m})u^\dagger\|_{H_1} \to 0, \qquad m \to \infty. \tag{3.27}$$

If we consider H_1^m being the finite element space V^{h_m}, c.f. Section 2.2.2, with mesh size $h_m = Ch^m$, $C > 0$ and $h > 0$ sufficiently small, H_1^m fulfill property (3.27). Clearly, the dimension of the spaces would increase in every iteration, thus the computational cost for solving (3.26) increases. However, one could tackle this problem by an adaptive grid refinement to not increase the finite element spaces too much, but also obtain accuracy and regularization [86–88]. An approach to satisfy (3.27) is to refine and coarsen the grid in each step to use little degrees of freedom, and thus have less computational cost, without loosing any accuracy [67].

3.2 Solving Inverse Medium Problems: The Adjoint Method

Consider a physical state formulated by a well-posed mathematical model given by partial differential equations (PDEs) with appropriate boundary conditions and initial conditions. This can be formulated abstractly as

$$A[u] : H_2 \to H_3, \qquad A[u]y = f, \tag{3.28}$$

where the operator $A[u]$ depends on the *medium* $u \in H_1$, for H_1, H_2, H_3 Hilbert spaces. The so-called *forward problem* now consists in solving (3.28) for y, given the source f and medium u. The inverse medium problem, on the other hand, is now the task of determining the cause u of the known behavior y, induced by the known action f. Thus, we have given data y and f and want to find the unknown u. The given data y is usually obtained by some measuring device and thus only a perturbed version of it is known. If we denote the exact, yet unknown, medium by $u^\dagger$ and the exact, but usually not available, data by $y^\dagger$, we denote the perturbed/noised given data by y^δ with known noise $\delta \geqslant 00$,

$$\|y^\dagger - y^\delta\|_{H_2} \leqslant \delta.$$

Thus, we can not hope to find the exact medium with given perturbed data. We only wish to find an approximate medium $u^{\dagger,\delta}$, satisfying $F(u^{\dagger,\delta}) = y^\delta$, of the exact unknown solution $u^\dagger$ that causes the exact, but unknown data $y^\dagger$.

Finding $u^{\dagger,\delta}$ can now be achieved by solving the constrained minimization problem

$$\begin{aligned} \min_{u,y} \quad & \frac{1}{2}\|y - y^\delta\|_{H_2}^2 \\ \text{s.t.} \quad & A[u]y - f = 0. \end{aligned} \tag{3.29}$$

This constrained optimization problem can be solved by two established standard approaches: minimizing the Lagrange functional or minimizing the reduced misfit.

The Lagrange approach [18, 64], or also called the *full-space* or *all-at-once* approach, eliminates the constraints by multiplying them with the Lagrange multiplier $\lambda \in H_3$ and then adding it to the misfit. Hence, the Lagrange functional is given by

$$L^\delta(u, y, \lambda) = \frac{1}{2}\|y - y^\delta\|_{H_2}^2 + (\lambda, A[u]y - f)_{H_3}$$

and we minimize with respect to $(u, y, \lambda) \in (H_1 \times H_2 \times H_3)$,

$$\min_{u,y,\lambda} L^\delta(u, y, \lambda).$$

Doing this, we obtain the Karush-Kuhn-Tucker (KKT) point $(u^{\dagger,\delta}, y^{\dagger,\delta}, \lambda^{\dagger,\delta})$ minimizing L^δ and thus, obtain the cause $u^{\dagger,\delta}$ for observed data y^δ. As the name full-space approach suggests, we have to save all three control variables which may lead to large memory consumption when minimizing L^δ numerically. To reduce the computational cost, we can use the *reduced-space* approach [51].

The reduced-space approach tries to set every variable in dependence of the unknown u. To acquire this, we rewrite the constraint $A[u]y = f$ as the parameter-to-field map $y = y[u] = A[u]^{-1}f$. Thus, we formally eliminated the constraint in (3.29) to obtain the *reduced misfit*

$$J^\delta(u) = \frac{1}{2}\|y[u] - y^\delta\|_{H_2}^2 = \frac{1}{2}\|F(u) - y^\delta\|_{H_2}^2, \tag{3.30}$$

where $F : H_1 \to H_2$, $F(u) = y[u]$ is the forward operator (1.1). Now, we only have to solve

$$\min_u J^\delta(u) \tag{3.31}$$

for one variable u, in contrast to the three control variables needed in the full-space Ansatz, hence reducing the memory cost.

To solve (3.31) we want to use the BFGS, as well as the L-BFGS Algorithm, explained in Sections 2.4 and 3.1.4. To do so, we need to compute the gradient of J^δ which may be done in two standard approaches, *discretize-then-optimize* and *optimize-then-discretize*. As the names suggest, the discretize-then-optimize approach first discretizes the misfit J^δ (3.30), e.g. by finite elements introduced in Section 2.2.2. This results in a finite dimensional least squares problem, where the gradient then has to be computed in each unit direction $\mathbf{e}_j$. However, we will focus on the optimize-then-discretize approach, where we compute the derivative $(J^\delta)'(u; v)$ in $u \in H_1$ with respect to the direction $v \in H_1$ first and discretize afterwards.

3.2.1 Elliptic Inverse Problem

Consider $H_1 = H_2 = H_3 = L^2(\Omega)$ and the misfit $J^\delta : L^2(\Omega) \to \mathbb{R}$ given by

$$J^\delta(u) = \frac{1}{2}\int_\Omega |y[u] - y^\delta|^2,$$

thus, we have available data y^δ in the whole domain Ω. To illustrate the computation of the gradient of J^δ, we consider, as an example, the elliptic inverse problem with forward problem given by (1.4),

$$\begin{aligned} -\nabla \cdot (u\nabla y) &= f \qquad && \text{in } \Omega, \\ y &= 0 && \text{on } \partial\Omega, \end{aligned}$$

and its corresponding weak formulation

$$\int_\Omega u\nabla y \cdot \nabla z = \int_\Omega fz \qquad \forall z \in H_0^1(\Omega). \tag{3.32}$$

Taking the derivative of J^δ in u in direction v yields

$$(J^\delta)'(u;v) = \int_\Omega y'[u;v](y[u] - y^\delta), \tag{3.33}$$

where $y'[u;v]$ denotes the derivative of y in u with respect to v. To calculate $y'[u;v]$ we first take the derivative of the weak form (3.32), where we use the chain rule to obtain

$$\int_\Omega v\nabla y[u] \cdot \nabla z + \int_\Omega u\nabla y'[u;v] \cdot \nabla z = 0 \qquad \forall z \in H_0^1,$$

since the right side of (3.32) does not depend on u. Then, for cosmetic reasons, we rewrite this as

$$\int_\Omega u\nabla y'[u;v] \cdot \nabla z = -\int_\Omega v\nabla y[u] \cdot \nabla z. \tag{3.34}$$

A naive idea would be to solve this problem for all directions v to obtain $y'[u;v]$, and thus $(J^\delta)'(u;v)$. However, this would result in solving multiple, if not millions, of PDEs. To avoid this, we define the auxiliary problem, the *adjoint problem*, by

$$\int_\Omega u\nabla z \cdot \nabla y^* = \int_\Omega z(y[u] - y^\delta), \qquad \forall z \in H_0^1, \tag{3.35}$$

with solution $y^* \in H_0^1$, thus having zero boundary. Since (3.34) also holds for $z = y^*$ and (3.35) holds for $z = y'[u;v]$, both imply

$$\begin{aligned} \int_\Omega u\nabla y'[u;v] \cdot \nabla y^* &= -\int_\Omega v\nabla y \cdot \nabla y^*, \\ \int_\Omega u\nabla y'[u;v] \cdot \nabla y^* &= \int_\Omega y'[u;v](y[u] - y^\delta). \end{aligned}$$

Combining the above equations with (3.33) yields the derivative

$$(J^\delta)'(u;v) = -\int_\Omega v\nabla y \cdot \nabla y^*, \tag{3.36}$$

where y is the solution of the forward problem and y^* is the solution to the adjoint problem. Thus, the three steps to compute the gradient are:

(i) Compute the solution y to the forward problem (3.32).

(ii) Compute the solution y^* to the adjoint problem (3.35).

(iii) Compute the derivative $(J^\delta)'(u;v)$ via (3.36) for every direction v with an appropriate quadrature rule. Note that we can precompute $\nabla y \cdot \nabla y^*$ on the quadrature nodes once and reuse it. Afterwards, we obtain the full gradient $\nabla J^\delta(u)$ by (2.1).

Extension to Mixed Boundary Conditions

Now, we consider the elliptic problem together with Dirichlet, Neumann, and Robin boundary conditions

$$\begin{aligned} -\nabla \cdot (u\nabla y) &= f && \text{in } \Omega, \\ y &= 0 && \text{on } \Gamma_D, \\ \tfrac{\partial y}{\partial n} &= g && \text{on } \Gamma_N, \\ u\tfrac{\partial y}{\partial n} + y &= 0 && \text{on } \Gamma_R, \end{aligned} \tag{3.37}$$

where $\partial\Omega = \Gamma_D \cup \Gamma_N \cup \Gamma_R$ and its weak form given by

$$\int_\Omega u\nabla y \cdot \nabla z + \int_{\Gamma_R} yz = \int_\Omega fz + \int_{\Gamma_N} ugz$$

for all $z \in H^1_D(\Omega)$, where $H^1_D(\Omega)$ corresponds to all functions in $H^1(\Omega)$ with zero boundary on Γ_D. Analogously to the argumentation above, we obtain the derivative of the weak form

$$\int_\Omega u\nabla y'[u;v] \cdot \nabla z + \int_{\Gamma_R} y'[u;v]z = -\int_\Omega v\nabla y[u] \cdot \nabla z + \int_{\Gamma_N} vgz. \tag{3.38}$$

Next, we define the adjoint problem in its weak form as

$$\int_\Omega u\nabla z \cdot \nabla y^* + \int_{\Gamma_R} zy^* = \int_\Omega z(y[u] - y^\delta) \qquad \forall z \in H^1_G(\Omega). \tag{3.39}$$

If we take $z = y^*$ in (3.38) and $z = y'[u; v]$ in (3.39) this yields the representation of the derivative as

$$(J^\delta)'(u; v) = -\int_\Omega v\nabla y \cdot \nabla y^* + \int_{\Gamma_N} vgy^*,$$

where y and y^* are the solutions to the forward and adjoint problem, respectively.

Note that the strong formulation corresponding to the weak form of the adjoint problem (3.39) is given by

$$\begin{aligned} -\nabla \cdot (u\nabla y^*) &= y[u] - y^\delta && \text{in } \Omega, \\ y^* &= 0 && \text{on } \Gamma_D, \\ \tfrac{\partial y^*}{\partial n} &= 0 && \text{on } \Gamma_N, \\ u\tfrac{\partial y^*}{\partial n} + y^* &= 0 && \text{on } \Gamma_R. \end{aligned}$$

Thus, we obtain homogeneous Neumann boundary conditions, in comparison to non-homogeneous conditions to the forward problem (3.37).

Extension to Partially Available Data

Now that we understand the concept of the adjoint method, we will consider data y^δ that is not available everywhere in Ω, but only on a subset $B \subset \Omega$ or on (parts of the) boundary $\Gamma_B \subset \partial\Omega$.

We first consider the case where we only know data on a subset $B \subset \Omega$. Thus the misfit is given by

$$J^\delta(u) = \frac{1}{2}\int_B |y[u] - y^\delta|^2 = \frac{1}{2}\int_\Omega |y[u] - y^\delta|^2 \chi_B,$$

where χ_B is the indicator/characteristic function of B. Considering χ_B in the analysis above, this only changes the right side of the adjoint problem, c.f. (3.35) and (3.39), to

$$\int_B z(y[u] - y^\delta) = \int_\Omega z(y[u] - y^\delta)\chi_B.$$

However, if we consider given data on the boundary $\Gamma_B \subset \partial\Omega$, where of course we assume that $\Gamma_B \cap \Gamma_D = \emptyset$, we can not simply use the indicator function χ_{Γ_B} since Γ_B is a null-set with respect to Ω and thus, the integral of χ_{Γ_B} over Ω vanishes. But since the misfit with this known data is

$$J^\delta(u) = \frac{1}{2}\int_{\Gamma_B} |y[u] - y^\delta|^2 \tag{3.40}$$

and we define the adjoint problem in its weak formulation, we have to simply consider the right side of the adjoint problem as the integral over the boundary $\Gamma_B \subset \partial\Omega$:

$$\int_{\Gamma_B} z(y[u] - y^\delta).$$

If we apply this to the adjoint problem (3.39), we obtain

$$\int_\Omega u\nabla z \cdot \nabla y^* + \int_{\Gamma_R} zy^* = \int_{\Gamma_B} z(y[u] - y^\delta) \qquad \forall z \in H^1_D(\Omega).$$

Due to this, the strong formulation admits a slightly different form

$$\begin{aligned}
-\nabla \cdot (u\nabla y^*) &= 0 && \text{in } \Omega,\\
y^* &= 0 && \text{on } \Gamma_D,\\
\tfrac{\partial y^*}{\partial n} &= 0 && \text{on } \Gamma_N \setminus \Gamma_B,\\
u\tfrac{\partial y^*}{\partial n} &= y[u] - y^\delta && \text{on } \Gamma_N \cap \Gamma_B,\\
u\tfrac{\partial y^*}{\partial n} + y^* &= 0 && \text{on } \Gamma_R \setminus \Gamma_B,\\
u\tfrac{\partial y^*}{\partial n} + y^* &= y[u] - y^\delta && \text{on } \Gamma_R \cap \Gamma_B.
\end{aligned} \tag{3.41}$$

If we introduce δ_{Γ_B}, the delta distribution with support on $\Gamma_B \subset \partial\Omega$ c.f. [37], such that

$$\int_\Omega f(\mathbf{x})\delta_{\Gamma_B}(\mathbf{x})\, d(\mathbf{x}) = \int_{\Gamma_B} f(\mathbf{x}(x))\, ds$$

holds, we can write the strong formulation (3.41) more cleaner as

$$\begin{aligned}
-\nabla \cdot (u\nabla y^*) &= (y[u] - y^\delta)\delta_{\Gamma_B} && \text{in } \Omega,\\
y^* &= 0 && \text{on } \Gamma_D,\\
\tfrac{\partial y^*}{\partial n} &= 0 && \text{on } \Gamma_N,\\
u\tfrac{\partial y^*}{\partial n} + y^* &= 0 && \text{on } \Gamma_R,
\end{aligned}$$

understood in a distributional sense, where we can use δ_{Γ_B} to express the misfit with boundary measures (3.40), $\Gamma_B \subset \partial\Omega$, as

$$J^\delta(u) = \frac{1}{2}\int_\Omega |y[u] - y^\delta|^2 \delta_{\Gamma_B}.$$

3.2.2 Inverse Scattering Problem for the Wave Equation

Now we dedicate our attention to the inverse scattering problem for the wave equation in time domain from Section 1.2.2,

$$\begin{aligned} \frac{\partial^2}{\partial t^2} y(\mathbf{x},t) - \nabla \cdot (u(\mathbf{x}) \nabla y(\mathbf{x},t)) &= f(\mathbf{x},t), && \mathbf{x} \in \Omega,\ t \in (0,T), \\ y(\mathbf{x},0) = \tfrac{\partial}{\partial t} y(\mathbf{x},0) &= 0, && \mathbf{x} \in \Omega, \\ \tfrac{\partial}{\partial t} y(\mathbf{x},t) + \sqrt{u(\mathbf{x})} \tfrac{\partial}{\partial n} y(\mathbf{x},t) &= 0, && \mathbf{x} \in \partial\Omega,\ t \in (0,T), \end{aligned} \tag{3.42}$$

for a bounded spatial domain $\Omega \subset \mathbb{R}^d$, $d \geqslant 1$ and time domain $(0,T)$, $T > 0$, where we impose zero initial conditions and first order absorbing boundary conditions. Here, u denotes the squared wave speed and f the known source. Since we only consider given data at the boundary, yet for all times $t \in (0,T)$ the misfit is given by

$$J^\delta(u) = \frac{1}{2} \int_0^T \int_{\partial\Omega} |y[u] - y^\delta|^2 = \frac{1}{2} \int_0^T \int_\Omega |y[u] - y^\delta|^2 \delta_{\partial\Omega},$$

where $\delta_{\partial\Omega}$ corresponds the delta distribution as introduced before.

Since we want to omit the lengthy and technical derivation of the adjoint problem we simply refer to the excellent pedagogical article by Givoli [42, Section 5 & 7.3]. Following these steps, the derivative of the misfit in u in direction v is

$$(J^\delta)'(u;v) = -\int_0^T \int_\Omega u(\mathbf{x}) \nabla y(\mathbf{x},t) \cdot \nabla y^*(\mathbf{x},t)\, d\mathbf{x}\, dt, \tag{3.43}$$

where y solves the forward problem (3.42) and y^* corresponds to the solution to the adjoint problem

$$\begin{aligned} \frac{\partial^2}{\partial t^2} y^* - \nabla \cdot (u \nabla y^*) &= (y[u] - y^\delta)\delta_{\partial\Omega} && \text{in } \Omega \times (0,T), \\ y^* = \tfrac{\partial}{\partial t} y^* &= 0 && \text{in } \Omega \times \{T\}, \\ \tfrac{\partial}{\partial t} y^* - \sqrt{u(\mathbf{x})} \tfrac{\partial}{\partial n} y^* &= 0 && \text{on } \partial\Omega \times (0,T). \end{aligned} \tag{3.44}$$

This would require stepping backward in time to solve it. If we shift the time via $t \mapsto T - t$ and introduce $\hat{y}^*(t) = y^*(T-t)$, and set $\hat{y}, \hat{y}^\delta$ analogously, (3.44) yields the adjoint problem forward in time,

$$\begin{aligned} \frac{\partial^2}{\partial t^2} \hat{y}^* - \nabla \cdot (u) \nabla \hat{y}^*) &= (\hat{y}[u] - \hat{y}^\delta)\delta_{\partial\Omega} && \text{in } \Omega \times (0,T), \\ \hat{y}^* = \tfrac{\partial}{\partial t} \hat{y}^* &= 0 && \text{in } \Omega \times \{0\}, \\ \tfrac{\partial}{\partial t} \hat{y}^* + \sqrt{u(\mathbf{x})} \tfrac{\partial}{\partial n} \hat{y}^* &= 0 && \text{on } \partial\Omega \times (0,T). \end{aligned}$$

Thus, to compute the adjoint solution y^*, we can reuse the algorithm to compute the forward problem (3.42) with right side $(\hat{y}[u] - \hat{y}^\delta)\delta_{\partial\Omega}$. This yields the shifted adjoint solution $\hat{y}^*$ and thus, the adjoint solution y^* by transforming $\hat{y}^*$ back in time.

We now want to comment on how to compute the gradient (3.43). Since v is time independent, we can rewrite (3.43) equivalently to

$$(J^\delta)'(u; v) = \int_\Omega v \int_0^T \nabla y \cdot \nabla y^*$$

and precompute $\int_0^T \nabla y \cdot \nabla y^*$ on the quadrature nodes. This allows us to reuse the time integration for the spatial integration for every direction v, thus obtaining the full gradient $\nabla J^\delta(u)$.

Part II

The Adaptive Spectral Decomposition

Chapter 4

Analysis of the Adaptive Spectral Decomposition

In this chapter we consider, for given media $u \in W^{1,\infty}(\Omega)$, with $\Omega \subset \mathbb{R}^d$, the expansion

$$u = \varphi_0 + \sum_{k=1}^{\infty} \beta_k \varphi_k$$

into the eigenfunctions $\{\varphi_k\}_{k\geqslant 1}$ of an ε-dependent elliptic operator $L_\varepsilon[u]$, satisfying

$$L_\varepsilon[u]\varphi_k = \lambda_k \varphi_k \quad \text{in } \Omega, \qquad \varphi_k = 0 \quad \text{on } \partial\Omega, \tag{4.1}$$

for corresponding non-decreasing eigenvalues $\lambda_k \in \mathbb{R}$, and the solution φ_0 of the boundary value problem

$$L_\varepsilon[u]\varphi_0 = 0 \quad \text{in } \Omega, \qquad \varphi_0 = u \quad \text{on } \partial\Omega, \tag{4.2}$$

capturing information of u on the boundary $\partial\Omega$. Clearly, the operator $L_\varepsilon[u]$ is crucial to achieve a good approximation

$$u \approx \varphi_0 + \sum_{k=1}^{K} \beta_k \varphi_k \tag{4.3}$$

for u by utilizing only the first few K eigenfunctions. Here we solely focus on the *Adaptive Spectral (AS) operator* defined via

$$L_\varepsilon[u]v = -\nabla \cdot (\mu[u]\nabla v), \qquad \mu_\varepsilon[u](\mathbf{x}) = \frac{1}{\sqrt{|\nabla u(\mathbf{x})|^2 + \varepsilon^2}}, \tag{4.4}$$

where $\varepsilon > 0$ is a small parameter to avoid devision by zero.

Usually, we are interested in decomposing piecewise constant functions u into the eigenfunctions of the AS operator (4.4) with as few eigenfunctions $\{\varphi_k\}_{k\geqslant 1}$ as possible. However, due to the discontinuity of u we can not apply (4.4) directly since $\mu_\varepsilon[u]$ depends on ∇u. To address this, we first approximate u by a more regular function u_h such that $L_\varepsilon[u_h]$ is well defined. Subsequently, we compute the first K eigenfunctions φ_k of the AS operator $L_\varepsilon[u_h]$ to obtain the (truncated) AS decomposition of u as given by (4.3).

Next, we follow [10, 11] to prove properties of the eigenfunctions and φ_0 obtained via (4.1) – (4.2) and estimates of the truncation error of u in relation to its (truncated) AS decomposition. In contrast to [10, 11], we will only consider $u_h \in V^h$ to be the standard H^1-conforming $\mathcal{P}^r$-FE interpolant of u, c.f. Section 2.2.2. However, the theory presented can be extended to encompass more general $u_h \in \mathcal{V}^h$ for a closed subspace $\mathcal{V}^h \subset H^1(\Omega)$, also referred to as *admissible approximations* in [10].

4.1 Notation and Definitions

4.1.1 Piecewise Constant Medium

We consider a piecewise constant function $u : \Omega \to \mathbb{R}$, where $\Omega \subset \mathbb{R}^d$, with $d \geqslant 2$, being a bounded Lipschitz domain. Additionally, we further assume that u admits the form

$$u(\mathbf{x}) = u^0(\mathbf{x}) + \tilde{u}(\mathbf{x}), \qquad \mathbf{x} \in \Omega, \tag{4.5}$$

where we refer to u^0 as the *background* and to $\tilde{u}$ as the *interior inclusion* given by

$$u^0 = \sum_{m=1}^{M} \omega_m \chi_{\Omega^m}, \quad \omega_m \in \mathbb{R}, \qquad \tilde{u} = \sum_{k=1}^{K} \alpha_k \chi_{A^k}, \quad \alpha_k \in \mathbb{R} \setminus \{0\}, \tag{4.6}$$

with χ_W the characteristic function of a set $W \subset \mathbb{R}^d$. Thus, we want to distinguish the sets Ω^m that are connected to the boundary $\partial\Omega$ of Ω such that

$$\overline{\Omega} = \bigcup_{m=1}^{M} \overline{\Omega^m} \qquad \text{and} \qquad \partial\Omega^m \cup \partial\Omega \text{ is open},$$

from the sets A^k. For each $k = 1, \ldots, K$, the sets A^k are Lipschitz domains with mutually disjoint boundaries such that ∂A^k is connected and $A^k \subset\subset \Omega^m$ for some $m = 1, \ldots, M$. A possible configuration of the sets Ω^m and A^k in two dimensions is illustrated in Figure 4.1.

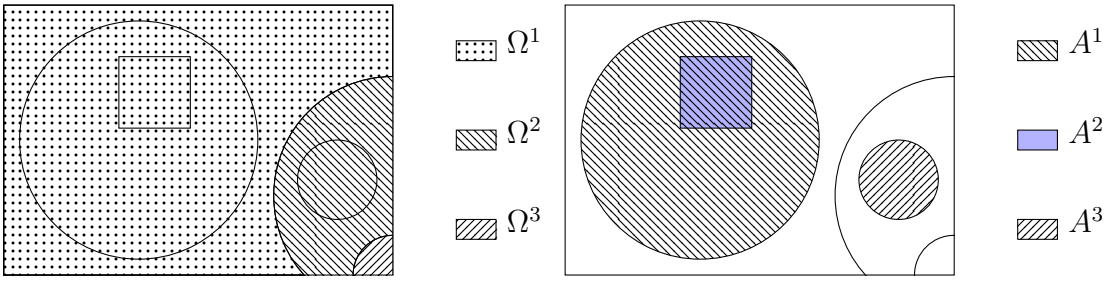

Fig. 4.1: Background and interior inclusions: A typical configuration in two dimensions of a piecewise constant function of the form (4.5) decomposed into the sets Ω^m, $m = 1, 2, 3$, to cover Ω and the sets A^k, $k = 1, 2, 3$, representing the interior inclusions, such that decomposition (4.6) holds.

Next, we define M_h as the open h-wide neighbourhood around all interfaces by

$$\begin{aligned} M_h = \tilde{U}_h \cup U_h, \qquad \tilde{U}_h &= \bigcup_{k=1}^{K} \{\mathbf{x} \in \Omega : \ \operatorname{dist}(\mathbf{x}, \partial A^k) < h\}, \\ U_h &= \bigcup_{m=1}^{M} \{\mathbf{x} \in \Omega : \ \operatorname{dist}(\mathbf{x}, \partial \Omega^m \cap \Omega) < h\}, \end{aligned} \tag{4.7}$$

and its open complement by

$$D_h = \Omega \setminus \overline{M_h}. \tag{4.8}$$

Furthermore, we want to partition D_h and M_h into their connected components. Let B_h^k be the connected components of D_h, given via

$$B_h^k = B^k \cap D_h, \qquad B^k = A^k \setminus \bigcup_{i>k} \overline{A^i}, \quad k = 1, \dots, K, \tag{4.9}$$

and E_h^m as the connected components of the outside inclusions given by

$$E_h^m = E^m \cap D_h, \qquad E^m = \Omega^m \setminus \bigcup_{k=1}^{K} \overline{A^k}, \quad m = 1, \dots, M, \tag{4.10}$$

where we assume that $h > 0$ is sufficiently small such that each B_h^k and E_h^m are, indeed, connected. Thus, we may express D_h as the disjoint union

$$D_h = E_h \cup \bigcup_{k=1}^{K} B_h^k, \qquad E_h = \bigcup_{m=1}^{M} E_h^m. \tag{4.11}$$

A possible configuration of the sets M_h, E^m, $m = 1, \dots, M$, and B^k, $k = 1, \dots, K$ is depicted in Figure 4.2.

Next, we will introduce the *Adaptive Spectral Decomposition* (AS decomposition), the AS operator $L_\varepsilon[v]$ as in (4.4), and a more general form of the weight function $\mu_\varepsilon[v]$.

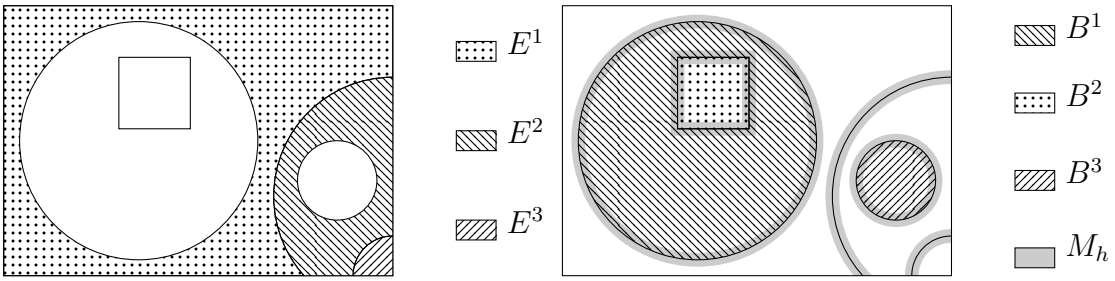

Fig. 4.2: Decomposition of Ω: A typical configuration in two dimension of the domain Ω as displayed in Figure 4.1: Decomposition of the sets D_h and M_h from (4.7) and (4.8), respectively, into its connected components B^k and E^m, $k, m = 1, \dots, 3$, c.f. (4.9) and (4.10).

4.1.2 The Adaptive Spectral Decomposition

The weight function

Let $\varepsilon > 0$ and consider $v \in H^1(\Omega)$ such that $\nabla v \in L^\infty(\Omega)$. Assume that the *weight function* $\mu_\varepsilon[v]$ explicitly depends on $|\nabla v|$. Thus, it admits the form

$$\mu[v](\mathbf{x}) = \hat{\mu}_\varepsilon(|\nabla v(\mathbf{x})|), \qquad \mathbf{x} \in \Omega, \tag{4.12}$$

where $\hat{\mu}_\varepsilon : [0, \infty) \to \mathbb{R}$ is a non-increasing function that satisfies

$$\hat{\mu}_\varepsilon(0) = {}^1\!/_\varepsilon, \quad 0 < \hat{\mu}_\varepsilon(t), \quad t\hat{\mu}_\varepsilon(t) \leqslant 1, \qquad t \geqslant 0 \tag{4.13}$$

and

$$\exists\, C > 0, \text{ s.t. for every sufficiently large } t,\ C \leqslant t\hat{\mu}_\varepsilon(t). \tag{4.14}$$

From this we immediately deduce that, for almost all $x \in \Omega$,

$$\mu_\varepsilon[v](\mathbf{x})|\nabla v(\mathbf{x})| < 1, \quad \text{and} \quad 0 < \hat{\mu}_\varepsilon(\|\nabla v\|_{L^\infty(\Omega)}) \leqslant \mu_\varepsilon[v](\mathbf{x}).$$

In particular, common weight functions that satisfy (4.12) – (4.14) are

$$\mu_\varepsilon[v] = \frac{1}{(|\nabla v|^q + \varepsilon^q)^{1/q}}, \qquad q \geqslant 1, \tag{4.15}$$

$$\mu_\varepsilon[v] = \frac{1}{\max(|\nabla v|, \varepsilon)},$$

$$\mu_\varepsilon[v] = \begin{cases} {}^1\!/_\varepsilon & \text{for } |\nabla v| \leqslant \nu, \\ {}^1\!/_{|\nabla v|} & \text{for } |\nabla v| > \nu, \end{cases} \qquad \nu > 0.$$

The Adaptive Spectral Decomposition

Let $\varepsilon, h > 0$, and consider $V^h \subset H^1(\Omega)$, the standard H^1-conforming $\mathcal{P}^r$-FE subspace and let $V_0^h = V^h \cap H_0^1(\Omega)$. Consider a given piecewise constant function u as in (4.5) – (4.6) and let $u_h \in V^h$ be its standard FE-interpolant on a regular and quasi-uniform mesh $\mathcal{T}_h$, c.f. Section 2.2.2. If we denote the FE-interpolant of χ_{Ω^m} and χ_{A^k} in V^h by

$$\begin{aligned} &\chi_h^{0,m}, && m = 1, \dots M, \\ &\chi_h^k, && k = 1, \dots, K, \end{aligned}$$

respectively, due to [10, Section 2.2 & Proposition 2.2] we obtain the properties:

(i)

$$u_h = u_h^0 + \tilde{u}_h, \qquad u_h^0 \in V^h, \quad \tilde{u}_h \in V_0^h, \tag{4.16}$$

$$u_h^0 = \sum_{m=1}^{M} \omega_m \chi_h^{0,m}, \qquad \tilde{u}_h = \sum_{k=1}^{K} \alpha_k \chi_h^k. \tag{4.17}$$

(ii)

$$u = u_h \qquad \text{a.e. in } D_h.$$

(iii)

$$\lim_{h\to 0} \|\chi_h^{0,m} - \chi_{\Omega^m}\|_{L^2(\Omega)} \to 0, \qquad \lim_{h\to 0} \|\chi_h^k - \chi_{A^k}\|_{L^2(\Omega)} \to 0,$$

for $m = 1, \dots, M$ and $k = 1, \dots, K$, and thus

$$\lim_{h\to 0} \|u_h - u\|_{L^2(\Omega)} \to 0.$$

(iv)

$$\begin{aligned} \|\chi_h^{0,m}\|_{L^1(\Omega)} &\leqslant C, \qquad h\|\chi_h^{0,m}\|_{L^\infty(\Omega)} \leqslant C, && m = 1, \dots, M, \\ \|\chi_h^k\|_{L^1(\Omega)} &\leqslant C, \qquad h\|\chi_h^k\|_{L^\infty(\Omega)} \leqslant C, && k = 1, \dots, K. \end{aligned} \tag{4.18}$$

for generic constants $C > 0$ independent of h.

(v)

$$u = u_h = u_h^0, \quad \tilde{u} = \tilde{u}_h = 0 \qquad \text{a.e. in } E_h.$$

(vi)

$$\nabla u_h \in L^\infty(\Omega), \qquad \operatorname{supp}(\nabla u_h^0) \subset \overline{U_h}, \qquad \operatorname{supp}(\nabla \tilde{u}_h) \subset \overline{\tilde{U}_h}, \tag{4.19}$$

where U_h and $\tilde{U}_h$ are given according to (4.7).

(vii) For $m = 1, \ldots, M$, $k = 1, \ldots, K$

$$\nabla u_h = 0 \quad \text{a.e. in } B_h^k \text{ and } E_h^m. \tag{4.20}$$

Thus, the operator $L_\varepsilon[u_h]$ defined by

$$L_\varepsilon[u]v = -\nabla \cdot (\mu[u]\nabla v) \tag{4.21}$$

is well defined for small $\varepsilon > 0$ and, for sufficiently small $h > 0$, even uniformly elliptic in Ω [10, Section 3.2]. Hence, the eigenfunctions $\{\varphi_k\}_{k\geqslant 1}$ of $L_\varepsilon[u_h]$, sorted according to their positive eigenvalues $\lambda_1 \leqslant \lambda_2 \leqslant \ldots \leqslant \lambda_k \leqslant \ldots$, form an L^2-orthonormal basis of V_0^h. Since u, and thus u_h, might have non-zero boundary u_h^0, we define $\varphi_0 \in V^h$ as the lifting of the boundary of u_h into Ω. More precisely, $\varphi_0 \in V^h$ satisfies

$$\begin{aligned} L_\varepsilon[u_h]\varphi_0 &= 0 \qquad && \text{in } \Omega, \\ \varphi_0 &= u_h && \text{on } \partial\Omega, \end{aligned} \tag{4.22}$$

and for $k \geqslant 1$, $\varphi_k \in V_0^h$, let $\varphi_k \neq 0$ satisfy the eigenvalue problem

$$\begin{aligned} L_\varepsilon[u_h]\varphi_k &= \lambda_k\varphi_k \qquad && \text{in } \Omega, \\ \varphi_k &= 0 && \text{on } \partial\Omega. \end{aligned} \tag{4.23}$$

Clearly, (4.22) and (4.23) are understood in a weak sense with respect to the bilinear form

$$B_{\varepsilon,h}[v, w] = (\mu_\varepsilon[u_h]\nabla v, \nabla w)_{L^2(\Omega)}$$

in V^h, thus their Galerkin FE formulations are: Find $\varphi_0 \in \{v \in V^h,\ v = u_h \text{ on } \partial\Omega\}$ and $\varphi_k \in V_0^h$ such that

$$\begin{aligned} B_{\varepsilon,h}[\varphi_0, \varphi] &= 0 && \forall \varphi \in V^h, \\ B_{\varepsilon,h}[\varphi_k, \varphi] &= \lambda_k(\varphi_k, \varphi) && \forall \varphi \in V_0^h. \end{aligned} \tag{4.24}$$

Note that by (4.13) and (4.20) we have

$$\mu_\varepsilon[u_h] = {}^1\!/_\varepsilon \qquad \text{a.e. in } D_h,$$

from which we conclude that

$$\|\nabla\varphi\|^2_{L^2(D_h)} \leqslant \varepsilon B_{\varepsilon,h}[\varphi,\varphi], \qquad \forall\varphi \in H^1(\Omega). \tag{4.25}$$

Next, we define the Adaptive Spectral (AS) space $\Phi^K \subset L^2(\Omega)$ as the span of the first K eigenfunctions $\{\varphi_k\}_{k=1}^K$,

$$\Phi^K = \operatorname{span}\{\varphi_1, \ldots, \varphi_K\},$$

and denote by $\Pi_K[u_h]$ the standard L^2-orthogonal projection onto Φ^K, given by

$$\Pi_K[u_h] : L^2(\Omega) \to \Phi^K, \quad (v - \Pi_K[u_h]v, \varphi)_{L^2(\Omega)} = 0, \qquad \forall\varphi \in \Phi^K, \tag{4.26}$$

as well as the L^2-orthogonal projection into $\varphi_0 + \Phi^K$ by

$$Q_K[u_h](v) = \varphi_0 + \Pi_K[u_h](v - \varphi_0). \tag{4.27}$$

Remark 1. *Since $L_\varepsilon[u_h]$ depends on ε and u_h, it also indirectly depends on h and u. Consequently, the eigenpairs $\{\lambda_k, \varphi_k\}_{k\geqslant 1}$, the AS space Φ^K, and the projections $\Pi_K[u_h]$ and $Q_K[u_h]$ also depend on u, h, and ε. For ease of notation, we will not always denote this dependency explicitly.*

Now we can introduce the *Adaptive Spectral Decomposition* (AS decomposition): Given u piecewise constant function with K (interior) inclusions of the form (4.5) – (4.6),

$$\begin{aligned} u(\mathbf{x}) &= u^0(\mathbf{x}) + \tilde{u}(\mathbf{x}), && \mathbf{x} \in \Omega, \\ u^0 &= \sum_{m=1}^{M} \omega_m \chi_{\Omega^m}, && \omega_m \in \mathbb{R}, \\ \tilde{u} &= \sum_{k=1}^{K} \alpha_k \chi_{A^k}, && \alpha_k \in \mathbb{R} \setminus \{0\}, \end{aligned}$$

we compute $u_h \in V^h$, solve the boundary value problem (4.22) for $\varphi_0 \in V^h$, and solve the eigenvalue problem (4.23) to obtain the first K eigenfunctions $\{\varphi_k\}_{k=1}^K \subset V_0^h$. Next, we can project every function $v \in u + X^K$, where

$$X^K = \operatorname{span}\{\chi_{A^k}\}_{k=1}^K = \operatorname{span}\{\chi_{B^k}\}_{k=1}^K, \tag{4.28}$$

on $\varphi_0 + \Phi^K$ using (4.27),

$$Q_K[u_h](v) = \varphi_0 + \Pi_K[u_h](v - \varphi_0).$$

Then $Q_K[u_h](v)$ is the AS decomposition of v (into $\varphi_0 + \Phi^K$). Note that if u has zero boundary, i.e. $u = \tilde{u}$, (4.22) immediately implies that $\varphi_0 = 0$, and thus $Q_K[u_h] = \Pi_K[u_h]$.

Remark 2. *In principle, we do not require u to be piecewise constant to perform the AS decomposition. It suffices to assume that $u : \Omega \to \mathbb{R}$ such that there exists the H^1-conforming FE-interpolant $u_h \in V^h$ of u and that the projection $\Pi_K[u_h]u$ is well defined for any $K \geqslant 1$.*

To illustrate the AS decomposition, we consider the piecewise constant function $u : \Omega \subset \mathbb{R}^2 \to \mathbb{R}$ given as in Figure 4.3 (a). Hence, u admits the form $u = u_0 + \tilde{u}$, see (4.5), where u_0 and $\tilde{u}$ are illustrated in Figures 4.4 (a) and (b), respectively. The background u_0 and the interior $\tilde{u}$ thus admit the form

$$u^0 = \sum_{m=1}^{M} \omega_m \chi_{\Omega^m}, \quad \omega_m \in \mathbb{R}, \qquad \tilde{u} = \sum_{k=1}^{K} \alpha_k \chi_{A^k}, \quad \alpha_k \in \mathbb{R} \setminus \{0\},$$

for $M = K = 3$, c.f. (4.6), where the sets Ω^m and A^k correspond to the configuration presented in Figure 4.1.

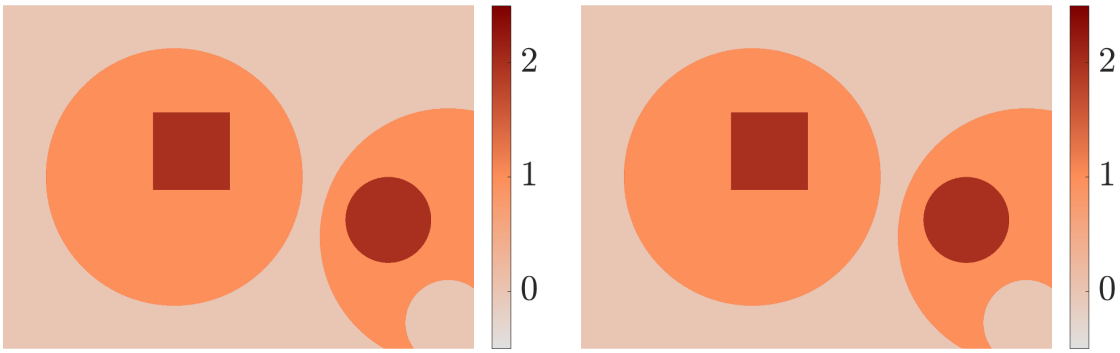

(a) u (or u_h) **(b)** $Q_K[u_h](u)$ for $K = 3$

Fig. 4.3: Adaptive Spectral Decomposition: A piecewise constant function $u : \Omega \to \mathbb{R}$, such that $u = u_0 + \tilde{u}$ as in (4.5) and its AS decomposition $Q_K[u_h](u)$ for $K = 3$.

To obtain the AS decomposition $Q_K[u_h](u)$ of u, we first discretize u by u_h using $\mathcal{P}^1$-FE on a mesh with mesh size $h = 0.05/2^6$. Next, we solve the boundary value and eigenvalue problem (4.22) and (4.23) with $\varepsilon = 10^{-8}$ and the weight function $\mu_\varepsilon[u_h]$ as defined in (4.15) with $q = 2$, to obtain φ_0 and the first $K = 3$ eigenfunctions $\varphi_1, \varphi_2, \varphi_3$, shown in Figures 4.4 (c) – (f). As observed in Figure 4.4, φ_0 captures all the information of u_0, and the first $K = 3$ eigenfunctions $\{\varphi_k\}_{k=1}^K$ capture the interior inclusions of $\tilde{u}$ very well, whereas the subsequent eigenfunctions resemble (local) eigenfunctions of the Laplacian with corresponding eigenvalues that scale with $1/\varepsilon$. Next, we obtain the AS decomposition $Q_K[u_h](u)$ of u for $K = 3$ by projecting it into $\varphi_0 + \Phi^3$, $\Phi^3 = \text{span}\{\varphi_1, \varphi_2, \varphi_3\}$ via (4.27). As seen in Figure 4.3 (b), the AS decomposition $Q_3[u_h]u$ of u is hardly distinguishable from u itself.

Although the illustration in Figure 4.4 may suggest that the first $K = 3$ eigenfunctions are piecewise constant, they are, in fact, only "almost piecewise constant", as we will prove later.

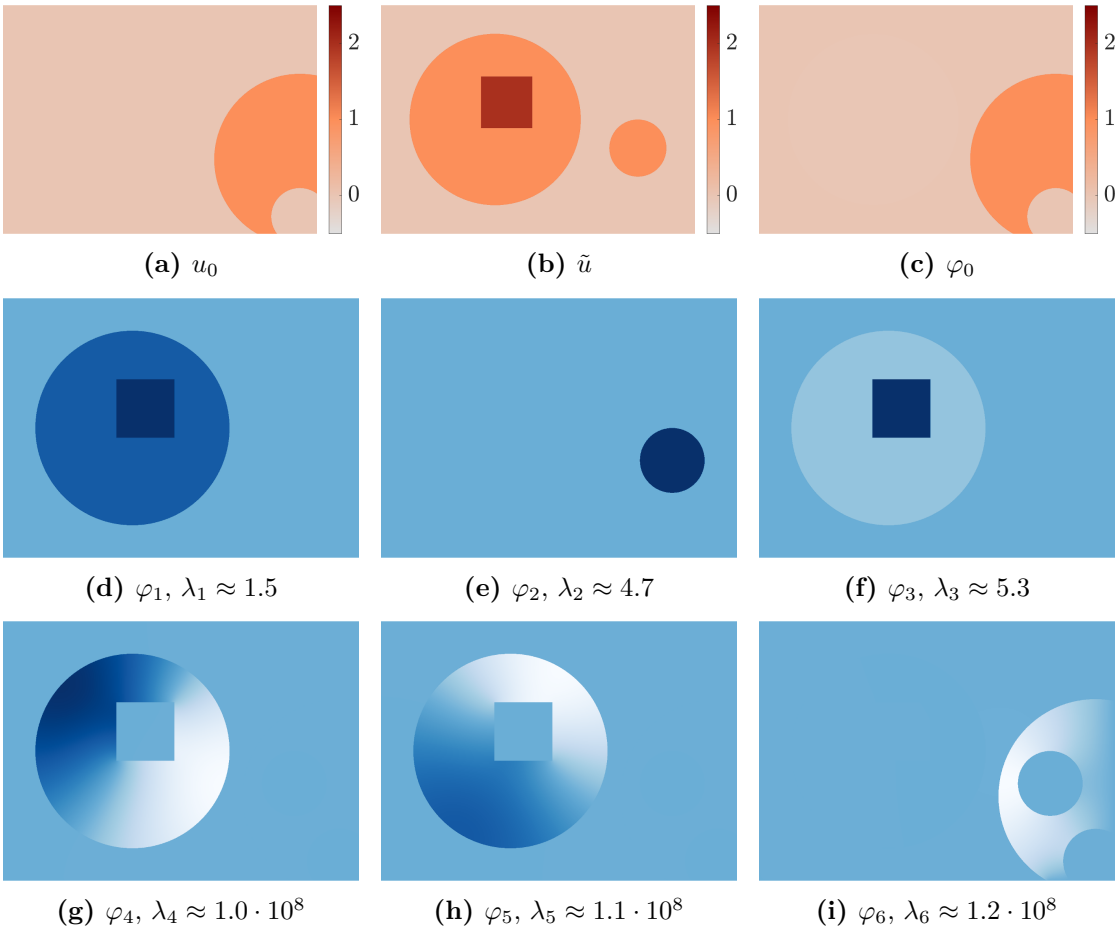

(a) u_0 **(b)** $\tilde{u}$ **(c)** φ_0

(d) φ_1, $\lambda_1 \approx 1.5$ **(e)** φ_2, $\lambda_2 \approx 4.7$ **(f)** φ_3, $\lambda_3 \approx 5.3$

(g) φ_4, $\lambda_4 \approx 1.0 \cdot 10^8$ **(h)** φ_5, $\lambda_5 \approx 1.1 \cdot 10^8$ **(i)** φ_6, $\lambda_6 \approx 1.2 \cdot 10^8$

Fig. 4.4: Eigenfunctions and background: The background u_0 and interior inclusions $\tilde{u}$ to decompose $u = u_0 + \tilde{u}$, as well as the solution φ_0 to the boundary value problem (4.22), and the first few eigenfunctions φ_k satisfying (4.23).

Finally, we remark on the connection between $L_\varepsilon[v]$ and the regularized TV functional (Section 3.1.3)

$$\mathrm{TV}_\varepsilon(v) = \int_\Omega \sqrt{|\nabla v|^2 + \varepsilon^2}, \qquad v \in H_0^1(\Omega),$$

where this connection was first established in [48, Remark 1]. Clearly, the gradient

of TV_ε is given by

$$\nabla \mathrm{TV}_\varepsilon(v) = -\nabla \cdot \left(\frac{\nabla v}{\sqrt{|\nabla v|^2 + \varepsilon^2}} \right) = -\nabla \cdot (\mu_\varepsilon[v] \nabla v) = L_\varepsilon[v] v$$

with $\mu_\varepsilon[v]$ as defined in (4.15) for $q = 2$. Thus $\nabla \mathrm{TV}_\varepsilon$ coincides with the AS operator $L_\varepsilon[v]$. Moreover, for $v \approx u_h$, where u_h is the interpolant (of any suitable) u into V^h, we obtain

$$\begin{aligned} (L_\varepsilon[u_h]v, v)_{L^2(\Omega)} &= \int_\Omega \mu_\varepsilon[u_h] |\nabla v|^2 = \int_\Omega \frac{|\nabla v|^2}{\sqrt{|\nabla u_h|^2 + \varepsilon^2}} \\ &\approx \int_\Omega |\nabla v| = \mathrm{TV}(v). \end{aligned} \tag{4.29}$$

for $\varepsilon > 0$ sufficiently small. Thus $L_\varepsilon[u_h]$ essentially corresponds to the TV-energy. Additionally, the AS decomposition exhibits a remarkable resemblance to the spectral decomposition of the nonlinear TV-functional [21, 41].

4.2 Error Estimates

As observed in the example above, given $u = u^0 + \tilde{u}$ piecewise constant, where $\tilde{u}$ consists of K interior inclusions A^k, $k = 1, \dots, K$, φ_0 given by (4.22) and the first K eigenfunctions $\{\varphi_k\}_{k=1}^K$ given by (4.23) seem to be piecewise constant, c.f. Figure 4.4. However, they are only "almost" piecewise constant (in D_h). To prove this, we follow [10, 11].

For this section, we assume that u is piecewise constant given by (4.5) and (4.6), u_h as in (4.16) and (4.17), X^K given by (4.28), and $\varphi_0, \varphi_1, \dots, \varphi_K$ satisfy (4.24). The positiv constants C, C_1, C_2 are generic constants, independent of ε and h.

Lemma 4.1. *There exists a constant $C > 0$, independent of ε, h, and u, such that for every $\varepsilon, h > 0$ sufficiently small, and $k = 1, \dots, K$, the following inequality holds:*

$$\lambda_k \leqslant \frac{C|\tau|}{\min_j |\alpha_j|}, \qquad \tau = (\tau_k) \in \mathbb{R}^K, \quad \tau_k = \tau_k(h) = \|\chi_h^k\|_{L^1(\Omega)}.$$

Next, we will prove that φ_0 and φ_k, $k = 1, \dots, K$ are, indeed, "almost" piecewise constant when the interior $\tilde{u}$ is comprised of K inclusions.

Theorem 4.2. *Let $u = u_0 + \tilde{u}$ be given by (4.5) such that (4.6),*

$$u^0 = \sum_{m=1}^M \omega_m \chi_{\Omega^m}, \quad \omega_m \in \mathbb{R}, \qquad \tilde{u} = \sum_{k=1}^K \alpha_k \chi_{A^k}, \quad \alpha_k \in \mathbb{R} \setminus \{0\},$$

holds. Let u_h be its FE-interpolant given by (4.16), φ_0 given by (4.22), and $\{\lambda_k, \varphi_k\}_k$ with $k \geqslant 1$ satisfy (4.23), where $\{\lambda_k\}_k$ is non-decreasing and $\{\varphi_k\}_k$ orthonormal in $L^2(\Omega)$. Then, for $\varepsilon, h > 0$ sufficiently small, the following estimates hold:

$$\|\nabla\varphi_0\|^2_{L^2(D_h)} \leqslant C_1 \max_m |\omega_m|\, \varepsilon \tag{4.30}$$

$$\|\nabla\varphi_k\|^2_{L^2(D_h)} \leqslant \frac{C_1}{\min_j |\alpha_j|}\varepsilon, \qquad \lambda_k \leqslant \frac{C_1}{\min_j |\alpha_j|}, \quad k = 1, \ldots, K. \tag{4.31}$$

Proof. We shall first prove assertion (4.30). Since φ_0 minimizes $B_{\varepsilon,h}[v, v]$ in $u_h + V_0^h$, we conclude that $B_{\varepsilon,h}[\varphi_0, \varphi_0] \leqslant B_{\varepsilon,h}[u_h^0, u_h^0]$. Next, (4.19) yields

$$B_{\varepsilon,h}[\varphi_0, \varphi_0] \leqslant B_{\varepsilon,h}[u_h^0, u_h^0] = \int_\Omega \mu_\varepsilon[u_h]|\nabla u_h^0|^2 = \int_{U_h} \mu_\varepsilon[u_h]|\nabla u_h^0|^2$$

and since $\nabla u_h = \nabla u_h^0$ in U_h we deduce

$$B_{\varepsilon,h}[\varphi_0, \varphi_0] \leqslant \int_{U_h} \mu_\varepsilon[u_h]|\nabla u_h^0|^2 \leqslant \int_{U_h} \mu_\varepsilon[u_h^0]|\nabla u_h^0|^2 \leqslant \|\nabla u_h^0\|_{L^1(D_h)},$$

where the last inequality follows from (4.13). Thus, (4.25) implies

$$\|\varphi_0\|^2_{L^2(D_h)} \leqslant \varepsilon B_{\varepsilon,h}[\varphi_0, \varphi_0] \leqslant \varepsilon\|\nabla u_h^0\|_{L^1(D_h)}. \tag{4.32}$$

Using the expansion (4.17),

$$\nabla u_h^0 = \sum_{m=1}^{M} \omega_m \nabla\chi_h^{0,m}, \quad \text{and estimate} \quad \|\chi_h^{0,m}\|_{L^1(\Omega)} \leqslant C,$$

see (4.18), the conclusion follows by (4.32) due to

$$\|\nabla\varphi_0\|^2_{L^2(D_h)} \leqslant \varepsilon\|\nabla u_h^0\|_{L^1(\Omega)} \leqslant C_1 \max_m |\omega_m|\, \varepsilon.$$

The proof of estimate (4.31) relies on Lemma 4.1, as well as equations (4.18), (4.24), and (4.25). Due to Lemma 4.1, there exists $C > 0$ independent of ε and h such that

$$\lambda_k \leqslant \frac{C|\tau|}{\min_j |\alpha_j|}, \qquad \tau_k = \tau_k(h) = \|\nabla\chi_h^k\|_{L^1(\Omega)}, \quad k = 1, \ldots, K,$$

By (4.18) we may bound τ_k from above by a positive constant, independent of ε, h. Thus, there exists $C_1 > 0$ independent of ε, h, such that

$$\lambda_k \leqslant \frac{C_1}{\min_j |\alpha_j|}.$$

Since for each $k \geqslant 1$, φ_k is L^2-normalized, (4.24) and (4.25) yield

$$\|\nabla\varphi_k\|^2_{L^2(D_h)} \leqslant \varepsilon B_{\varepsilon,h}[\varphi_k,\varphi_k] = \varepsilon\lambda_k \leqslant \frac{C_1}{\min_j |\alpha_j|}\varepsilon, \qquad k = 1,\dots,K.$$

□

From this, we can deduce the following corollary.

Corollary 4.3. *Since D_h is the union of all its connected components E_h^m and B_h^k, $m = 1,\dots,M$ and $k = 1,\dots,K$, see (4.9) – (4.11), Poincaré's inequality and estimates (4.30) – (4.31) imply*

$$\begin{aligned} \|u^0 - \varphi_0\|^2_{L^2(W)} &\leqslant C_2 \max_m |\omega_m|\, \varepsilon, \\ \|\varphi_k\|^2_{L^2(W)} &\leqslant \frac{C_2}{\min_j |\alpha_j|}\varepsilon, \qquad k = 1,\dots,K, \end{aligned} \tag{4.33}$$

for any $W = E_h^m$ or $W = B_h^k$, $m = 1,\dots,M$ and $k = 1,\dots,K$, where $u = u^0 + \tilde{u}$ is piecewise constant given by (4.5) and C_2 independent of ε and h.

In summary, (4.30) implies that φ_0 is essentially "almost" piecewise constant and due to (4.33) may approximates u^0, or u_h^0, very well in each connected component of D_h, see Figures 4.4 (a) and (c). Similarly, if $\tilde{u}$ consists of K interior inclusions $A^1,\dots,A^K$, the first K eigenfunctions φ_k of $L_\varepsilon[u_h]$ are also "almost" piecewise constant due to (4.31). Thus, $\{\varphi_k\}_{k=1}^K$ cover all information of $\tilde{u}$ in each connected component of D_h very well. Note that each φ_k does not have to resemble a single interior inclusion A^j, $j = 1,\dots,K$ (see Figure 4.4), though the span of $\{\varphi_k\}_{k=1}^K$ is able to approximate $\tilde{u}$, or $\tilde{u}_h$, very well. Consequently, the AS decomposition $Q_k[u_h](u)$ of u, i.e. the projection of u into $\varphi_0 + \Phi^K$, is able to represent u, as presumed by Figure 4.3. To prove this, we need the following results from [10], where denote by

$$\langle f\rangle_W = \frac{1}{\mathcal{L}(W)}\int_W f(\mathbf{x})\, d\mathbf{x},$$

the average of f in $W \subset \Omega$, with Lebesgue measure $\mathcal{L}(W)$.

Corollary 4.4. *There exists a constant $C > 0$ independent of ε and h such that for every $\varepsilon, h > 0$ sufficiently small and $1 \leqslant j \leqslant K$,*

$$\|\varphi_0 - u^0\|^2_{L^2(E_h)} \leqslant C\varepsilon, \qquad \|\varphi_0 - \langle\varphi_0\rangle_{B_h^j}\|^2_{L^2(B_h^j)} \leqslant C\varepsilon$$

and

$$\|\varphi_k\|^2_{L^2(E_h)} \leqslant C\varepsilon, \quad \|\varphi_k - \langle\varphi_k\rangle_{B_h^j}\|^2_{L^2(B_h^j)} \leqslant C\varepsilon, \qquad k = 1,\dots,K.$$

Lemma 4.5. *There exists a constant $C > 0$ independent of ε and h such that for every $\varepsilon, h > 0$ sufficiently small*

$$\begin{aligned} \|\varphi_0 - u^0\|^2_{L^2(M_h)} &\leqslant Ch, \\ \|\varphi_k\|^2_{L^2(M_h)} &\leqslant Ch, \qquad k = 1, \dots, K. \end{aligned}$$

Note that Corollary 4.4 and Lemma 4.5 essentially express that the difference $\varphi_0 - u^0$ and the eigenfunctions φ_k, $k = 1, \dots, K$ behave like $\mathcal{O}(\sqrt{h})$ in the h-tube M_h around the jump-discontinuities of u, and behave like $\mathcal{O}(\sqrt{\varepsilon})$ otherwise. This may indicate that the error made when projecting u, or any $v \in u^0 + X^K$, into $\varphi_0 + \Phi^K$, asymptotically behaves like $\mathcal{O}(\sqrt{\varepsilon + h})$, for $\varepsilon, h > 0$ sufficiently small. To prove this, we first need lower and upper bounds of Σ, the matrix of the averages of φ_k:

Lemma 4.6. *Let the matrix $\Sigma \in \mathbb{R}^{K \times K}$ of the averages of φ_j be defined as*

$$\Sigma = (\sigma)_{k,j}, \quad \sigma_{k,j} = \langle \varphi_j \rangle_{B_h^k}, \qquad k, j = 1, \dots, K.$$

Then there exist constants $0 < C_1 \leqslant C_2$ independent of ε and h, such that for every sufficiently small $\varepsilon, h > 0$

$$C_1|\beta| \leqslant |\Sigma\beta| \leqslant C_2|\beta|, \qquad \beta \in \mathbb{R}^K.$$

This automatically implies that Σ is invertible.

Lemma 4.7. *There exists a positive constant C independent of ε and h, such that for each $\varepsilon, h > 0$ sufficiently small*

$$\|\varphi_0 - u^0\|_{L^2(\Omega)} \leqslant C, \qquad k = 1, \dots, K.$$

Now we can prove the main result. Here, as above, we assume that u is piecewise constant given by (4.5) and (4.6), u_h as in (4.16) and (4.17), X^K given by (4.28), and $\varphi_0, \varphi_1, \dots, \varphi_K$ satisfy (4.24).

Theorem 4.8. *(i) Let $\Pi_K[u_h]$ be the orthogonal projection on Φ^K given by (4.26). Then there exists a constant $C > 0$ independent of ε and h such that for every $v \in X^K$ and every $\varepsilon, h > 0$ sufficiently small*

$$\|v - \Pi_K[u_h]v\|_{L^2(\Omega)} \leqslant C\sqrt{\varepsilon + h}\|v\|_{L^2(\Omega)}. \tag{4.34}$$

In particular, $v = \tilde{u}$ and $v = \chi_{A^k}$ $(k = 1, \dots, K)$ satisfy (4.34).

(ii) Let $Q_K[u_h]$ be the L^2-orthogonal projection on $\varphi_0+\Phi^K$ given by (4.27). Then there exists a constant $C > 0$ independent of ε and h such that for every $v \in u^0 + X^K$ and every $\varepsilon, h > 0$ sufficiently small

$$\|v - Q_K[u_h](v)\|_{L^2(\Omega)} \leqslant C\sqrt{\varepsilon + h}\left(\|v - u^0\|_{L^2(\Omega)} + 1\right). \tag{4.35}$$

In particular, $v = u$ and $v = u^0$ satisfy (4.35).

Proof. We only show (4.35) since the proof of (4.34) is similar. Note that

$$\|v - Q_k[u_h]v\|_{L^2(\Omega)} = \min_{\beta\in\mathbb{R}^K} \left\|(v-\varphi_0) - \sum_{k=1}^K \beta_k\varphi_k\right\|_{L^2(\Omega)}.$$

Since we have

$$\|v - Q_k[u_h]v\|_{L^2(\Omega)} \leqslant \|v-\varphi\|_{L^2(\Omega)}, \qquad \forall\varphi \in \varphi_0 + \Phi^K,$$

by the triangle inequality we obtain

$$\begin{aligned}\|v-\varphi\|_{L^2(\Omega)} \leqslant &\|v-\varphi\|_{L^2(E_h)} + \|v-u^0\|_{L^2(M_h)} + \|u^0-\varphi\|_{L^2(M_h)} \\ &+ \sum_{k=1}^K \|v-\varphi\|_{L^2(B_h^k)}.\end{aligned} \tag{4.36}$$

The idea of the proof is to find a particular φ, i.e. to construct a suitable $\beta \in \mathbb{R}^K$ and set

$$\varphi = \varphi_0 + \tilde{\varphi}, \qquad \tilde{\varphi} = \sum_{k=1}^K \beta_k\varphi_k \ \in \Phi^K, \tag{4.37}$$

such that we can estimate each term of the right side of (4.36) with respect to ε and h.

We first construct a suitable φ. Due to Lemma 4.6, the matrix $\Sigma \in \mathbb{R}^{K\times K}$ of the averages is invertible. This implies the existence of a unique $\beta \in \mathbb{R}^K$ such that

$$(\Sigma\beta)_k = \sum_{j=1}^K \beta_j\langle\varphi_j\rangle_{B_h^k} = \langle v-\varphi_0\rangle_{B_h^k}, \qquad k = 1,\dots,K, \tag{4.38}$$

and hence, we obtain the estimate

$$|\beta|^2 \leqslant C_1 \sum_{k=1}^K \langle v-\varphi_0\rangle_{B_h^k}$$

for $C_1 > 0$ independent of ε and h. Thus we get

$$|\beta| \leqslant \sqrt{C_1} \left(\sum_{k=1}^{K} \|v - \varphi_0\|^2_{L^2(B_h^k)} \right)^{1/2}. \tag{4.39}$$

By Lemma 4.7 we now estimate $\|v - \varphi_0\|$ to obtain

$$\|v - \varphi_0\|_{L^2(B_h^k)} \leqslant \|v - u_0\|_{L^2(B_h^k)} + \|u_0 - \varphi_0\|_{L^2(B_h^k)} \leqslant \|v - u_0\|_{L^2(B_h^k)} + C$$

for $C > 0$ independent of ε, h, which yields

$$|\beta| \ \leqslant C(\|v - u^0\|_{L^2(\Omega)} + 1).$$

Next, we will use this particular β from (4.38) to construct φ defined by (4.37):

$$\varphi = \varphi_0 + \tilde{\varphi}, \qquad \tilde{\varphi} = \sum_{k=1}^{K} \beta_k \varphi_k \ \in \Phi^K.$$

Now we can estimate each term on the right side of (4.36). Due to Corollary 4.4 and (4.39), from $v = u^0$ in E_h follows that

$$\begin{aligned} \|v - \varphi\|_{L^2(E_h)} &\leqslant \|u^0 - \varphi_0\|_{L^2(E_h)} + \|\tilde{\varphi}\|_{L^2(E_h)} \\ &\leqslant \|u^0 - \varphi_0\|_{L^2(E_h)} + \sum_{k=1}^{K} |\beta_k| \|\varphi_k\|_{L^2(E_h)} \\ &\leqslant C\sqrt{\varepsilon}(\|v - u^0\|_{L^2(\Omega)} + 1). \end{aligned}$$

To obtain and estimate of the piecewise constant function $w = v - u^0 \in X^K$ in M_h of (4.36), we employ that $w = 0$ almost everywhere in $\Omega \setminus \overline{\cup_{k=1}^{K} B^k}$, thus

$$\|v - u^0\|^2_{L^2(M_h)} = \int_{M_h} w^2 = \sum_{k=1}^{K} \int_{M_h \cap B^k} w^2. \tag{4.40}$$

Since w^2 is constant in each set B^k and $\mathcal{L}(M_h \cap B^k) = \mathcal{O}(h)$, see [11, Lemma 4], this implies

$$\int_{M_h \cap B^k} w^2 = \mathcal{L}(M_h \cap B^k) w^2|_{B^k} \leqslant Ch\mathcal{L}(B^k) w^2|_{B^k} = Ch \int_{B^k} w^2.$$

Together with (4.40), this yields the estimate of the second term in (4.36) with respect to h:

$$\|v - u^0\|_{L^2(M_h)} \leqslant C\sqrt{h} \|v - u^0\|_{L^2(\Omega)}.$$

Now, by Lemma 4.5 and (4.39) we estimate the third term $\|u^0 - \varphi\|_{L^2(M_h)}$ as

$$\begin{aligned}\|u^0 - \varphi\|_{L^2(M_h)} &\leqslant \|u^0 - \varphi^0\|_{L^2(M_h)} + \sum_{k=1}^{K} |\beta_k| \|\varphi_k\|_{L^2(M_h)} \\ &\leqslant C\sqrt{h}(\|v - u^0\|_{L^2(\Omega)} + 1).\end{aligned}$$

To estimate each $\|v-\varphi\|_{L^2(B_h^k)}$, we use that β solves (4.38) and thus $\langle v-\varphi\rangle_{B_h^k} = 0$. Hence, the Poincaré-Wirtinger inequality implies

$$\|v - \varphi\|_{L^2(B_h^k)} \leqslant C\|\nabla(v - \varphi)\|_{L^2(B_h^k)}.$$

Since $\nabla v = 0$ in each B_h^k,

$$\begin{aligned}\|v - \varphi\|_{L^2(B_h^k)} &\leqslant C_1\|\nabla\varphi\|_{L^2(B_h^k)} \leqslant C_1 \left(\|\varphi_0\|_{L^2(B_h^k)} + \sum_{j=1}^{K} |\beta_j| \|\nabla\varphi_j\|_{L^2(B_h^k)} \right) \\ &\leqslant C_2\sqrt{\varepsilon}(\|v - u^0\|_{L^2(\Omega)} + 1).\end{aligned}$$

Finally, we combine the estimates above to obtain

$$\|v - Q_k[u_h](v)\|_{L^2(\Omega)} \leqslant \|v - \varphi\|_{L^2(\Omega)} \leqslant C\sqrt{\varepsilon + h}(\|v - u^0\|_{L^2(\Omega)} + 1).$$

□

Remark 3. *In practice, we can project any $w \in L^2(\Omega)$ into Φ^K or $\varphi_0 + \Phi^K$, for particular the FE-interpolant $w = u_h$ of u. From Theorem 4.8 we immediately obtain error estimates for arbitrary L^2-functions. Since the norm of every projection is less than one, the triangle inequality yields*

$$\|w - \Pi_K[u_h]w\|_{L^2(\Omega)} \leqslant C\sqrt{\varepsilon + h}\|w\|_{L^2(\Omega)} + \|w - v\|_{L^2(\Omega)} \tag{4.41}$$

for every $v \in X^K$. Similarly, if $v \in u_0 + X^K$, then

$$\|w - Q_K[u_h](w)\|_{L^2(\Omega)} \leqslant C\sqrt{\varepsilon + h}(\|w - u^0\|_{L^2(\Omega)} + 1) + \|w - v\|_{L^2(\Omega)}. \tag{4.42}$$

This means that the projection error additionally depends on the error made from the approximation of v by w in the L^2-norm.

Chapter 5

Numerical Results

In this chapter, we present numerical examples that illustrate the analysis and error estimates of Section 4.2, especially Theorem 4.8, and demonstrate the accuracy of the AS decomposition for piecewise constant media. At first, we consider four different but simple media with homogeneous background u^0, where each media is comprised of a single characteristic function. The second example is the medium shown in Figure 4.3 (a), where the background u^0 consists of $M = 3$ sets Ω^m, $m = 1, \dots, M$, and the interior $\tilde{u}$ consists of $K = 3$ interior shapes A^k, $k = 1, \dots, K$. The third medium consists of a uniform background and four interior adjacent inclusions. Even though this constellation is not admissible for our analysis, the convergence rate of Theorem 4.8 still holds true. In the last remaining two examples, we consider more complex media that are not covered by our analysis: a polygonal approximation of the map of Switzerland with its 26 cantons and Anna's Mountains[1].

In all the numerical examples, the domain $\Omega \subset \mathbb{R}^2$ is rectangular. If not explicitly stated otherwise, we use a uniform triangular mesh $\mathcal{T}_h$ of mesh size $h > 0$, see Section 2.2.2, whose vertices lie on an equidistant cartesian grid of grid size h. As the underlying finite dimension space V^h we use standard $\mathcal{P}^1$-FE, the standard space of piecewise polynomials of degree 1, and let $V_0^h = V^h \cap H_0^1(\Omega)$. As mentioned above, we denote by $u_h \in V^h$ the H^1-conforming continuous interpolant of u onto V^h.

We let $L_\varepsilon[u_h]$ be as in (4.21) with weight function given by (4.15) with $q = 2$. Thus, we consider

$$L_\varepsilon[u_h]v = -\nabla \cdot (\mu_\varepsilon[u_h]\nabla v), \qquad \mu_\varepsilon[u_h](v) = \frac{1}{\sqrt{|\nabla u_h|^2 + \varepsilon^2}}.$$

[1]This abstract illustration of mountains was kindly supported by my former flatmate Anna Frommherz.

To obtain $\varphi_0 \in V^h$ and $\varphi_k \in V_0^h$ for $k = 1, \dots, K$, we employ the Galerkin finite element method introduced in Section 2.2.2 to numerically solve (4.24). This results in the generalized eigenvalue problem

$$\mathbf{A}_\varepsilon \varphi_k = \lambda_k \mathbf{M} \varphi_k, \qquad k = 1, \dots, K,$$

where $\mathbf{A}_\varepsilon$ corresponds to the discretization of the operator $L_\varepsilon[u_h]$ and $\mathbf{M}$ denotes the mass matrix. In principle, $\varepsilon > 0$ should be as small as possible, yet large enough to ensure that $\mathbf{A}_\varepsilon$ is still well-posed. Unless specified otherwise, we consistently use $\varepsilon = 10^{-8}$.

After obtaining φ_0 and φ_k, $k = 1, \dots, K$, we proceed to compute the AS decomposition of u, which involves computing the projections $\Pi_K[u_h](u)$ and $Q_K[u_h](u)$ as defined in (4.26) and (4.27), respectively. Since the eigenfunctions φ_k are computed numerically, they may not satisfy $(\varphi_k, \varphi_j)_{L^2(\Omega)} = \delta_{k,j}$ exactly. Thus, we do not compute the Fourier expansion

$$\Pi_K[u_h]v = \sum_{k=1}^{K} (\varphi_k, u)_{L^2(\Omega)} \varphi_k$$

directly to obtain the projection. To avoid these numerical errors, we instead solve the K-dimensional least squares problem

$$\Pi_K[u_h]v = \operatorname*{argmin}_{w \in \Phi^K} \|v - w\|_{L^2(\Omega)}, \qquad \Phi^K = \operatorname{span}\{\varphi_k\}_{k=1}^K.$$

In the subsequent numerical examples we monitor two errors, $e = e(\varepsilon, h)$ and $e_h = e_h(\varepsilon, h)$ given by

$$e = \|u - Q_K[u_h](u)\|_{L^2(\Omega)} \quad \text{and} \quad e_h = \|u_h - Q_K[u_h](u_h)\|_{L^2(\Omega)}. \tag{5.1}$$

The first error validates (4.35) of Theorem 4.8, whereas the second error validates (4.42) of Remark 3 with $w = u_h$. Calculating (5.1) requires the evaluation of inner products on L^2. Since all functions involved in e_h lie in V^h, we can calculate the L^2-norm exactly. The error e on the left, however, involves discontinuous functions whose discontinuities are not necessarily aligned with the mesh. To account for these discontinuities, we use the numerical quadrature rule from ACM TOMS Algorithm #584 [74] with degree of precision 8 and 19 quadrature nodes to precisely take the discontinuities into account.

5.1 Convergence Rates of the Adaptive Spectral Decomposition

5.1.1 Four Simple Shapes

In this first example, we consider the four different media $u : \Omega \to \mathbb{R}$, $\Omega = (0,1)^2$, as in Figure 5.1. All four possess zero boundary values, thus $u^0 = 0$, and their interior is comprised by a single inclusion. Hence they admit the form (4.5) with

$$u(\mathbf{x}) = \tilde{u}(\mathbf{x}) = \chi_{A^1}(\mathbf{x}), \qquad \mathbf{x} \in \Omega.$$

All four geometries are chosen on purpose with the following properties: the disk is convex with a smooth boundary and the square is also convex but only admits a piecewise smooth boundary. The open wedge and star are non-convex, also with piecewise smooth boundaries. Thus, all four shapes are therefore covered by our analysis.

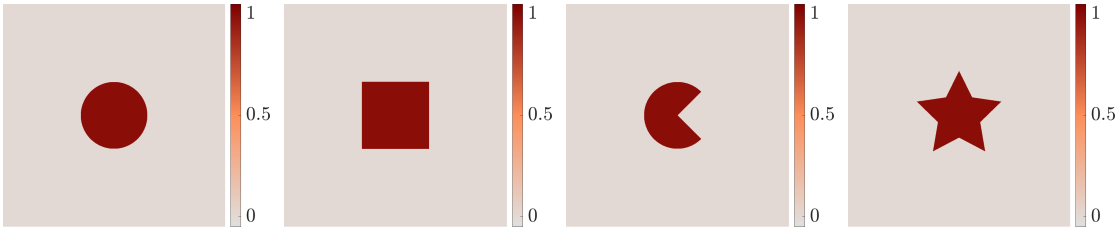

(a) disk **(b)** square **(c)** open wedge **(d)** star

Fig. 5.1: Four simple shapes: The exact media u, all consisting of a single inclusion A^1 and homogeneous boundary.

Next, we measure the error $e = e(\varepsilon, h)$, first with respect to h by keeping $\varepsilon = 10^{-8}$ fixed, then with respect to ε by using the finest mesh with mesh size $h = 0.05/2^6$. To measure the error $e = e(h)$ with respect to h, we compute (5.1) for six different meshes with varying mesh size $h = 0.05/2^m$, $m = 1, \dots 6$. In Figure 5.2 (a) the error $e(h)$ decays as $\mathcal{O}(\sqrt{h})$ for every single shape, thus we obtain the optimal convergence rate from Theorem 4.8. Figure 5.2 (b) illustrates the error $e(\varepsilon)$ for varying $\varepsilon = 10^{-m}$, $m = 1, \dots, 8$, where it first decays as $\mathcal{O}(\varepsilon)$, thus with a slightly better convergence rate as predicted in Theorem 4.8, but then stagnates at about 10^{-2} for subsequent ε. This is due to the dominant error made from discretization, thus we can only improve the error decay with respect to ε by further refining the mesh.

To eliminate the discretization error with respect to h by interpolation on V_0^h, we now monitor the error $e_h = e_h(\varepsilon, h)$, see Remark 3 (4.41) with $w = u_h$. The error $e_h(h)$ remains nearly constant at about 10^{-9} for the three media, where the

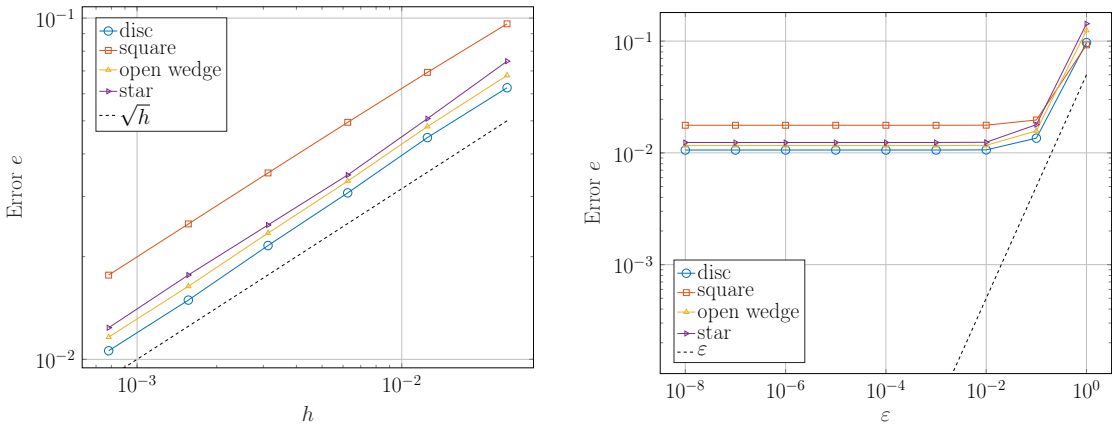

(a) $e = e(h)$ **(b)** $e = e(\varepsilon)$

Fig. 5.2: Four simple shapes: The error $e = \|u - \Pi_1[u_h]u\|_{L^2(\Omega)}$ as a function of h for fixed $\varepsilon = 10^{-8}$ (left) and as a function of ε for $h = 0.05/2^6$ (right).

single inclusion is given by the disk, square, and open wedge, whereas the error for the star-shaped medium decays with $\mathcal{O}(h)$, however, 6 magnitudes larger compared to the three other shapes, see Figure 5.3 (a). Thus, we achieve a slightly improved convergence order compared to (4.41). The error $e_h(\varepsilon)$ for varying ε and fixed h shown in Figure 5.3 (b) is improved to $\mathcal{O}(\varepsilon)$ for the disks, square, and open wedge shaped media, whereas the star-shaped inclusion again levels off at about 10^{-3}. This is due to the star-shaped discontinuities not being aligned with the mesh, whose vertices lie on an equidistant grid.

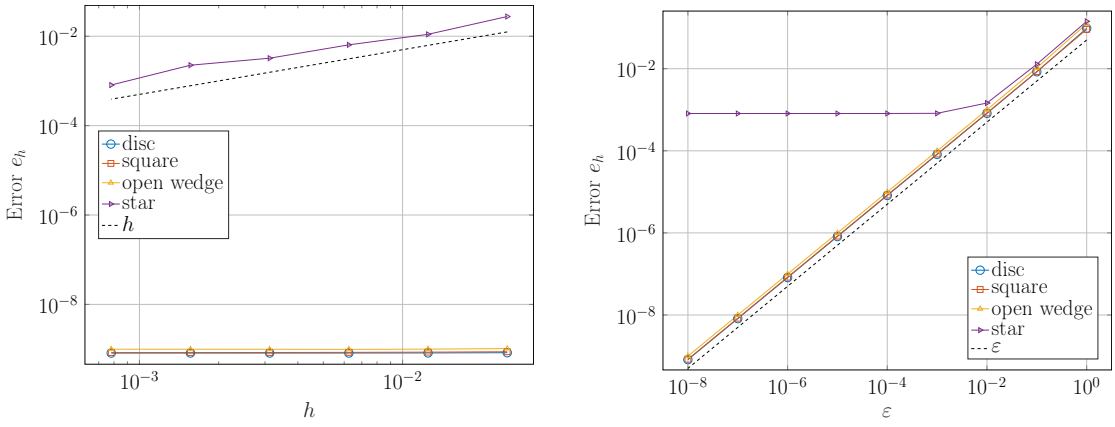

(a) $e_h = e_h(h)$ **(b)** $e_h = e_h(\varepsilon)$

Fig. 5.3: Four simple shapes: The error $e_h = \|u_h - \Pi_1[u_h]u_h\|_{L^2(\Omega)}$ as a function of h for fixed $\varepsilon = 10^{-8}$ (left) and as a function of ε for $h = 0.05/2^6$ (right).

If we align the mesh to the star-shaped discontinuity as in Figure 5.4 (a), the error $e_h(h)$ again decays with $\mathcal{O}(h)$ and also decreases to 10^{-9}, similar to the other three inclusions.

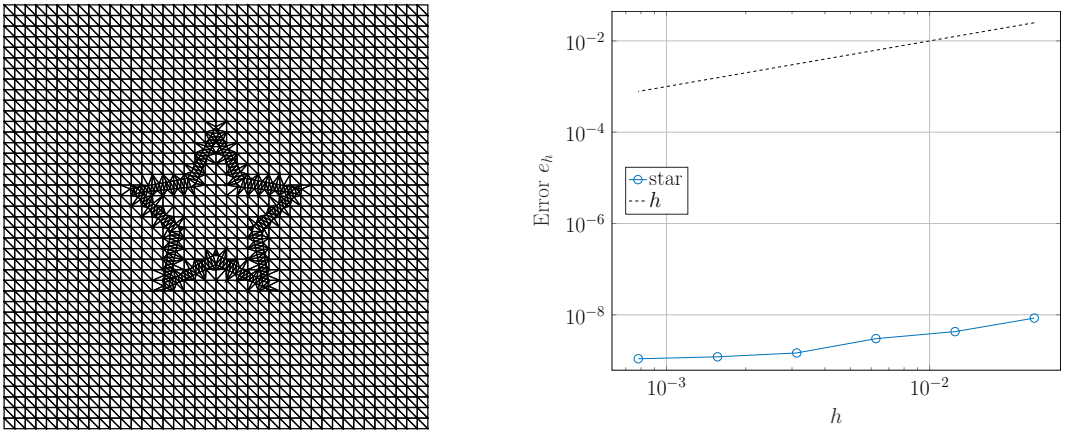

(a) Aligned star-shaped mesh **(b)** $e_h = e_h(h)$

Fig. 5.4: Four simple shapes: The error $e_h(h)$ for the star-shaped inclusion on a mesh aligned to the discontinuities.

5.1.2 Nonuniform Background

Next, we consider the medium u as in Figure 5.5 (a), see also Figure 4.3 (a), consisting of a non-vanishing background u^0 comprised of $M = 3$ sets Ω^m, $m = 1, \dots, M$, and $K = 3$ interior inclusions A^k, $k = 1, \dots, K$. Thus u admits the form

$$u(\mathbf{x}) = u^0(\mathbf{x}) + \tilde{u}(\mathbf{x}), \qquad \mathbf{x} \in \Omega,$$

where

$$u^0 = \sum_{m=1}^{M} \omega_m \chi_{\Omega^m}, \quad \omega_m \in \mathbb{R}, \qquad \tilde{u} = \sum_{k=1}^{K} \alpha_k \chi_{A^k}, \quad \alpha_k \in \mathbb{R} \setminus \{0\},$$

see (4.5) – (4.6). Figure 5.5 shows φ_0 given by (4.22), covering all information of the background u^0, and the first three eigenfunctions φ_k, $k = 1, \dots, 3$ given by (4.23) of $L_\varepsilon[u_h]u$, as well as the AS decomposition $Q_3[u_h](u)$ of u.

Here, we only focus on the errors

$$e(h) = \|u - Q_3[u_h](u)\|_{L^2(\Omega)}$$

with respect to h and fixed ε, as well as

$$e_h(\varepsilon) = \|u_h - Q_3[u_h](u_h)\|_{L^2(\Omega)}$$

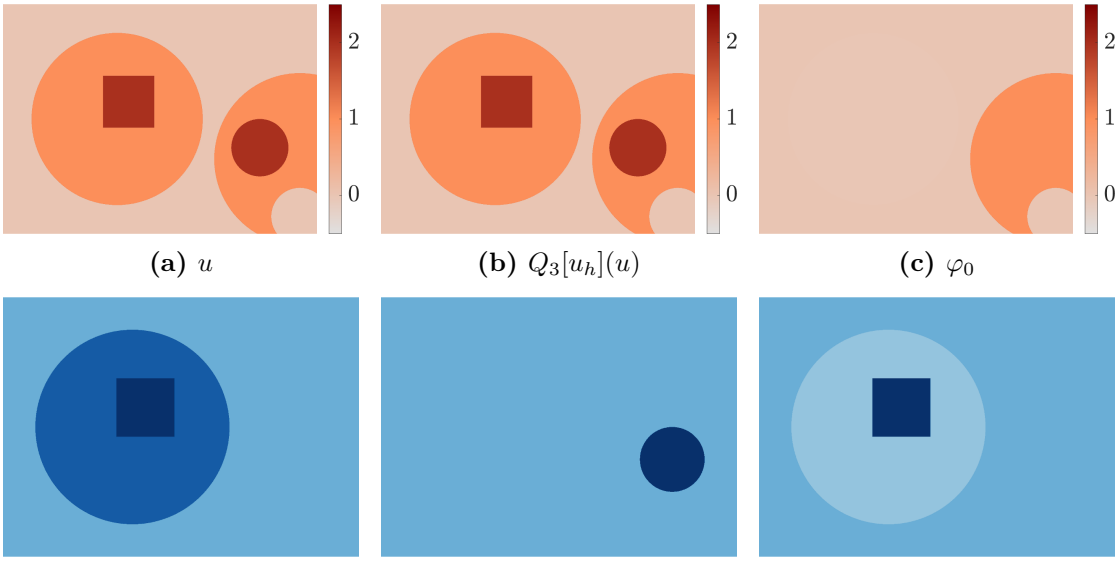

(a) u **(b)** $Q_3[u_h](u)$ **(c)** φ_0

(d) φ_1, $\lambda_1 \approx 1.5$ **(e)** φ_2, $\lambda_2 \approx 4.7$ **(f)** φ_3, $\lambda_3 \approx 5.3$

Fig. 5.5: Nonuniform background: The exact medium u, φ_0, the first three eigenpairs (λ_k, φ_k), and its projection $Q_3[u_h](u)$ on $\varphi_0 + \Phi^3$.

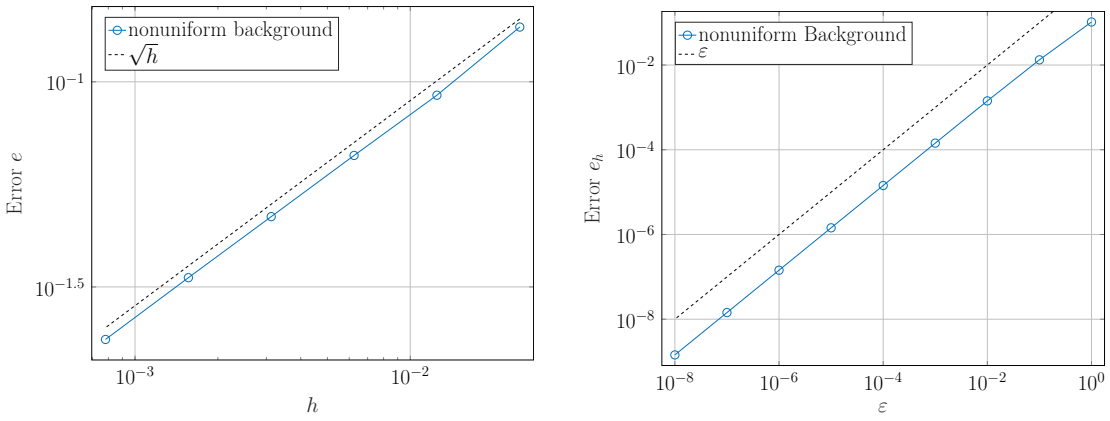

(a) $e = e(h)$ **(b)** $e_h = e_h(\varepsilon)$

Fig. 5.6: Nonuniform background: The errors $e(h) = \|u - Q_3[u_h](u)\|_{L^2(\Omega)}$ with $\varepsilon = 10^{-8}$ fixed and $e_h(\varepsilon) = \|u_h - Q_3[u_h](u_h)\|_{L^2(\Omega)}$ on the finest mesh with mesh size $h = 0.05/2^6$.

with respect to ε and fixed h, since e_h removes the dominant error made due to projection on V^h. Figure 5.6 (a) shows the error $e(h)$ for six different mesh sizes $h = 0.05/2^m$, $m = 1, \ldots, 6$, where we observe the error decay of $\mathcal{O}(h)$, thus validating the estimate of Theorem 4.8. The error $e_h(\varepsilon)$, for varying $\varepsilon = 10^{-m}$, $m = 1, \ldots, 8$, on the finest mesh with mesh size $h = 0.05/2^6$ is illustrated in Figure

5.6 (b). Clearly, the numerical order of convergence $\mathcal{O}(\varepsilon)$ is half an order improved compared to the convergence order $\mathcal{O}(\sqrt{\varepsilon})$ proved by Theorem 4.8.

5.1.3 Four Adjacent Squares

The third example consists of a medium $u : \Omega \to \mathbb{R}$, $\Omega = (0,1)^2$, with vanishing boundary $u^0 = 0$, and four interior inclusions as illustrated in Figure 5.7 (a). Thus the medium admits the form

$$u(\mathbf{x}) = \tilde{u}(\mathbf{x}) = \sum_{k=1}^{4} \chi_{A^k},$$

where each A^k, $k = 1, \dots, 4$, admits the shape of a square. Note that since the squares A^k do not have mutually disjoint boundaries ∂A^k, this medium is not covered by our analysis. However, we can still compute the AS decomposition $\Pi_4[u_h]$ and measure the errors $e(h)$, $e_h(\varepsilon)$ as in (5.1).

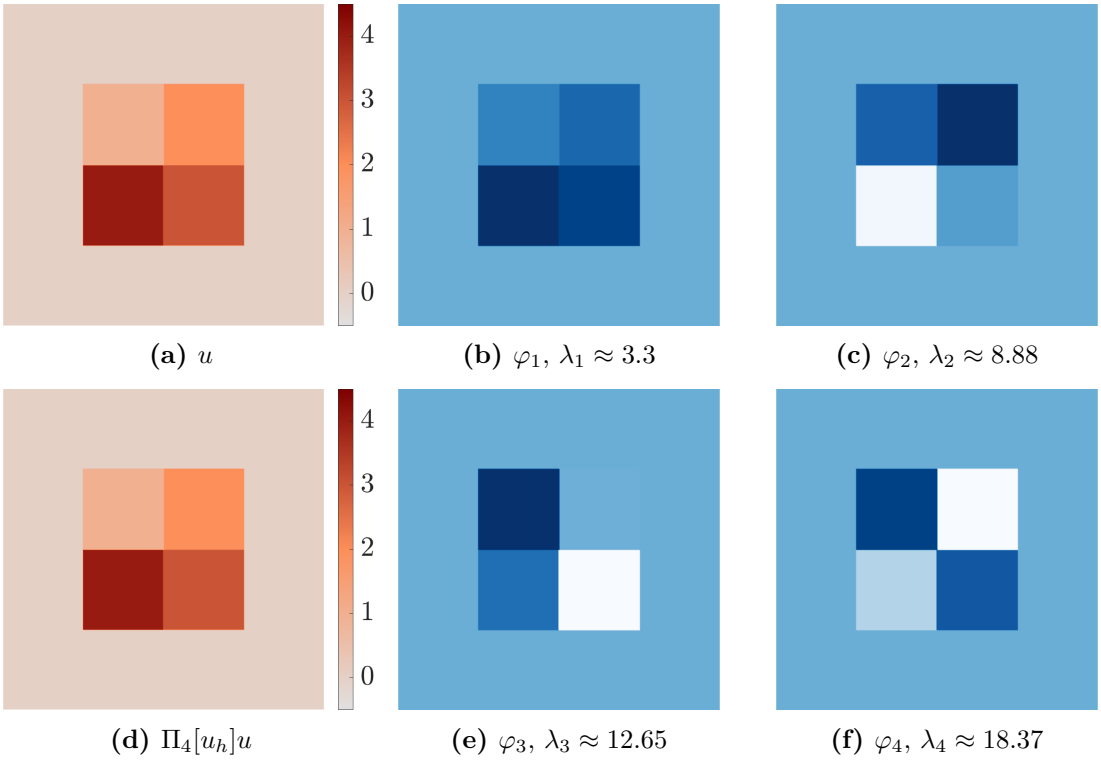

(a) u **(b)** φ_1, $\lambda_1 \approx 3.3$ **(c)** φ_2, $\lambda_2 \approx 8.88$

(d) $\Pi_4[u_h]u$ **(e)** φ_3, $\lambda_3 \approx 12.65$ **(f)** φ_4, $\lambda_4 \approx 18.37$

Fig. 5.7: Four adjacent squares: The medium u and its projection $\Pi_4[u_h]u$ into the first four eigenfunctions $\varphi_1, \dots, \varphi_4$ of the operator $L_\varepsilon[u_h]$.

Similar to the example above, the error $e(h)$, $h = 0.05/2^m$, $m = 1, \dots 6$, converges as $\mathcal{O}(\sqrt{h})$, see Figure 5.8 (a). Thus, the error estimate of Theorem 4.8 also

holds true, even though the boundaries of the inclusions are not mutually disjoint. Figure 5.8 (b) shows the error $e_h(\varepsilon)$ on the finest mesh with mesh size $h = 0.05/2^6$ for varying $\varepsilon = 10^{-m}$, $m = 1, \dots, 8$. Here, the convergence order with respect to ε is linear, in contrast to $1/2$ as in (4.34) and (4.41).

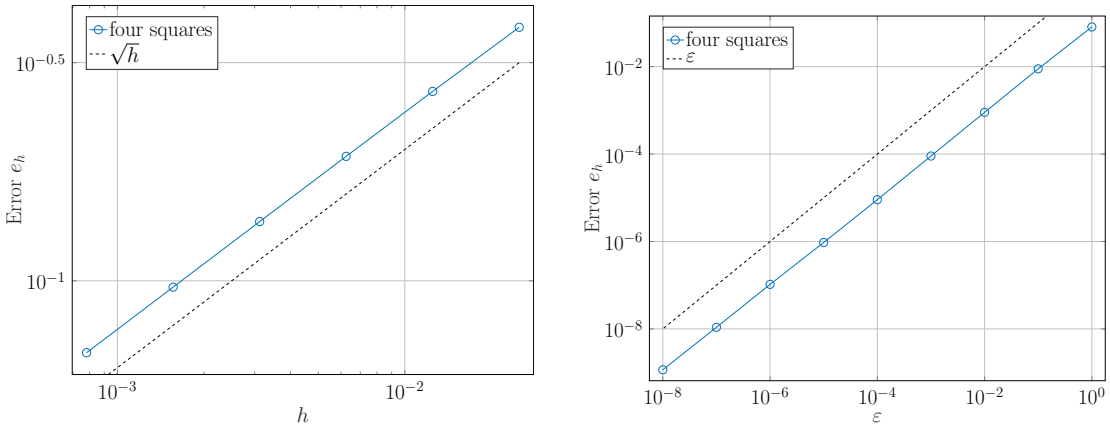

(a) $e = e(h)$ **(b)** $e_h = e_h(\varepsilon)$

Fig. 5.8: Four adjacent squares: The errors $e(h) = \|u - \Pi_4[u_h]u\|_{L^2(\Omega)}$ with $\varepsilon = 10^{-8}$ fixed and $e_h(\varepsilon) = \|u_h - \Pi_4[u_h]u_h\|_{L^2(\Omega)}$ on the finest mesh with mesh size $h = 0.05/2^6$.

5.2 The Adaptive Spectral Decomposition for Complex Geometries

In this section, we will compute the AS decomposition for complex media that do not, in general, admit the form (4.5) – (4.6), where the data are given on a discrete rectangular pixel based grid.

5.2.1 Map of Switzerland

First, we consider a polygonal approximation $u_h \in V_0^h$ of Switzerland and its $K = 26$ cantons, as in Figure 5.9 (a), on a 1563 px × 1002 px pixel based grid, where each canton is assigned a constant value. Thus, u_h is given by

$$u_h = \sum_{k=1}^{K} \alpha_k \chi_h^k, \qquad \alpha_k \neq 0,$$

where each $\chi_h^k \in V^h$ corresponds to a single canton u_h^c. Next, we compute the first $K = 26$ eigenfunctions $\varphi_1, \dots, \varphi_K$ of $L_\varepsilon[u_h]$, see Figure 5.9 (b) – (e), to obtain

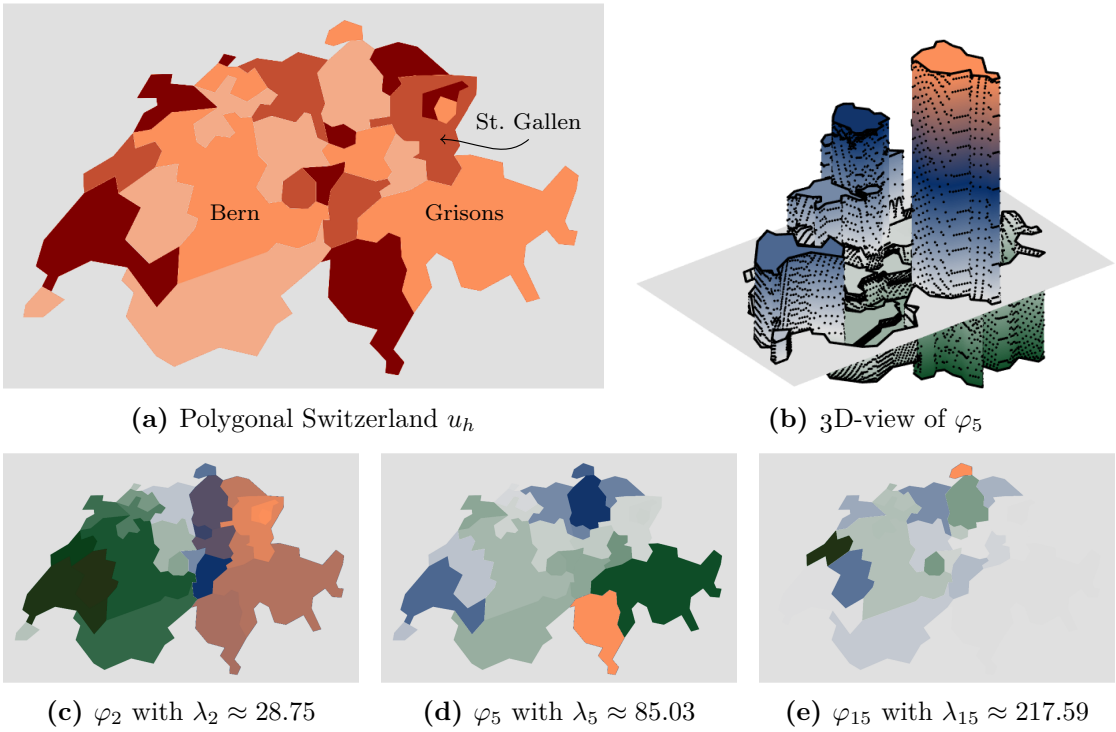

(a) Polygonal Switzerland u_h **(b)** 3D-view of φ_5

(c) φ_2 with $\lambda_2 \approx 28.75$ **(d)** φ_5 with $\lambda_5 \approx 85.03$ **(e)** φ_{15} with $\lambda_{15} \approx 217.59$

Fig. 5.9: Map of Switzerland: Polygonal representation of the map of Switzerland u_h with its 26 cantons, together with three eigenfunctions φ_k, $k = 2, 5, 15$.

$\Phi^{26} = \text{span}\{\varphi_k\}_{k=1}^{K}$. Even tough each eigenfunction does not correspond to a single canton u_h^c, we may still project each canton into Φ^{26}. Thus, the AS decomposition

$$\Pi_{26}[u_h]u_h^c = \sum_{k=1}^{K} \beta_k \varphi_k$$

of a single canton is a good approximation to the canton u_h^c itself. Figure 5.10 shows the projection $\Pi_{26}[u_h]$ for the canton of Bern, Grisons, and St. Gallen onto the space Φ^{26}. Note that although the canton of St. Gallen surrounds the cantons of Appenzell Innerrhoden and Ausserrhoden, the projection $\Pi_{26}[u_h]$ does not include these two cantons, and thus resembles the canton of St. Gallen.

5.2.2 Anna's Mountains

As a last example, we consider u_h shown in Figure 5.11 (a), where the discrete data u_h are given on a 676 px $\times$ 500 px pixel based grid. We compute φ_0 and the first $K = 250$ eigenfunctions φ_k, $k = 1, \ldots, K$, of $L_\varepsilon[u_h]$ and calculate the relative

(a) Canton of Bern **(b)** Canton of Grisons **(c)** Canton of St. Gallen

Fig. 5.10: Map of Switzerland: Three cantons projected onto Φ^{26}.

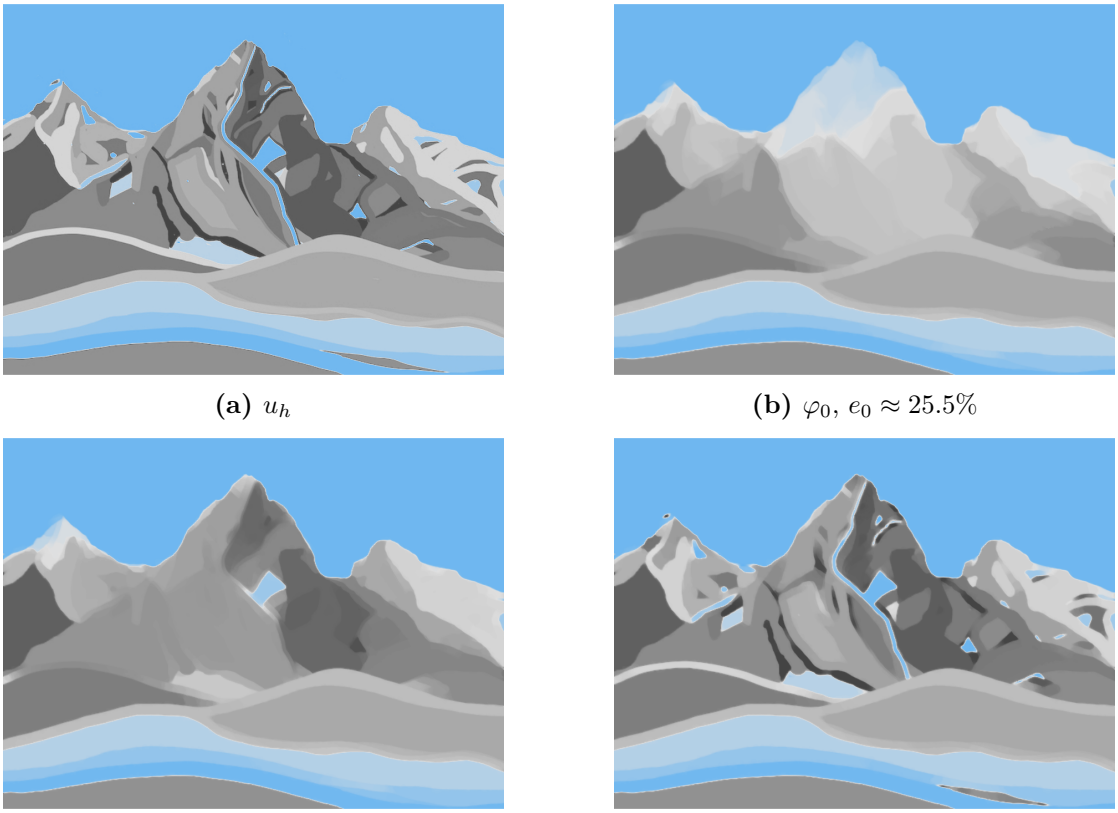

(a) u_h **(b)** φ_0, $e_0 \approx 25.5\%$

(c) $Q_{10}[u_h](u_h)$, $e_{10} \approx 14.5\%$ **(d)** $Q_{200}[u_h](u_h)$, $e_{200} \approx 4.5\%$

Fig. 5.11: Anna's Mountains: The medium u_h, φ_0 and the projections $Q_K[u_h](u_h)$ for $K = 10, 200$, together with its relative L^2-errors e_K.

L^2-error

$$e_K = \frac{\|u_h - Q_K[u_h](u_h)\|_{L^2(\Omega)}}{\|u_h\|_{L^2(\Omega)}}.$$

Remarkably, φ_0 itself is a good approximation of u_h with a relative error $e_0 \approx 25.5\%$, representing most information of u_h that is connected to the bound-

ary, such as the shapes of the mountains, see Figure 5.11 (b). When comparing φ_0 to u_h, however, φ_0 misses covering details in the interior of u_h, e.g. the lakes and rivers that flows down the mountains, as well as its structure. When we take the first 10 eigenfunctions φ_k $(k = 1, \ldots, K)$ into account, the projection $Q_{10}[u_h](u_h)$ on $\varphi_0 + \Phi^{10}$ is able to represent the broader details of the interior, such as the lake and the coarser details of the mountains, see Figure 5.11 (c). Now, if we use the first 200 eigenfunctions to project u_h into $\varphi_0 + \Phi^{200}$, we are able to essentially recover all interior details, c.f. Figure 5.11 (d), such as the rivers and the finer structure of all mountains, resulting in a relative L^2-error of 4.5%.

Part III

The Adaptive Spectral Inversion

Chapter 6

The Adaptive Inversion Algorithm

In this section, we focus on solving inverse (medium) problems, see Section 3.2. Therefore, we consider the forward operator

$$F : H_1 \to H_2, \qquad F(u) = y,$$

where H_1, H_2 are Hilbert spaces. The unknown true medium is denoted by $u^\dagger \in H_1$, and its corresponding exact data is given by $y^\dagger = F(u^\dagger) \in H_2$. However, in practice the exact data $y^\dagger$ is often unknown due to noise in the measurements. Instead, we have access to perturbed/noisy data y^δ such that

$$\|y^\dagger - y^\delta\|_{H_2} \leqslant \delta, \tag{6.1}$$

with known noise $\delta > 0$. Thus, we wish to solve the inverse problem

$$F(u) = y^\delta, \tag{6.2}$$

given noisy data y^δ, which we reformulate as a least squares problem

$$u^{\dagger,\delta} = \operatorname*{argmin}_{u \in H_1} J^\delta(u), \tag{6.3}$$

where the *misfit* $J^\delta : H_1 \to \mathbb{R}$ is given by

$$J^\delta(u) = \frac{1}{2}\|F(u) - y^\delta\|_{H_2}^2 = \frac{1}{2}\|y[u] - y^\delta\|_{H_2}^2.$$

In other words, we seek the medium u that minimizes the error between the data $y[u] = F(u)$ and the noisy observations y^δ in the Hilbert space H_2.

Assumptions 1. *In this entire chapter we assume that the forward operator F is continuous and the misfit J^δ is Fréchet differentiable with derivative $(J^\delta)'(u)$ for every $u \in H_1$. Since H_1 and H_2 are Hilbert spaces, the gradient $\nabla J^\delta(u) \in H_1$ also exists for every $u \in H_1$ where $\|(J^\delta)'(u)\|_{H_1 \to \mathbb{R}} = \|\nabla J^\delta(u)\|_{H_1}$, see Section 2.1.1. To simplify notation, we drop the index on the H_1 norm of the gradient and only write $\|\nabla J^\delta(u)\|$. Further, we denote the inner product on H_1 by $\langle \cdot, \cdot \rangle$*

Following [43], to determine a solution to the inverse problem (6.2), we solve the least squares problem (6.3) successively in a sequence of (closed) finite dimensional subspaces $\Psi^m \subset H_1$, where we do not necessarily have *a priori* knowledge of the entire sequence $\{\Psi^m\}_{m \geqslant 1}$. Furthermore, each subspace might also depent on δ. This leads us to the *Adaptive Inversion Algorithm*:

Algorithm 5 Adaptive Inversion

Input: initial guess $u^{0,\delta}$, search space $\Psi^1 \subset H_1$, $m = 1$.

1. **while** $\|\nabla J^\delta(u^{m,\delta})\| \neq 0$ **do**
2. *Solve*

$$u^{m,\delta} = \operatorname*{argmin}_{u \in \Psi^m} J^\delta(u).$$

3. *Determine* new search space Ψ^{m+1}, such that $u^{m,\delta} \in \Psi^{m+1}$.
4. $m \leftarrow m + 1$

Since we ensure that $u^{m,\delta}$ also belongs to the next new search space Ψ^{m+1}, we guarantee that the sequence $\{u^{m,\delta}\}_{m \geqslant 1}$ obtained by the Adaptive Inversion Algorithm 5 is a minimizing sequence of J^δ. Consequently, the misfit does not increase in every iteration m, i.e.

$$J^\delta(u^{m+1,\delta}) \leqslant J^\delta(u^{m,\delta}), \qquad \forall m \geqslant 1.$$

However, without further assumptions, we do not know yet whether this algorithm is well defined and converges.

6.1 Convergence

To prove the convergence of the Adaptive Inversion Algorithm, we establish a crucial angle condition for $\{u^{m,\delta}\}_{m \geqslant 1}$ with $\delta \geqslant 0$ fixed. This angle condition now ensures that the norm of the gradient $\|\nabla J^\delta(u^{m,\delta})\|$ converges to zero with respect to m, leading to the convergence of Algorithm 5. Under suitable assumptions from convex optimization theory, we can then deduce that the minimizing sequence $\{u^{m,\delta}\}_{m \geqslant 1}$ indeed converges to $u^{\dagger,\delta}$.

Theorem 6.1. *Let the misfit J^δ satisfy Assumptions 1 and its gradient be Lipschitz continuous for every direction $d \in H_1$, i.e.*

$$|\langle \nabla J^\delta(u+v), d\rangle - \langle \nabla J^\delta(u), d\rangle| \leqslant L\|v\|_{H_1}\|d\|_{H_1} \qquad \forall u, v \in H_1, \quad L > 0.$$

Further assume that $J^\delta(u) \geqslant C > -\infty$ for all $u \in H_1$. Then, if the correction terms $d^{m,\delta} = u^{m+1,\delta} - u^{m,\delta}$ satisfy the angle condition

$$|\langle \nabla J^\delta(u^{m,\delta}), d^{m,\delta}\rangle| \geqslant \varepsilon_\theta \|d^{m,\delta}\|_{H_1}\|\nabla J^\delta(u^{m,\delta})\|, \qquad 0 < \varepsilon_\theta < 1 \tag{6.4}$$

uniformly in m, we have

$$\|\nabla J^\delta(u^{m,\delta})\| \to 0, \qquad m \to \infty.$$

Proof. First, we claim that

$$J^\delta(u^{m+1,\delta}) - J^\delta(u^{m,\delta}) \leqslant -\frac{\alpha_m}{2}\mu_m \langle \nabla J^\delta(u^{m,\delta}), d^{m,\delta}\rangle, \tag{6.5}$$

where

$$\alpha_m = \frac{\mu_m}{L}\frac{\langle \nabla J^\delta(u^{m,\delta}), d^{m,\delta}\rangle}{\|d^{m,\delta}\|^2} > 0, \qquad \mu_m = \operatorname{sign}(\langle \nabla J^\delta(u^{m,\delta}), d^{m,\delta}\rangle). \tag{6.6}$$

As both $u^{m+1,\delta}, u^{m,\delta} \in \Psi^{m+1}$, the correction $d^{m,\delta}$ is also in Ψ^{m+1}. Furthermore, since $J^\delta(u^{m+1,\delta}) \leqslant J^\delta(u)$ for all $u \in \Psi^{m+1}$, we may choose $u = u^{m,\delta} - \alpha_m\mu_m d^{m,\delta}$ to obtain $J^\delta(u^{m+1,\delta}) \leqslant J^\delta(u^{m,\delta} - \alpha_m\mu_m d^{m,\delta})$. The linearity and Lipschitz continuity of the gradient thus yields

$$\begin{aligned}
&J^\delta(u^{m+1,\delta}) - J^\delta(u^{m,\delta}) + \alpha_m\mu_m\langle \nabla J^\delta(u^{m,\delta}), d^{m,\delta}\rangle \\
&\quad\leqslant J^\delta(u^{m,\delta} - \alpha_m\mu_m d^{m,\delta}) - J^\delta(u^{m,\delta}) + \alpha_m\mu_m\langle \nabla J^\delta(u^{m,\delta}), d^{m,\delta}\rangle \\
&\quad= \alpha_m\mu_m \int_0^1 \left\langle \left(\nabla J^\delta(u^{m,\delta}) - \nabla J^\delta(u^{m,\delta} - \tau\alpha_m\mu_m d^{m,\delta})\right), d^{m,\delta}\right\rangle d\tau \\
&\quad\leqslant \frac{\alpha_m L}{2}\|d^{m,\delta}\|^2\alpha_m = \frac{\alpha_m}{2}\mu_m\langle \nabla J^\delta(u^{m,\delta}), d^{m,\delta}\rangle,
\end{aligned}$$

which proves (6.5).

By assumption J^δ is bounded from below by $C > 0$ and decreases in every iteration, thus, there exists a constant $C_0 \geqslant 0$ such that by (6.5)

$$\begin{aligned}
-C_0 &\leqslant C - J^\delta(u^{(1),\delta}) \leqslant J^\delta(u^{m+1,\delta}) - J^\delta(u^{(1),\delta}) \\
&= \sum_{m=1}^{M}\left(J^\delta(u^{m+1,\delta}) - J^\delta(u^{m,\delta})\right) \leqslant -\sum_{m=1}^{M}\frac{\alpha_m}{2}\mu_m\langle \nabla J^\delta(u^{m,\delta}), d^{m,\delta}\rangle \\
&= -\frac{1}{2L}\sum_{m=1}^{M}\frac{\|\nabla J^\delta(u^{m,\delta})\|^2}{\|d^{m,\delta}\|^2} \leqslant 0.
\end{aligned} \tag{6.7}$$

Next, we define the angle θ_m via

$$\cos(\theta_m) = \mu_m \frac{\langle \nabla J^\delta(u^{m,\delta}), d^{m,\delta} \rangle}{\|\nabla J^\delta(u^{m,\delta})\| \|d^{m,\delta}\|} > 0$$

and rewrite (6.7) using (6.6) as

$$-C_0 \leqslant -\frac{1}{2L} \sum_{m=1}^{M} \cos^2(\theta_m) \|\nabla J^\delta(u^{m,\delta})\|^2 \leqslant 0.$$

Taking the limit $M \to \infty$ then yields the well known *Zoutendijk condition* [90]

$$\sum_{m=1}^{\infty} \cos^2(\theta_m) \|\nabla J^\delta(u^{m,\delta})\|^2 < \infty,$$

which immediately implies

$$\cos^2(\theta_m) \|\nabla J^\delta(u^{m,\delta})\|^2 \to 0, \qquad m \to \infty.$$

Since the angle condition (6.4) holds uniformly in m for all $u^{m,\delta}$, i.e. $\cos(\theta_m) \geqslant \varepsilon_\theta$ for all $m \geqslant 1$, with $0 < \varepsilon_\theta < 1$, we thus conclude that

$$\|\nabla J^\delta(u^{m,\delta})\| \to 0, \qquad m \to \infty.$$

□

Theorem 6.1 assures that the Adaptive Inversion Algorithm generates a minimizing sequence $\{u^{m,\delta}\}_{m \geqslant 1}$ such that the gradient of the misfit tends to zero. Consequently, the algorithm is well defined and converges. However, without further assumptions concerning the misfit, this does not automatically imply that the sequence $\{u^{m,\delta}\}_{m \geqslant 1}$ converges (weakly) to a (local) minimizer or accumulation point.

Assuming the misfit is coercive and proper, we can apply [16, Corollary 11.30] to obtain the following convergence result for $u^{m,\delta}$.

Theorem 6.2. *Let $J^\delta : H_1 \to \mathbb{R}$ be continuous, convex, coercive, and proper. Then, for every $\delta \geqslant 0$, the sequence $\{u^{m,\delta}\}_{m \geqslant 1}$ from the Adaptive Inversion Algorithm 5*

(i) has a weak accumulation point, which is a minimizer of J^δ.

(ii) If J^δ is strictly convex, then J^δ admits a unique minimizer $u^{\dagger,\delta}$ and

$$u^{m,\delta} \rightharpoonup u^{\dagger,\delta}, \qquad m \to \infty.$$

(iii) If J^δ is also uniformly convex, then J^δ admits a unique minimizer $u^{\dagger,\delta}$ and

$$u^{m,\delta} \to u^{\dagger,\delta}, \qquad m \to \infty.$$

Note that the assumptions made in Theorem 6.2 seldom hold in practice, especially for inverse medium problems. Thus, we can not always guarantee that the sequence $\{u^{m,\delta}\}_{m\geqslant 1}$ from Algorithm 5 converges. However, the angle condition (6.4) from Theorem 6.1 ensures convergence of the gradient to zero. Now that we have established convergence of the Adaptive Inversion Algorithm, we will show that it is also a regularization method c.f. Section 3.1, when stopped by the discrepancy principle.

6.2 Regularization

Since usually only perturbed noisy data y^δ is available, that satisfies (6.1) for known noise $\delta \geqslant 0$, it does not seam feasible to improve the minimizer $u^{m,\delta}$ of $J^\delta(u)$ to exactly fit the misfit in the observed data beyond the error δ. Therefore, we wish to stop the iteration whenever $F(u^{m,\delta})$ approximates y^δ closely enough. Thus, given a parameter $\tau > 1$, we stop the Adaptive Inversion Algorithm at iteration $m_*(\delta)$ defined by the *discrepancy principle*:

$$m_* = m_*(\delta) = \min\{m \in \mathbb{N} : \ \|F(u^{m,\delta}) - y^\delta\|_{H_2} \leqslant \tau\delta\}. \tag{6.8}$$

If we assume that the search spaces Ψ^m satisfy

$$\|(I - \Pi_{\Psi^m})u^\dagger\|_{H_1} \to 0, \qquad m \to \infty,$$

where Π_{Ψ^m} denotes the projection into Ψ^m and $u^\dagger$ the exact (noise-free) solution, the following lemma always guarantees the existence of a finite m_*. This implies that the Adaptive Inversion Algorithm always satisfies the discrepancy principle and stops after finitely many iterations.

Lemma 6.3. *Suppose that Assumptions 1 for the forward operator F hold and that the spaces $\{\Psi^m\}_{m\geqslant 1}$ satisfy*

$$\|(I - \Pi_{\Psi^m})u^\dagger\|_{H_1} \to 0, \qquad m \to \infty. \tag{6.9}$$

Then, for $\tau > 1$, there exists for every $\delta \geqslant 0$ an index $m_*(\delta)$ such that the discrepancy principle (6.8) *is satisfied.*

Proof. By minimality of $u^{m,\delta}$, the residual is bounded by

$$\begin{aligned}\|F(u^{m,\delta}) - y^\delta\|_{H_2} &\leqslant \|F(\Pi_{\Psi^m}u^\dagger) - y^\delta\|_{H_2} \\ &\leqslant \|F(\Pi_{\Psi^m}u^\dagger) - F(u^\dagger)\|_{H_2} + \|F(u^\dagger) - y^\delta\|_{H_2} \\ &\leqslant \|F(\Pi_{\Psi^m}u^\dagger) - F(u^\dagger)\|_{H_2} + \delta.\end{aligned}$$

From the continuity of F and (6.9) we obtain

$$\|F(u^{m,\delta}) - y^\delta\|_{H_2} \leqslant \tau\delta, \qquad \tau > 1,$$

for $m \geqslant M$ sufficiently large. Thus $m_*(\delta) := M$ is always well defined. □

Next, we consider the sequence $\{u^{m_*,\delta}\}_{\delta\geqslant 0}$ obtained from the Adaptive Inversion Algorithm when stopped by the discrepancy principle (6.8). To show that the Adaptive Inversion Algorithm is indeed a regularization method, that is

$$u^{m_*,\delta} \to u^\dagger, \qquad \delta \to 0,$$

we additionally assume that the forward operator F is Fréchet differentiable with derivative $F'(u)$, weakly sequentially closed, and satisfies the *tangential cone condition* (also known as *Scherzer condition*),

$$\|F(u) - F(v) - F'(u)(u - v)\|_{H_2} \leqslant \eta\|F(u) - F(v)\|_{H_2} \tag{6.10}$$

for all $u, v \in H_1$ and $\eta \in (0, 1)$. Then we conclude from [68, Theorem 3.4] that the Adaptive Inversion Algorithm is a genuine regularization method according to Definition 3.3:

Theorem 6.4. *Let Ψ^m satisfy (6.9), F be weakly sequentially closed, Fréchet differentiable, and also satisfy (6.10). Then, the sequence $\{u^{m_*,\delta}\}_{\delta\geqslant 0}$ obtained from the Adaptive Inversion Algorithm 5, stopped at iteration $m_* = m_*(\delta)$ according to (6.8), admits a subsequence converging to a minimizer of J^δ. Moreover, if the minimizer is unique, then the sequence $\{u^{m_*,\delta}\}_{\delta\geqslant 0}$ converges to the exact (noise-free) solution $u^\dagger$ of the inverse problem (6.2), that is*

$$u^{m_*,\delta} \to u^\dagger, \qquad \delta \to 0.$$

Remark 4. *If the nullspace of the Fréchet derivative $F'(u)$ is trivial, the Scherzer condition (6.10) immediately implies the uniqueness of $u^{\dagger,\delta}$ for each $\delta \geqslant 0$. Using the triangle inequality, (6.10) implies*

$$\|F'(u)(u - v)\| \leqslant (1 + \eta)\|F(u) - F(v)\| \qquad \forall u, v \in H_1.$$

Thus, for two distinct solutions $u^{\dagger,\delta} \neq v^{\dagger,\delta}$ to (6.2), we have

$$0 = \|F(u^{\dagger,\delta}) - F(v^{\dagger,\delta})\| \geqslant \frac{1}{\eta + 1}\|F'(u^{\dagger,\delta})(u^{\dagger,\delta} - v^{\dagger,\delta})\|.$$

This contradiction then implies the uniqueness of $u^\dagger$. Consequently, if the nullspace of the Fréchet derivative $F'(u)$ is trivial for all $u \in H_1$, then Theorem 6.4 immediately implies the convergence of $\{u^{m_*,\delta}\}_{\delta\geqslant 0}$ to the exact solution.

Summary. *The Adaptive Inversion Algorithm 5 generates a minimizing sequence* $\{u^{m,\delta}\}_{m\geqslant 1}$*, i.e.*

$$J^\delta(u^{m+1,\delta}) \leqslant J^\delta(u^{m,\delta}), \qquad \forall m \geqslant 1.$$

If we additionally assume that the angle condition

$$|\langle \nabla J^\delta(u^{m,\delta}), d^{m,\delta}\rangle| \geqslant \varepsilon_\theta \|d^{m,\delta}\|_{H_1} \|\nabla J^\delta(u^{m,\delta})\|, \qquad 0 < \varepsilon_\theta < 1$$

for the correciton $d^{m,\delta} = u^{m+1,\delta} - u^{m,\delta}$ *holds uniformly in* m*, Theorem 6.1 ensures convergence of the gradient to zero:*

$$\|\nabla J^\delta(u^{m,\delta})\| \to 0, \qquad m \to 0.$$

These assumptions alone are not sufficient to ensure the convergence of the sequence $\{u^{m,\delta}\}_{m\geqslant 1}$ *to the exact solution. But under standard assumptions from convex optimization, we even obtain convergence of the minimizing sequence from Theorem 6.2.*

Moreover, if the forward operator F *satisfies standard assumptions for inverse problems, we further deduce that the algorithm acts as a regularization method when stopped at iteration* m_* *by the discrepancy principle* (6.8)*. Therefore, for decreasing noise* δ *tending to zero, the sequence* $\{u^{m_*,\delta}\}_{\delta\geqslant 0}$ *converges to the exact noise free solution* $u^\dagger$ *of the inverse problem* (6.2)*.*

Chapter 7

The Adaptive Spectral Inversion Algorithm

In this chapter, we combine the Adaptive Spectral Decomposition from Chapter II with the iterative Adaptive Inversion Algorithm 5 from Section 6. Thus, let $\Omega \subset \mathbb{R}^d$, $d \geqslant 1$ be a bounded Lipschitz domain and $H_1 = L^2(\Omega)$. In each iteration m of the algorithm, we seek a minimizer $u^{m,\delta}$ of the misfit J^δ within a finite dimensional affine subspace $\varphi_0^m + \Psi^m$. To construct the subsequent search space $\varphi_0^{m+1} + \Psi^{m+1}$, we compute φ_0^{m+1} and the first few eigenfunctions $\{\varphi_k^{m+1}\}_{k\geqslant 1}$ using (4.22) – (4.23), sorted in non-decreasing order according to their eigenvalues. We then merge $\{\varphi_k^{m+1}\}_{k\geqslant 0}$ with Ψ^m and reduce its dimension such that $u^{m,\delta}$ remains well represented in Ψ^{m+1}. Although the exact medium $u^\dagger$ is unknown, we assume that its values on the boundary are known. Therefore, each $u^{m,\delta}$ should coincide with $u^\dagger$ on the boundary and we deduce the subsequent minimizer in $\varphi_0^{m+1} + \Psi^{m+1}$. Clearly, φ_0^{m+1} inherits the boundary values of $u^\dagger$ (and thus $u^{m,\delta}$), while Ψ^{m+1} accounts for the interior variations.

Next, we wish to incorporate the angle condition (6.4) from Theorem 6.1 required to obtain convergence. Consider the given minimizer $u^{m,\delta} \in \varphi_0^m + \Psi^m$ of J^δ in the m-th iteration. Then, we first have to determine the minimizer $u^{m+1,\delta}$ of J^δ in $\varphi_0^{m+1} + \Psi^{m+1}$, compute the correction term $d^{m,\delta} = u^{m+1,\delta} - u^{m,\delta}$, and validate the angle condition (6.4)

$$|\langle \nabla J^\delta(u^{m,\delta}), d\rangle| \geqslant \varepsilon_\theta \|d\|_{H_1} \|\nabla J^\delta(u^{m,\delta})\|, \qquad 0 < \varepsilon_\theta < 1. \tag{7.1}$$

for $d = d^{m,\delta}$ If the angle condition is not satisfied, we have to choose a different search space, for example by using more eigenfunctions, and repeat with determining a new minimizer.

To circumvent this, we want to construct a space where we know *a priori* that there exists at least one element that satisfies the angle condition. To do so, we

consider the eigenfunctions $\{\varphi_k\}_{k\geqslant 1}$ of $L_\varepsilon[u^{m,\delta}]$ c.f. (4.23). Then, we reorder them according to their *sensitivities*

$$|\sigma_1| \geqslant |\sigma_2| \geqslant \ldots \geqslant |\sigma_k|, \geqslant \ldots, \qquad \sigma_k = \langle \nabla J^\delta(u^{m,\delta}), \varphi_k \rangle. \tag{7.2}$$

and shall include in Ψ^{m+1} the most *sensitive* eigenfunctions φ_k. Now, we construct a subspace $\Phi_{N_\theta} = \operatorname{span}\{\varphi_k\}_{k=1}^{N_\theta} \subset L^2(\Omega)$, with dimension N_θ, which contains at least one $d \in \Phi_{N_\theta}$ that satisfies the angle condition (7.1) for a fixed $0 < \varepsilon_\theta < 1$. Following [43], the next two lemmas yield subspaces Φ_{N_∞}, Φ_{N_2}, that contain at least one element satisfying the angle condition.

Lemma 7.1. *Let N_∞ be the largest index such that*

$$|\sigma_k| = |\langle \nabla J^\delta(u^{m,\delta}), \varphi_k \rangle| \geqslant \varepsilon_\theta \|\nabla J^\delta(u^{m,\delta})\|, \qquad k = 1, \ldots, N_\infty, \tag{7.3}$$

holds. Then, $d = \sum_{k=1}^{N_\infty} \sigma_k \varphi_k \in \Phi_{N_\infty}$ satisfies the angle condition (6.4).

Proof. Since the eigenfunctions φ_k are orthonormal, we have $\|d\|_{L^2(\Omega)} = \|\sigma\|_{\ell^2}$ which yields

$$\begin{aligned}
|\langle \nabla J^\delta(u^{m,\delta}), d \rangle| = \left| \sum_{k=1}^{N_\infty} \sigma_k \langle \nabla J^\delta(u^{m,\delta}), \varphi_k \rangle \right| &= \sum_{k=1}^{N_\infty} |\langle \nabla J^\delta(u^m), \varphi_k \rangle|^2 \\
&\geqslant \varepsilon_\theta \|\nabla J^\delta(u^{m,\delta})\| \sum_{k=1}^{N_\infty} |\langle \nabla J^\delta(u^{m,\delta}), \varphi_k \rangle| \\
&= \varepsilon_\theta \|\nabla J^\delta(u^{m,\delta})\| \|\sigma\|_{\ell^1} \geqslant \varepsilon_\theta \|\nabla J^\delta(u^{m,\delta})\| \|\sigma\|_{\ell^2} \\
&= \varepsilon_\theta \|d\|_{L^2(\Omega)} \|\nabla J^\delta(u^{m,\delta})\|,
\end{aligned}$$

where the inequality follows from (7.3). Thus, the angle condition (6.4) is satisfied for $d = \sum_{k=1}^{N_\infty} \sigma_k \varphi_k \in \Phi_{N_\infty}$. □

Note that for $\varepsilon_\theta < 1$ there always exists $N_\infty \geqslant 1$ sufficiently large such that (7.3) is satisfied.

Lemma 7.2. *Let N_2, be the smallest index such that*

$$\sqrt{\sum_{k=1}^{N_2} |\langle \nabla J^\delta(u^{m,\delta}), \varphi_k \rangle|^2} \geqslant \varepsilon_\theta \|\nabla J^\delta(u^{m,\delta})\| \tag{7.4}$$

Then, $d = \sum_{k=1}^{N_2} \sigma_k \varphi_k \in \Phi_{N_2}$ satisfies the angle condition (6.4).

Proof. Similarly, since the eigenfunctions φ_k are orthonormal, we have

$$\begin{aligned}|\nabla J^\delta(u^{m,\delta})d| &= \sum_{k=1}^{N_2} |\langle \nabla J^\delta(u^{m,\delta}), \varphi_k\rangle|^2 \\ &= \|d\|_{L_2(\Omega)} \sqrt{\sum_{k=1}^{N_2} |\langle \nabla J^\delta(u^{m,\delta}), \varphi_k\rangle|^2} \\ &\geqslant \varepsilon_\theta \|d\|_{L^2(\Omega)} \|\nabla J^\delta(u^{m,\delta})\|,\end{aligned}$$

because of (7.4). Hence, the angle condition (6.4) is satisfied for $d = \sum_{k=1}^{N_2} \sigma_k \varphi_k \in \Phi_{N_2}$. □

We refer to (7.3) as the ℓ^∞-criterion and to (7.4) as the ℓ^2-criterion. If we let

$$N_\theta = \max\{N_\infty, N_2\}, \tag{7.5}$$

we ensure that there exists at least one element in the subspace

$$\Phi_{N_\theta} = \operatorname{span}\{\varphi_1, \ldots, \varphi_{N_\theta}\}$$

that satisfies the newly introduced angle condition (6.4). Clearly, (7.3) is more stringent than (7.4) and thus $N_2 \leqslant N_\infty$. As we only compute in practice a finite number of eigenfunctions φ_k, $1 \leqslant k \leqslant N$, ordered according to their non-decreasing eigenvalues, none might, in fact, satisfy (7.3). Then we set $N_\infty = 0$ and thereby $N_\theta = N_2$ in (7.5). In the unlikely case that no $N_2 \leqslant N$ satisfies (7.4), one needs to increase N until (7.4) holds to ensure the existence of $d \in \Phi_{N_\theta}$ which satisfies (6.4). This yields the full Adaptive Spectral Inversion (ASI) Algorithm below.

Algorithm 6 Adaptive Spectral Inversion

Input:
initial guess $u^{0,\delta}$, search space $\varphi_0^1 + \Psi^1$
set $m = 1$, $\tau_0 \geqslant 1$

Output: reconstruction $u^{m_*,\delta}$

1. **while** $\|\nabla J^\delta(u^{m,\delta})\| \neq 0$ **do**
2. *Minimize* J^δ in the current search space Ψ^m, $\dim \Psi^m = K_m$:

$$u^{m,\delta} = \operatorname*{argmin}_{u \in \varphi_0^m + \Psi^m} J^\delta(u). \tag{7.6}$$

3. *Compute* $\tau_m = {}^1\!/_\delta \|F(u^{m,\delta}) - y^\delta\|_{H_2}$.
4. **if** $\tau_m \leqslant \tau_0$ **then**
5. Discrepancy principle (6.8) is satisfied, return $u^{m_*,\delta} = u^{m-1,\delta}$.
6. *Determine* AS basis Φ^{m+1} and φ_0^{m+1} from $L_\varepsilon[u^{m,\delta}]$ via (4.22) – (4.23).
7. *Merge* AS basis and current search space:
$$\hat{\Psi}^{m+1} = \Psi^m \cup \Phi^{m+1} \cup \{\varphi_0^{m+1} - \varphi_0^m\}.$$
8. *Truncate* $\hat{\Psi}^{m+1}$ while maintaining the accuracy of $u^{m,\delta}$. This yields $\tilde{\Psi}^{m+1}$.
9. *Add sensitivities.* Include AS basis functions $\varphi_k^{m+1} \in \tilde{\Phi}^{m+1} \subset \Phi^{m+1}$ with maximal $|\sigma_k|$ in (7.2). This yields the new search space $\Psi^{m+1} = \tilde{\Psi}^{m+1} \cup \tilde{\Phi}^{m+1}$ with $\dim \Psi^{m+1} = K_{m+1}$.
10. $m \leftarrow m + 1$

By combining the previous search space Ψ^m with promising new search directions determined from the current iterate $u^{m,\delta}$, Steps 6 – 8 construct a low dimensional subspace $\tilde{\Psi}^{m+1}$ capable of representing $u^{m,\delta}$ up to a small error. In Step 9, we then add the basis functions that will likely contribute the most to the reduction of the misfit. Below, we provide a detailed discussion of Steps 6 – 9 of the ASI Algorithm 6.

Step 6: Determine $\varphi_0^{m+1} + \Phi^{m+1}$. Once the minimizer $u^{m,\delta}$ of J^δ in the current search space $\varphi_0^m + \Psi^m$ of dimension $\dim \Psi^m = K_m$ has been found, we we proceed to compute the boundary contribution φ_0^{m+1} and the first few eigenfunctions of the elliptic operator $L_\varepsilon[u^{m,\delta}]$. This involves numerically solving the (linear, symmetric, and positive definite) boundary and eigenvalue problem (4.22) – (4.23)

$$\begin{aligned} L_\varepsilon[u^{m,\delta}]\varphi_0^{m+1} &= 0 && \text{in } \Omega, && \varphi_0 = u_h && \text{on } \partial\Omega, \\ L_\varepsilon[u^{m,\delta}]\varphi_k^{m+1} &= \lambda_k \varphi_k^{m+1} && \text{in } \Omega, && \varphi_k = 0 && \text{on } \partial\Omega \end{aligned}$$

for the first few $k = 1, \dots, K_m$ eigenvalues, ordered with respect to their eigenvalues $0 < \lambda_1 \leqslant \ldots \leqslant \lambda_{K_m}$. This yields the new boundary contribution and AS basis,

$$\varphi_0^{m+1} \quad \text{and} \quad \Phi^{m+1} = \operatorname{span}\left\{\varphi_1^{m+1}, \dots, \varphi_{K_m}^{m+1}\right\}.$$

Here, we arbitrarily set the dimension of Φ^{m+1} to that of Ψ^m, though any other sufficiently large number of eigenfunctions could be chosen.

Step 7: Merge. Next we merge the previous search space Ψ^m with Φ^{m+1} and φ_0^{m+1} as

$$\begin{aligned}\hat{\Psi}^{m+1} &= \Psi^m \cup \Phi^{m+1} \cup \{\varphi_0^{m+1} - \varphi_0^m\} \\ &= \Psi^m + \operatorname{span}\left\{\varphi_0^{m+1} - \varphi_0^m, \varphi_1^{m+1}, \dots, \varphi_{K_{m+1}}^{m+1}\right\}.\end{aligned}$$

We then compute an L^2-orthonormal basis $\hat{\psi}_k$, $k = 1, \dots, \hat{K}_{m+1}$, of $\hat{\Psi}^{m+1}$ using modified Gram-Schmidt to obtain

$$\hat{\Psi}^{m+1} = \operatorname{span}\left\{\hat{\psi}_1, \dots, \hat{\psi}_{\hat{K}_{m+1}}\right\}.$$

Therefore, the previous minimizer $u^{m,\delta} \in \varphi_0^m + \Psi^m$ lies also in $\varphi_0^{m+1} + \hat{\Psi}^{m+1}$, i.e. $u^{m,\delta} \in \varphi_0^{m+1} + \hat{\Psi}^{m+1}$. However, since the dimension $\dim \hat{\Psi}^{m+1} = \hat{K}_{m+1}$ may become too large with every iteration, we now need to truncate $\hat{\Psi}^{m+1}$ to keep the number of control variables small.

Step 8: Truncate. To truncate $\hat{\Psi}^{m+1}$ and retain only the basis functions $\hat{\psi}_k$ essential to the contribution of $u^{m,\delta} - \varphi_0^{m+1}$, we proceed in two steps. First, we compute an indicator v close to $u^{m,\delta} - \varphi_0^{m+1}$, but has minimal TV-"energy", to remove noise and preserve edges. Instead of minimizing the TV-functional $\mathrm{TV}(v) = \int |\nabla v|$, which results in a nonlinear optimization problem, we keep the computational costs low by minimizing the linearized TV-functional (4.29). Thus, the indicator v satisfies

$$\begin{aligned}\min_{v \in \hat{\Psi}^{m+1}} \quad & \int_\Omega \mu_\varepsilon[u^{m,\delta}] |\nabla v|^2 \\ \text{s.t.} \quad & \|v - (u^{m,\delta} - \varphi_0^{m+1})\|_{L^2(\Omega)} \leqslant \varepsilon_\Psi \|u^{m,\delta} - \varphi_0^{m+1}\|_{L^2(\Omega)},\end{aligned} \tag{7.7}$$

for a prescribed truncation tolerance $\varepsilon_\Psi > 0$; typically set to $\varepsilon_\Psi = 5\%$. Since (7.7) is a quadratic optimization problem with quadratic inequality constraints, computing v is cheap and efficient.

Second, we reduce the dimension of $\hat{\Psi}^{m+1}$ by discarding all basis functions that do not significantly contribute much to the indicator v. Let γ_k denote the Fourier coefficients γ_k of v,

$$\gamma_k = (v, \hat{\psi}_k)_{L^2(\Omega)}, \qquad k = 1, \dots, \hat{K}_{m+1},$$

sorted in decreasing order and sort the L^2-orthonormal basis functions $\hat{\psi}_k^{m+1}$ accordingly. Next, we determine the index N_0 by

$$N_0 = \min \left\{ 1 \leqslant K \leqslant \hat{K}_{m+1} : \sum_{k=K+1}^{\hat{K}_{m+1}} \gamma_k^2 \leqslant {\varepsilon_\Psi}^2 \|\gamma\|_{\ell^2}^2 \right\},$$

to ensure that the relative L^2-error in the Fourier expansion truncated at N_0 is below ε_Ψ. To avoid drastic changes in the dimension of the search space, we now calculate $\rho = N_0/K_m$. For given ρ_0, ρ_1, where $0 < \rho_0 \leqslant 1 \leqslant \rho_1$ (typically $\rho_0 = 0.8$ and $\rho_1 = 1.2$), we choose the dimension $\tilde{K}_{m+1}$ of the truncated space $\tilde{\Psi}^{m+1}$ as follows:

(i) If $\rho \in [\rho_0, \rho_1]$, set $\tilde{K}_{m+1} = N_0$.

(ii) If $\rho < \rho_0$, the dimension decreases too fast. Set $\tilde{K}_{m+1} = \lceil \rho_0 K_m \rceil$ and halve ε_Ψ to avoid a rapid decrease in the dimension at the next iteration.

(iii) If $\rho > \rho_1$, the dimension increases too fast. Set $\tilde{K}_{m+1} = \lceil \rho_1 K_m \rceil$ and double ε_Ψ to avoid a rapid increase in the dimension at the next iteration.

This yields the truncated space as $\tilde{\Psi}^{m+1} = \operatorname{span}\left\{\hat{\psi}_1, \dots, \hat{\psi}_{\tilde{K}_{m+1}}\right\}$.

Step 9: Add sensitivities. Finally, we determine the most sensitive AS basis functions

$$\tilde{\Phi}^{m+1} = \operatorname{span}\{\varphi_1, \dots, \varphi_{N_\theta}\}$$

from Φ^{m+1}, reordered according to their sensitivities $|\sigma_k|$ as in (7.2). To determine N_θ, we use the ℓ^∞- and ℓ^2-criteria (7.3) and (7.4) from Lemmas 7.1 and 7.2, respectively. In the unlikely event that the AS space Φ^{m+1} from Step 6 contains no eigenfunction that satisfies (7.3) or (7.4), we can either increase the dimension of Φ^{m+1} or set $\tilde{\Phi}^{m+1} = \emptyset$, thus simply proceed. By combining $\tilde{\Psi}^{m+1}$ and $\tilde{\Phi}^{m+1}$, we obtain the subsequent search space

$$\Psi^{m+1} = \tilde{\Psi}^{m+1} \cup \tilde{\Phi}^{m+1} = \operatorname{span}\left\{\psi_1, \dots, \psi_{K_{m+1}}\right\}.$$

Now, we can proceed and seek a minimizer $u^{m+1,\delta}$ of J^δ in the affine search space $\varphi_0^{m+1} + \Psi^{m+1}$.

Note that the sensitivity based selection procedure in Step 9 only ensures that the angle condition (6.4) is satisfied by at least one element in $\tilde{\Phi}^{m+1} \subset \Psi^{m+1}$. However, it does not guarantee that the correction $d^{m,\delta} = u^{m+1,\delta} - u^{m,\delta}$ itself satisfies the condition (7.1) at every iteration. If we specifically require $d^{m,\delta}$ to satisfy the angle condition at each iteration, we would have to verify (7.1) for every m and potentially reject the new minimizer of (7.6) if the condition is not met. This would result in the need to choose a new search space, possibly leading to a further increase in the search space dimension. Instead, Lemmas 7.1 and 7.2 guarantee that at least one element in the search space satisfies the angle condition, thereby making it rather likely that it will also be satisfied by the correction $d^{m,\delta}$.

Remark 5. *In the above Adaptive Spectral Inversion (ASI) Algorithm, Steps 1 – 8 correspond to the ASI Algorithm previously introduced in [11]. This previous ASI Algorithm, however, did not include the growth control (iii) on the dimension K_{m+1} in Step 8. Step 9, however, where further eigenfunctions are included based on their sensitivites* (7.2)*, is new and will prove crucial for detecting even small-scale features in the medium. Henceforth, we denote by ASI_0 the above ASI Algorithm without Step 9, similar to the one from [11], to distinguish it from the present ASI Algorithm.*

The History of the Adaptive Spectral Inversion

This section is dedicated to the history of the Adaptive Spectral Inversion, from its origins, refinements, and to its current version as given by Algorithm 6.

De Buhan and Osses [29] first restricted the search space Ψ^m in each iteration m to the eigenfunctions of an elliptic operator that depends on the medium $u^{m,\delta}$ to solve the inverse problems (6.3). More precisely, in the context of Chapter II, they considered

$$L[u^{m,\delta}]v = -\nabla \cdot (\mu[u^{m,\delta}]\nabla v), \qquad \mu[u^{m,\delta}] = \frac{1}{|\nabla u^{m,\delta}|},$$

without any ε-dependency, to obtain the eigenfunctions for the subsequent search space Ψ^{m+1}. However, as $L[u^{m,\delta}]$ did not depend on the fixed parameter $\varepsilon > 0$, this could lead to an ill-posed operator for small gradients of $u^{m,\delta}$. After obtaining the minimizer, they dismissed the entire search space and constructed the subsequent search space by newly computing the eigenfunctions of $L[u^{m,\delta}]$. Despite referring to the method as *an adaptive method*, they only recomputed new eigenfunctions in each iteration but kept its dimension constant.

In [28], De Buhan and Kray first introduced the fixed but small parameter $\varepsilon > 0$ to the elliptic operator $L_\varepsilon[u^{m,\delta}]$ to avoid problems whenever the gradient

becomes close to zero, see [28, Remark in Section 3.3] They achieved this by using the weight function

$$\mu_\varepsilon[u^{m,\delta}] = \max(|\nabla u^{m,\delta}|, \varepsilon)^{-q}, \qquad q \geqslant 1,$$

and then obtained the new search space by the first few eigenfunctions of $L_\varepsilon[u^{m,\delta}]$. The authors then applied this found search space together with the TRAC method to solve an inverse problem for the wave equation without adapting the dimension of each search space and referred to this method as the *Adaptive Inversion* (AI). Later, de Buhan and Darbas applied this method to the time-harmonic Maxwell equation at a fixed frequency [27] and referred to it as the *Adaptive Eigenspace Inversion* (AEI) method.

Grote, Kray, and Nahum took the first step in adapting the number of basis functions used in the AEI method, c.f. [48], where they solved the inverse scattering problem for the Helmholtz equation using frequency stepping, increasing the number of basis functions linearly with every frequency. There, the authors discovered the connection of L_ε given by (4.4) with the gradient of the regularized TV functional, c.f. [48, Remark 1] and Chapter II. Later, Grote and Nahum applied the AEI from [48] to multi-parameter inversion, also comparing different elliptic operators, not necessarily of the form (4.21), to obtain the eigenfunctions that span the search space.

In [11], Baffet, Grote, and Tang introduced a fully adaptive basis choice criterion, resulting in the *Adaptive Spectral Inversio* (ASI). The idea was to construct a new search space, by combing the old search space with new eigenfunctions obtained from the AS operator $L_\varepsilon[u^{m,\delta}]$, ensuring that the current iterate $u^{m,\delta}$ is "well represented" in the new search space, while maintaining a low dimension. This algorithm essentially corresponds to Steps 1 – 8 in Algorithm 6. However, they did not include item (iii) from Step 8, thus the search space could grow arbitrarily fast.

The newly introduced ASI Algorithm 6 now prevents the search space from a fast growth of dimension by employing Step 8 (iii). Additionally, it incorporates the new key angle condition introduced in Step 9, where further eigenfunctions are included based on their sensitivities (7.2). This will prove crucial for detecting small-scale features located inside the medium.

Chapter 8

Numeric Examples

To illustrate the accuracy and usefulness of the ASI Algorithm introduced in Section 7, we shall now apply it to two inverse medium problems of the form: Find $u \in H_1, y \in H_2$ that satisfy

$$\begin{aligned} \min_{u,y} \quad & \frac{1}{2}\|y - y^\delta\|_{H_2}^2 \\ \text{s.t.} \quad & A[u]y - f = 0, \end{aligned} \tag{8.1}$$

for a given source f and noisy data $y^\delta \in H_2$ as in (6.1). Each inverse problem is governed by a distinct *forward problem* (8.1) whose solution, for any given medium u, is $y = A[u]^{-1}f$. Thus, we can eliminate the constraints in (8.1) to obtain the reduced misfit J^δ as in (3.30) from Section 3.2, which leads to the equivalent unconstrained minimization problem: Find $u^{\dagger,\delta} \in H_1$ such that

$$u^{\dagger,\delta} = \operatorname*{argmin}_{u \in H_1} \frac{1}{2}\|y[u] - y^\delta\|_{H_2}^2. \tag{8.2}$$

For each inverse problem, we aim to recover separately the two different (unknown) media $u^\dagger$ shown in Figure 8.1, by applying the ASI Algorithm 6 to (8.2) The first consists of six disks, each with a different value and radius. The second consists of three inclusions: An open wedge with a sharp 90° interior angle, making it non-convex with a piecewise smooth boundary, a convex drop-like inclusion with a sharp tip, and a kite-shaped inclusion, both non-convex with smooth boundaries.

In all cases, we apply the ASI Algorithm 6 from Section 7 with the following fixed parameter settings:

$$\rho_0 = 0.8, \quad \rho_1 = 1.2, \quad \varepsilon_\theta = 10^{-4}, \quad \varepsilon_\Psi = 0.05, \quad \tau_0 = 1.$$

As an initial guess, we always choose $u^{0,\delta} = 1$ constant. We also set the initial search space Ψ^1 to be the first K_1 L^2-orthonormal eigenfunctions of the Laplacian,

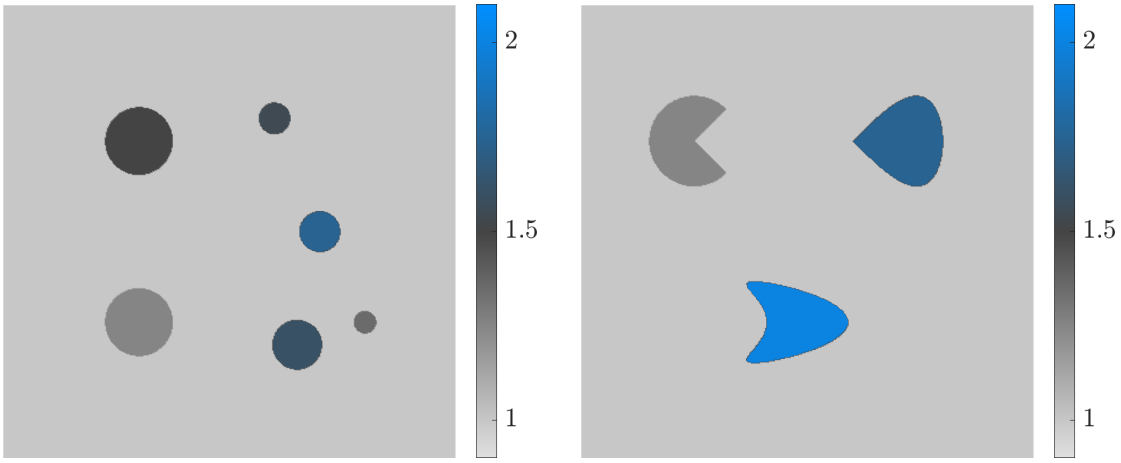

Fig. 8.1: Inverse Problem: The two distinct media $u^\dagger$ used in the numerical experiments. Left: six disks; right: three inclusions.

sorted in non-decreasing order with respect to their eigenvalues. Here, we choose $K_1 = 100$ for problem 8.1 and $K_1 = 50$ for problem 8.2.

To assess the accuracy of the ASI method, we shall monitor the following quantities: The dimension K_m of the search space Ψ^m, the relative error

$$e_m = \frac{\|u^{m,\delta} - u^\dagger\|_{H_1}}{\|u^\dagger\|_{H_1}}, \tag{8.3}$$

the ratio τ_m from the discrepancy principle, determined in Step 3,

$$\tau_m = \frac{\|y[u^{m,\delta}] - y^\delta\|_{H_2}}{\delta}, \tag{8.4}$$

and the total number of iterations m_*, where $m = m_* + 1$ is the first index such that $\tau_m \leqslant \tau_0$; hence, the discrepancy principle (6.8) is then satisfied with $\tau = \tau_{m_*}$. Note that $\tau_{m_*} \approx \tau_0 = 1$ implies that $u^{m_*,\delta}$ (nearly) yields an optimal data misfit since $\|y^\dagger - y^\delta\|_{H_2} \leqslant \delta$.

8.1 Elliptic Inverse Problem

First, we consider the forward problem described by the elliptic differential equation

$$\begin{aligned} -\nabla \cdot (u(\mathbf{x})\nabla y(\mathbf{x})) &= f(\mathbf{x}), && \mathbf{x} \in \Omega, \\ y(\mathbf{x}) &= 0, && \mathbf{x} \in \partial\Omega, \end{aligned} \tag{8.5}$$

from Section 1.2.1, with $\Omega = (0,1)^2$, constant right hand side $f = 100$, and $H_1 = H_2 = L^2(\Omega)$; Since $H_1 = L^2(\Omega)$, the observations y^δ are available throughout Ω. In [65, 66, 106], the one-dimensional version of (8.5) was considered and shown to satisfy the Scherzer condition (6.10), see Theorem 6.4.

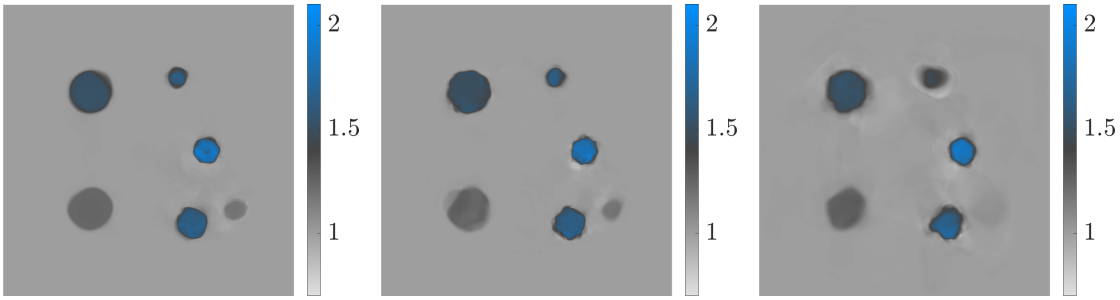

(a) ASI: $u^{m_*,\delta}$ for $\hat{\delta} = 1\%$ **(b)** ASI: $u^{m_*,\delta}$ for $\hat{\delta} = 2\%$ **(c)** ASI: $u^{m_*,\delta}$ for $\hat{\delta} = 5\%$

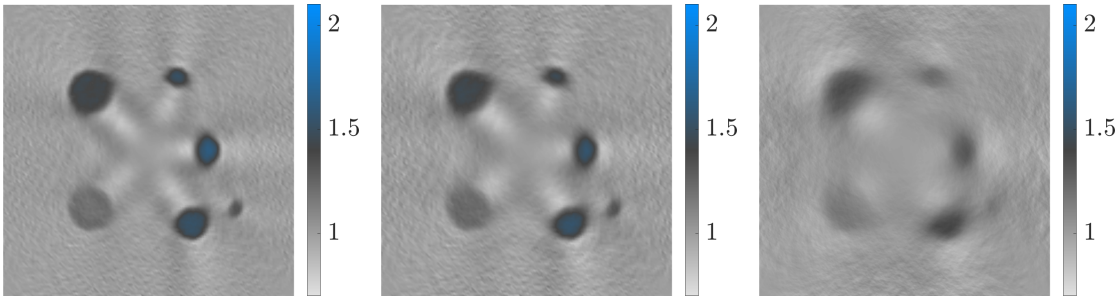

(d) Tikhonov: $u^{m_*,\delta}$for $\hat{\delta} = 1\%$ **(e)** Tikhonov: $u^{m_*,\delta}$for $\hat{\delta} = 2\%$ **(f)** Tikhonov: $u^{m_*,\delta}$for $\hat{\delta} = 5\%$

Fig. 8.2: Elliptic inverse problem, six disks: Reconstructed media using the ASI method (top) or standard L^2-Tikhonov regularization (bottom) for different noise levels $\hat{\delta}$.

Here, we compare the ASI Algorithm 6 from Section 7 with a standard grid based inversion method using Tikhonov regularization introduced in Section 3.1.3. To solve the forward problem (8.5), we employ a Galerkin piecewise linear $\mathbb{P}^1$ finite element discretization, thus $V^h = \mathcal{P}^1$, where both u and y are approximated using the same triangular mesh with vertices located on a 400×400 equidistant Cartesian grid.

Hence, we omit the index $u_h, y_h \in V^h$ and simply denote $u, y \in V^h$. Although the finite element representation involves a large number of degrees of freedom (nDof $= 160'000$), we recall that the ASI Algorithm determines the m-th iterate only in the much smaller subspace Ψ^m of dimension K_m. In the m-th step of the ASI Algorithm, we determine the minimizer $u^{m,\delta}$ of (7.6) using standard BFGS along with Armijo, instead of Wolfe-Powell line search, to keep the number of (expensive) gradient evaluation small, as outlined in Section 2.4.

For the standard Tikhonov L^2-regularization approach, we minimize

$$\min_{u\in L^2(\Omega)} \frac{1}{2}\|y[u]-y^\delta\|^2_{L^2(\Omega)} + \frac{\alpha}{2}\|u\|^2_{L^2(\Omega)}, \tag{8.6}$$

where $\alpha > 0$ denotes the regularization parameter. Due to the resulting large number of unknowns, we now solve (8.6) using standard *limited memory BFGS* (L-BFGS) together with Armijo line search as in Algorithm 3. Following Section 3.1.4, we set the regularization parameter $\alpha_n = 2^{-n}$ at the n-th L-BFGS iteration, as proposed in (3.20).

To avoid any potential inverse crime, the exact data $y^\dagger = y[u^\dagger]$ was computed from a 20% finer mesh and perturbed at each grid point $\mathbf{x}_j$ by

$$y^\delta(\mathbf{x}_j) = y^\dagger(\mathbf{x}_j) + \hat{\delta}\xi_j \qquad \forall \mathbf{x}_j \in \Omega$$

for the *noise level* $\hat{\delta} \geqslant 0$, where $(\xi_j)_j$ is a multivariate random variable with $\xi_j = \eta_j/\|\eta\|_{L^2(\Omega)}$ and η_j are i.i.d. Gaussian random variables with mean zero and variance one. Hence the data misfit satisfies exactly

$$\|y^\dagger - y^\delta\|_{L^2(\Omega)} = \hat{\delta} = \delta.$$

Tab. 8.1: Elliptic inverse problem, six disks: The relative error e_{m_*}, the total number of iterations m_*, the dimension K_{m_*}, and the ratio τ_{m_*} from the discrepancy principle of the search space are shown for the ASI method and L^2-Tikhonov regularization.

Method	ASI				L^2-regularization			
$\delta = \hat{\delta}$	1%	2%	5%	10%	1%	2%	5%	10%
e_{m_*}	2.7%	2.8%	3.9%	5.3%	5.3%	6.1%	8.0%	8.7%
m_*	50	19	15	10	5.3	39	15	11
K_{m_*}	67	95	76	51		nDof = 160′000		
τ_{m_*}	1.005	1.0001	1.000	1.0003	1.000	1.0008	1.005	1.001

Table 8.1 compares the relative error e_{m_*}, dimension K_{m_*} of the search space Ψ^{m_*}, and the ratio τ_{m_*} at the final iteration m_* for both, the ASI method and L^2-Tikhonov regularization. As expected, both methods require fewer iterations m_* to achieve (6.8) as the noise level $\hat{\delta}$ increases, while the relative error obtained by the ASI method is consistently smaller than that achieved by standard L^2-Tikhonov regularization. Even with $\delta = 10\%$ the ASI method yields a smaller relative error than standard Tikhonov regularization for smaller noise δ. In Figure 8.2, we

compare the reconstructed media $u^{m_*,\delta}$ obtained from both methods. Clearly, the ASI method yields reconstructions with sharper contrasts, crisper edges, and more accurate coefficients inside each disk. Moreover, the results from L^2-Tikhonov regularization display a noisy background and less accurate reconstructions of the coefficients inside the inclusions. Remarkably, the ASI method achieves better reconstructions, only using as few as $K_{m_*} = 100$ control variables, in contrast to grid based Tikhonov regularization, which involves over 160′000 unknowns.

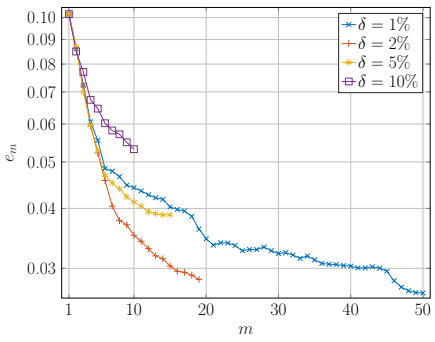

(a) relative L^2-error e_m

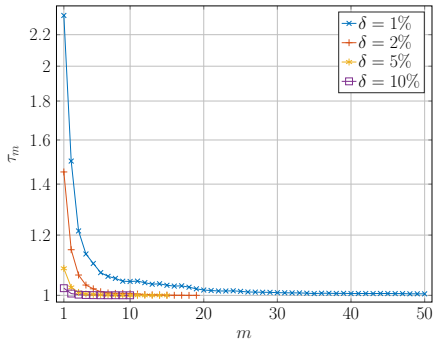

(b) ratio τ_m from the discrepancy principle

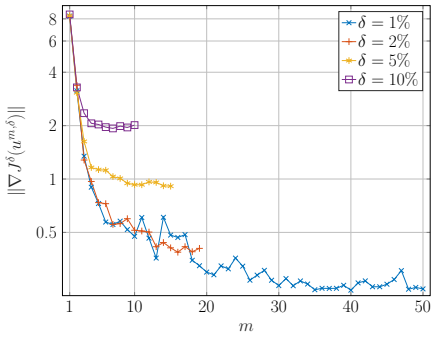

(c) $\|\nabla J(u^{m,\delta})\|$

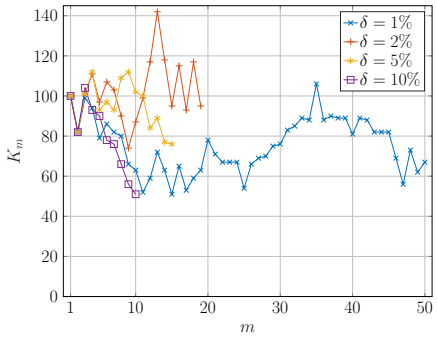

(d) dimension K_m

Fig. 8.3: Elliptic inverse problem, six disks: The relative error (8.3), the ratio τ_m from the discrepancy principle (8.4), the norm of the gradient, and the dimension of the search space at iteration m for different noise levels δ.

From Figure 8.3 we observe that the relative error e_m and $\|\nabla J^\delta(u^{m,\delta})\|$ decrease throughout all iterations, as expected from Theorem 6.1 in Section 6. Furthermore, τ_m tends to 1 until stopped by the discrepancy principle (6.8). Note that the dimension K_m, or equivalently the number of control variables, remains small for the ASI method regardless of δ. This keeps the computational effort low while achieving accurate reconstructions.

Next, we consider the inverse problem for the (unknown) medium $u^\dagger$ depicted in the right frame of Figure 8.1, which consists of three distinct inclusions. Again, the

ASI Algorithm from Section 7 successfully recovers the true medium at the various noise levels δ, as illustrated in Figure 8.4: all three inclusions are clearly visible with well defined contrast and sharp edges, except for the reentrant corner of the open wedge with 5% noise. On the other hand, the L^2-Tikhonov regularization method yields more noisy and blurred reconstructions, where the inclusions become hardly visible beyond 5% noise.

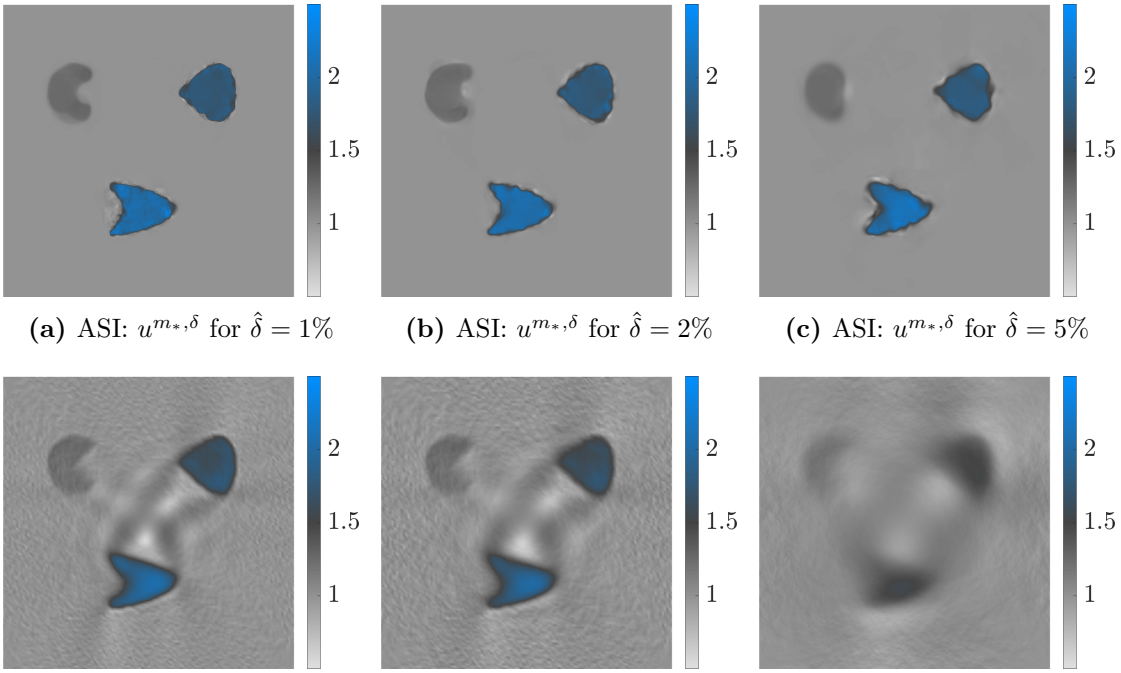

(a) ASI: $u^{m_*,\delta}$ for $\hat{\delta} = 1\%$ **(b)** ASI: $u^{m_*,\delta}$ for $\hat{\delta} = 2\%$ **(c)** ASI: $u^{m_*,\delta}$ for $\hat{\delta} = 5\%$

(d) Tikhonov: $u^{m_*,\delta}$ for $\hat{\delta} = 1\%$ **(e)** Tikhonov: $u^{m_*,\delta}$ for $\hat{\delta} = 2\%$ **(f)** Tikhonov: $u^{m_*,\delta}$ for $\hat{\delta} = 5\%$

Fig. 8.4: Elliptic inverse problem, three inclusions: Reconstructed medium using the ASI method (top) or standard L^2-Tikhonov regularization (bottom) for different noise levels $\hat{\delta}$.

From Table 8.2, we again conclude that the relative error e_{m_*} of the ASI method alway remains below that obtained with L^2-Tikhonov regularization. Even with $\delta = 10\%$ noise, the ASI method proves to be more accurate than L^2-Tikhonov regularization with as little as 1% noise. Moreover, the number of control variables K_{m_*} used in the ASI method never exceeds 160, in comparison to approximately 160′000 control variables used in the nodal FE representation for L^2-Tikhonov regularization. As a consequence, the computational effort of the ASI method always remains significantly lower than that with standard Tikhonov regularization.

In Figure 8.5, we observe that the relative error e_m and $\|\nabla J(u^{m,\delta})\|$ decrease with each iteration, while simultaneously the ratio τ_m tends to 1. Also, the number of basis functions K_m of the search space Ψ^m, i.e. the number of control variables,

remains small, which again translates to a low computational effort.

Tab. 8.2: Elliptic inverse problem, three inclusions: The relative error e_{m_*}, the total number of iterations m_*, the dimension K_{m_*}, and the ratio τ_{m_*} from the discrepancy principle of the search space are shown for the ASI method and L^2-Tikhonov regularization.

Method	ASI				L^2-regularization			
$\delta = \hat{\delta}$	1%	2%	5%	10%	1%	2%	5%	10%
e_{m_*}	3.3%	3.7%	5.0%	6.4%	7%	8.3%	12.9%	13.0%
m_*	50	25	12	8	69	48	15	15
K_{m_*}	153	120	110	72	nDof = 160′000			
τ_{m_*}	1.001	1.0001	1.0001	1.000	1.0004	1.0001	1.029	1.0014

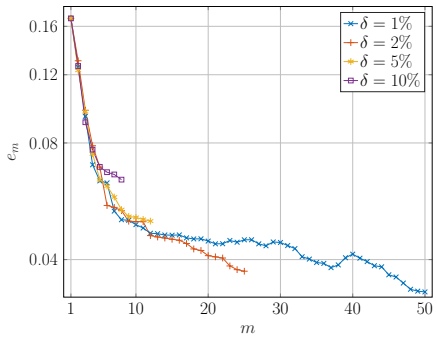

(a) relative L^2-error e_m

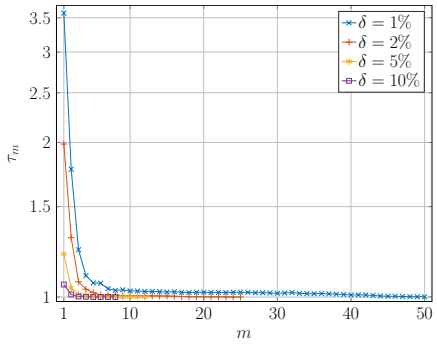

(b) ratio τ_m from the discrepancy principle

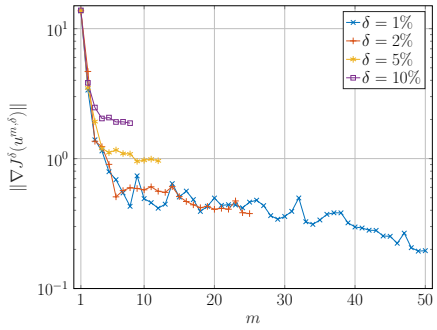

(c) $\|\nabla J(u^{m,\delta})\|$

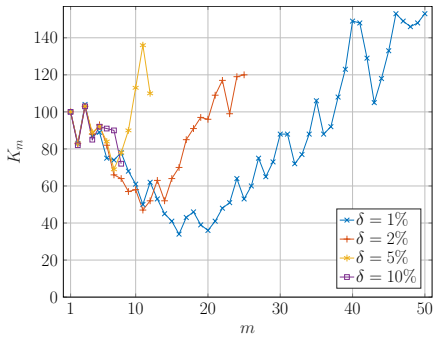

(d) dimension K_m

Fig. 8.5: Elliptic inverse problem, three inclusions: The relative error (8.3), the ratio τ_m from the discrepancy principle (8.4), the norm of the gradient, and dimension of the search space, for every iteration m for different noise levels $\hat{\delta} > 0$.

8.2 Time Dependent Inverse Scattering Problem

Next, we consider wave scattering from an unknown spatially distributed medium illuminated by surrounding point sources. Hence, the forward problem (8.1) now corresponds to the time dependent wave equation in $\Omega = (0,1)^2$,

$$\begin{aligned} \frac{\partial^2}{\partial t^2} y_\ell(\mathbf{x},t) - \nabla \cdot (u(\mathbf{x}) \nabla y_\ell(\mathbf{x},t)) &= f_\ell(\mathbf{x},t), && \mathbf{x} \in \Omega,\ t \in (0,T), \\ y_\ell(\mathbf{x},0) = \tfrac{\partial}{\partial t} y_\ell(\mathbf{x},0) &= 0, && \mathbf{x} \in \Omega, \\ \tfrac{\partial}{\partial t} y_\ell(\mathbf{x},t) + \sqrt{u(\mathbf{x})}\, \tfrac{\partial}{\partial n} y_\ell(\mathbf{x},t) &= 0, && \mathbf{x} \in \partial\Omega,\ t \in (0,T), \end{aligned} \tag{8.7}$$

with homogeneous initial conditions and first order absorbing boundary conditions as introduced in Section 1.2.2. Here, u denotes the squared wave speed whereas the sources $f_\ell(\mathbf{x},t) = g_\ell(\mathbf{x}) r(t)$, $\ell = 1, \dots, N_s$, correspond to smoothed Gaussian point sources

$$g_\ell(\mathbf{x}) = \kappa e^{\frac{(\mathbf{x}-\mathbf{x}_\ell)^2}{s}}, \qquad \mathbf{x} \in \Omega,$$

in space, centered about distinct locations $\mathbf{x}_\ell \in \Omega$, with $s = 10^{-2}$ and $\kappa = 200$, and a Ricker wavelet [28, 77] in time,

$$r(t) = (1 - 2\pi^2(\nu - t)^2) e^{-\pi^2(\nu t - 1)^2}, \qquad t \in [0,T],$$

with central frequency $\nu = 10$. In Figure 8.6, snapshots of the solution to the forward problem (8.7) are shown at different times for the source located at the top left corner.

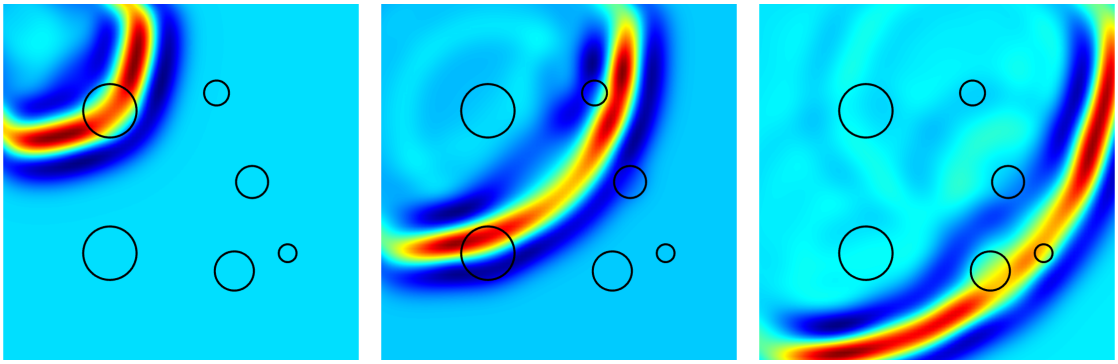

(a) $t = 0.4$ **(b)** $t = 0.7$ **(c)** $t = 1.0$

Fig. 8.6: Wave equation: Snapshots of the solution to the wave equation (8.7).

To generate the (synthetic) observations, we now place $N_s = 32$ sources located at $\mathbf{x}_\ell$ equidistributed near the boundary and illuminate the medium, one source at a time. In contrast to the previous example from Section 8.1, here the data y_ℓ^δ is only available at the boundary, yet for all $t \in (0, T)$ until the final time $T = 2$, when the incident wave has essentially left Ω. Hence, we set $H_1 = L^2(\Omega)$ and $H_2 = L^2(\partial\Omega \times (0, T))$ in (8.2). Thus, the misfit

$$J^\delta(u) = \frac{1}{2} \sum_{\ell=1}^{N_s} \|y_\ell[u] - y_\ell^\delta\|^2_{L^2(\partial\Omega\times(0,T))} \tag{8.8}$$

now accounts for the data y_ℓ^δ from multiple sources $\ell = 1, \dots, N_s$.

The forward problem (8.7) is solved by a standard Galerkin FE-method, where we again discretize u in V^h using $\mathcal{P}^1$-FE on a triangular mesh with vertices located on a 400×400 equidistant Cartesian grid. To discretize y in (8.7), we let $\tilde{V}^h$ be the FE space $\mathcal{P}^2_b$, the piecewise quadratic $\mathbb{P}^2$-FE space with bubble function $b \in \mathbb{P}^3$ to ensure mass lumping, see Section 2.2.2. However, we employ a separate triangular mesh with about 10 elements per wavelength, resulting in approximately 60′000 nodes. For the time integration, we use the standard (fully explicit) leap frog method with time step $\Delta t \approx 4.5 \cdot 10^{-4}$. Similar to the previous section, we may simply write $u \in V^h$ and, for every time step $t_n = n\Delta t$, $t = 0, \dots, N_T$, denote the fully discrete solution to (8.7) by $y_\ell(\cdot, t_n) \in \tilde{V}^h$, see also Section 2.3.

To avoid any potential inverse crime, the exact data $y_\ell^\dagger = y_\ell[u^\dagger]$ was computed from a 20% finer mesh. The perturbed (noisy) data y_ℓ^δ at each grid point $\mathbf{x}_j$ and time step t_n was then obtained via multiplicative noise, motivated by [25, 28], as

$$y_\ell^\delta(\mathbf{x}_j, t_n) = y_\ell^\dagger(\mathbf{x}_j, t_n) \left((1 + \hat{\delta}(\eta_\ell)_{j,n}\right) \qquad \forall (\mathbf{x}_j, t_n) \in \Omega \times (0, T)$$

for the noise level $\hat{\delta} \geqslant 0$. Here $(\eta_\ell)_{j,n}$ corresponds to normally distributed Gaussian noise. Thus

$$\sum_{\ell=1}^{N_s} \|y_\ell^\dagger - y_\ell^\delta\|_{L^2(\partial\Omega\times(0,T))} \leqslant \delta, \qquad \delta \geqslant 0.$$

To reduce computational cost during the inverse iteration, we do not minimize (8.8) directly, but instead use a standard *sample average approximation* (SAA) [53]: at each iteration, we combine all sources f_ℓ into a single "super-shot" f^m,

$$f^m = \sum_{\ell=1}^{N_s} \xi_\ell^m f_\ell,$$

where $\xi_\ell^m = \pm 1$ follow a Rademacher distribution with zero mean, resampled after each iteration m. Consequently, at each iteration m, we solve the minimization

problem

$$\min_{u\in\Psi^m} \frac{1}{2}\|y[u] - y^{m,\delta}\|_{L^2(\Gamma\times(0,T))},$$

with corresponding boundary observations

$$y^{m,\delta} = \sum_{\ell=1}^{N_s} \xi_\ell^m y_\ell^\delta.$$

Tab. 8.3: Inverse scattering problem, six disks: The relative error e_{m_*}, the total number of iterations m_*, the dimension K_{m_*}, and the ratio τ_{m_*} from the discrepancy principle of the search space are shown for the ASI and ASI_0 method.

Method	ASI				ASI_0			
$\hat{\delta}$	1%	2%	5%	10%	1%	2%	5%	10%
e_{m_*}	2.6%	2.4%	2.0%	1.8%	2.4%	3.4%	4.4%	3.2%
m_*	50	48	50	32	50	50	31	49
K_{m_*}	81	133	85	69	83	28	57	83
τ_{m_*}	1.076	1.006	1.0003	1.0001	1.047	1.26	1.061	1.017
δ	0.18%	0.35%	0.88%	1.76%	0.18%	0.35%	0.88%	1.76%

First, we compare the ASI Algorithm from Section 7 with the former ASI_0 Algorithm. In the ASI_0 Algorithm, we omit Step 9 and thus ignore the most sensitive AS basis functions required for the angle condition (see Remark 5). We consider the (unknown) medium $u^\dagger$ consisting of six disks shown in Figure 8.1, where we observe from Table 8.3 that the ASI and ASI_0 Algorithms perform similarly in terms of the relative error e_{m_*} and dimension of the search space K_{m_*}. However, when we compare the reconstructed media $u^{m_*,\delta}$ from Figure 8.7, we see that the ASI_0 Algorithm (Figures 8.7 (d) – (f)) fails to reconstruct the smallest disk with increasing noise. In contrast, the ASI Algorithm (Figures 8.7 (a) – (c)) consistently recovers even the smallest disk.

In Figure 8.8, we observe that the relative error e_m decreases throughout all iterations, while the number of control variables K_m remains small, which effectively keeps the overall computational cost low. As expected from Theorem 6.1, the norm of the gradient $\|\nabla J^\delta(u^{m,\delta})\|$ decreases and the ratio τ_m from the discrepancy principle (8.4) tends to 1.

Finally, we consider the medium $u^\dagger$ shown in Figure 8.1 with three geometric inclusions. As shown in Figure 8.9, the ASI Algorithm recovers the shape and

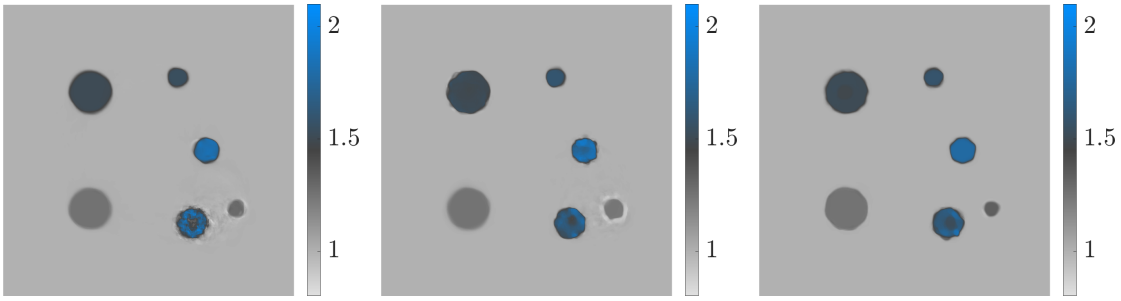

(a) ASI: $u^{m_*,\delta}$ for $\hat{\delta} = 1\%$ **(b)** ASI: $u^{m_*,\delta}$ for $\hat{\delta} = 2\%$ **(c)** ASI: $u^{m_*,\delta}$ for $\hat{\delta} = 5\%$

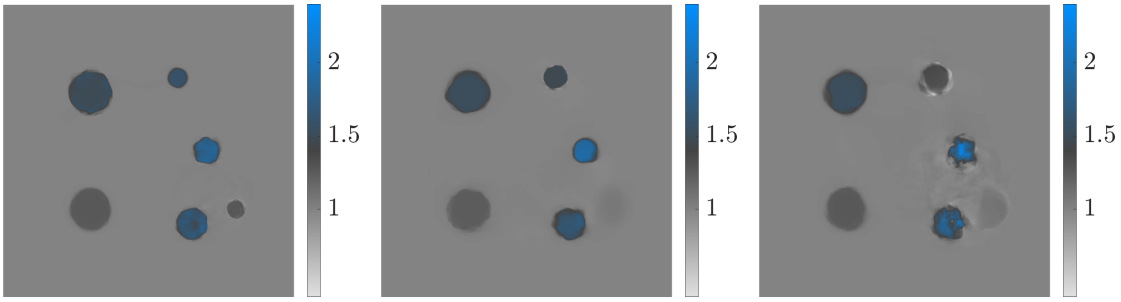

(d) ASI_0: $u^{m_*,\delta}$ for $\hat{\delta} = 1\%$ **(e)** ASI_0: $u^{m_*,\delta}$ for $\hat{\delta} = 2\%$ **(f)** ASI_0: $u^{m_*,\delta}$ for $\hat{\delta} = 5\%$

Fig. 8.7: Inverse scattering problem, six disks: Comparison of ASI (top) and ASI_0 (bottom) for different noise levels $\hat{\delta}$.

Tab. 8.4: Inverse scattering problem, three inclusions: The relative error e_{m_*}, the total number of iterations m_*, the dimension K_{m_*}, and the ratio τ_{m_*} from the discrepancy principle of the search space are shown for the ASI method.

Method	ASI			
$\hat{\delta}$	1%	2%	5%	10%
e_{m_*}	4.0%	3.4%	3.2%	3.4%
m_*	50	49	50	50
K_{m_*}	114	83	61	45
τ_{m_*}	1.075	1.015	1.005	1.002
δ	0.18%	0.35%	0.88%	1.46%

height of all three inclusions with high fidelity and regardless of the noise level $\hat{\delta}$. In Table 8.4 and Figure 8.10, we observe that the relative error e_m consistently remains low for all $\hat{\delta}$ and decreases throughout all iterations. Again, the ratio τ_m from (8.4) tends to 1 while $\|\nabla J^\delta(u^{m,\delta})\|$ decreases. Notably, for all noise levels

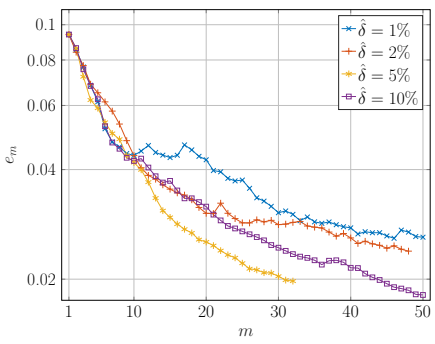

(a) relative L^2-error e_m

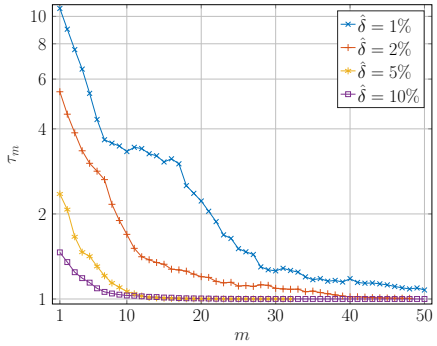

(b) ratio τ_m from the discrepancy principle

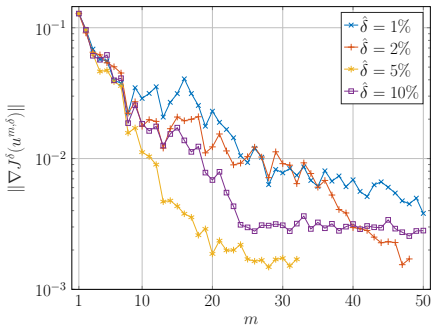

(c) $\|\nabla J(u^{m,\delta})\|$

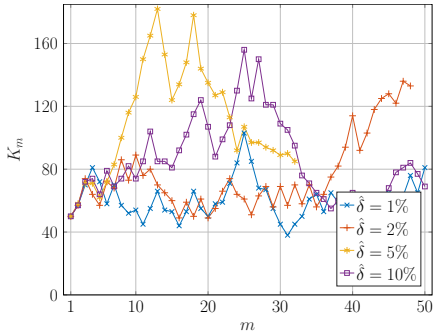

(d) dimension K_m

Fig. 8.8: Inverse scattering problem, six disks: The relative error (8.3), the ratio τ_m from the discrepancy principle (8.4), the norm of the gradient, and the dimension of the search space are shown at every iteration m for the ASI method and the different noise levels $\hat{\delta}$.

$\hat{\delta}$, the number of basis functions K_m never exceeds 140, significantly reducing the computational effort compared to a standard nodal based optimization approach with 160′000 control variables. As the ASI and ASI_0 Algorithms performed similarly, the results from the latter are omitted here.

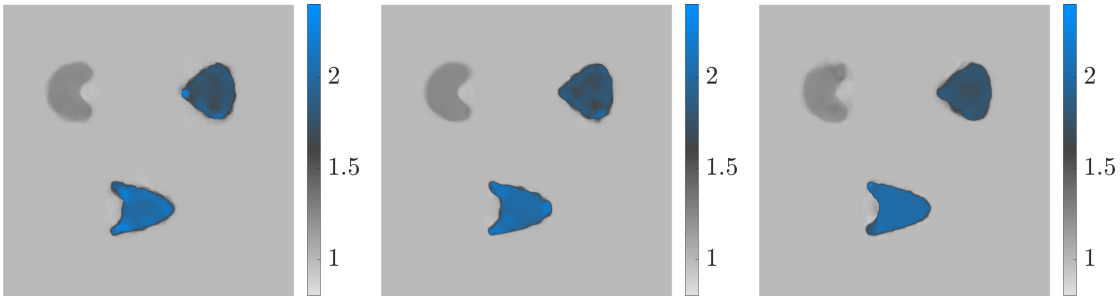

(a) ASI: $u^{m_*,\delta}$ for $\hat{\delta} = 1\%$ **(b)** ASI: $u^{m_*,\delta}$ for $\hat{\delta} = 2\%$ **(c)** ASI: $u^{m_*,\delta}$ for $\hat{\delta} = 5\%$

Fig. 8.9: Inverse scattering problem, three inclusions: Reconstructed medium using the ASI method for different noise levels $\hat{\delta}$.

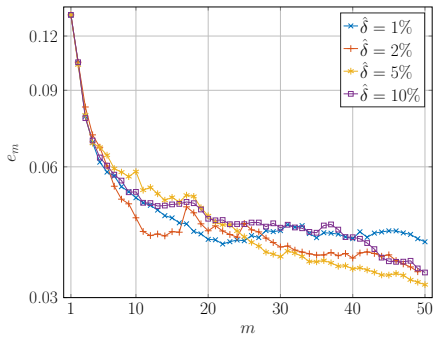

(a) relative L^2-error e_m

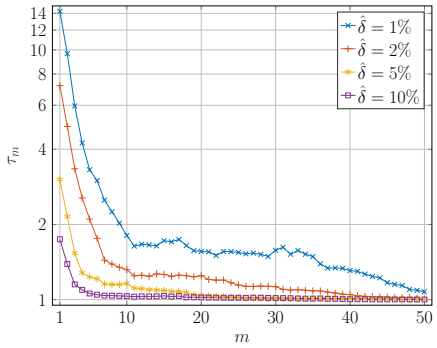

(b) ratio τ_m from the discrepancy principle

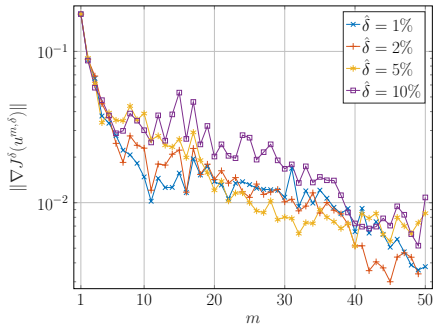

(c) $\|\nabla J(u^{m,\delta})\|$

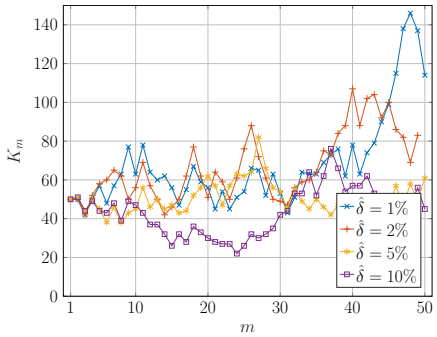

(d) dimension K_m

Fig. 8.10: Inverse scattering problem, three inclusions: The relative error (8.3), the ratio τ_m from the discrepancy principle (8.4), the norm of the gradient, and the dimension of the search space, at iteration m for the ASI method and different noise levels $\hat{\delta}$.

Conclusion and Future Work

In this Thesis, we have introduced the *Adaptive Spectral Inversion* (ASI) method, a nonlinear iterative optimization technique for solving inverse (medium) problems, which is based on the iteratively *Adaptive Inversion* Algorithm 5. Unlike a grid based finite element or finite difference Ansatz, that lead to a large number of unknowns, the AEI method adopts a different strategy. In each iteration m, the inverse problem is solved by minimizing the data misfit with added noise δ within a small finite dimensional search space Ψ^m, effectively reducing the number of control variables.

The subsequent search space Ψ^{m+1} is constructed using the first few eigenfunctions of a judicious chosen elliptic operator $L_\varepsilon[u^{m,\delta}]$, which itself depends on the minimizer $u^{m,\delta} \in \Psi^m$ of the misfit. Thus, the first few eigenfunctions depend on $u^{m,\delta}$ and inherit crucial information from the previous step, transported to the subsequent search space. Additionally, we newly added those eigenfunctions with the largest *sensitivities* (7.2) to obtain a sufficient decrease of the misfit in each step m.

In Section 6.2, we demonstrate that the ASI method, when stopped by the discrepancy principle (6.8) after a finite number of m_* iterations, is a genuine regularization method. Consequently, as the noise δ approaches zero, the solution $u^{m_*,\delta}$ obtained by the discrepancy principle, converges to the exact minimizer $u^\dagger$ of the inverse problem. Furthermore, by incorporating the eigenfunctions with the largest sensitivities, satisfying the ℓ^∞- and ℓ^2-criteria from Lemmas 7.1 and 7.2, respectively, into the ASI method, we introduce the newly determined *angle condition* (6.4). We have established in Theorem 6.1 that under this angle condition, the algorithm is well defined and converges, meaning the gradient of the misfit tends to zero. In summary, we have successfully proven that under appropriate assumptions, the ASI method is both well defined and convergent, and serves as a regularization method. Consequently, regularization is naturally embedded into the ASI method, and thus there is no need for additional regularization strategies, such as adding a penalization term to the misfit, in order to obtain robust solutions.

In Section 8, we underpin the remarkable accuracy of the ASI, first by com-

paring it to standard grid based Tikhonov regularization for an elliptic inverse problem. Here, the ASI method is, even for increasing noise, able to reconstruct the unknown medium with its shapes and values, where it surpasses L^2-Tikhonov regularization. Next, we demonstrate the practical applicability of the newly incorporated angle condition by solving time dependent inverse scattering problems. By including the most sensitive eigenfunctions, we can detect even the smallest inclusions, where the ASI algorithm without taking the sensitivities into account failed. This demonstrates the effectiveness of the angle condition, making the ASI method even more robust.

Obviously, the choice of the operator $L_\varepsilon[u^{m,\delta}]$ is crucial to obtain valid solutions for inverse problems. In Chapter II, we introduce the elliptic operator $L_\varepsilon[v]$, initially established in [29], which depends on a sufficiently small $\varepsilon > 0$ and a suitable function v. When considering a piecewise constant medium u with K interiour inclusions, we have proven in Section 4.2 that the first K eigenfunctions obtained by $L_\varepsilon[u_h]$, where u_h corresponds to the finite element interpolant of u and h denotes the mesh size, are "almost" piecewise constant and effectively represent the inclusions inside the medium. As a result, the projection of u into these eigenfunctions, the *Adaptive Spectral* (AS) decomposition of u, accurately represents u with its inclusions. Furthermore, we have proven this by deploying convergence rates of the projection error with respect to ε and h. In various examples, we have verified these convergence rates and highlighted the remarkable approximation of piecewise constant functions u by only using the first few eigenfunctions of the operator $L_\varepsilon[u_h]$.

For the AS decomposition, it is essential to assume that we know the values of the medium on the boundary. Therefore, employing this decomposition in the ASI method may not be practical in real life applications, especially in scenarios like seismic imaging, see Figure 1.1, where a priori information of the medium at the boundary, or certain parts it, might be unknown. However, when we assume that the medium is piecewise constant, we can also deduce that its normal derivative at the boundary vanishes. Hence, we can consider the AS decomposition with homogeneous Neumann conditions, allowing us to obtain the first few eigenfunctions without requiring a priori information about the unknown medium on the boundary.

As demonstrated in the numerical examples, the ASI method yields a robust approximation to the unknown medium, requiring only a few control parameters compared to grid based representations. This reduction in control parameters significantly reduces the numerical cost of the method. Moreover, the eigenfunctions of the operator $L_\varepsilon[u^{m,\delta}]$ are highly localized, allowing for easy "sparsification" [48] by setting all small values in their discrete representation to zero, further reducing the computational cost. We may even improve the efficiency of ASI method

further by employing a mesh refinement when solving (4.24), as in [28]. Clearly, the ASI method could also be applied to other inverse problems, or combined with alternative (globally convergent) inversion methods [17].

Starting from the iteratively adaptive inversion, we can also deduce a grid based method with a similar framework: Instead of minimizing the misfit $J^\delta(u)$ for $u \in \Psi^m$ in iteration m, we minimize the misfit with respect to the correction term. To do so, we find $d^{m,\delta}$ that minimizes $J^\delta(u^{m-1,\delta} + d)$ for $d \in \Theta^m$, and then set $u^{m,\delta} = u^{m-1,\delta} + d^{m,\delta}$. Then an analog version of Theorem 6.1 holds true, where the angle condition is still necessary to prove convergence. Clearly, Θ^m should not consist of all grid based basis functions. Instead, it should only consist of a few nodal basis functions with the largest sensitivities, satisfying the ℓ^∞- and ℓ^2-criterion.

Bibliography

[1] *https://defelement.com/*.

[2] *https://www.iris.edu/gallery3/research/lrsp/SB13*.

[3] *https://www.open.edu/openlearn*.

[4] G. S. Abdoulaev, K. Ren, and A. H. Hielscher, *Optical tomography as a PDE-constrained optimization problem*, Inverse Problems, 21 (2005), pp. 1507–1530.

[5] R. Acar and C. R. Vogel, *Analysis of bounded variation penalty methods for ill-posed problems*, Inverse Problems, 10 (1994), pp. 1217–1229.

[6] R. A. Adams and J. J. F. Fournier, *Sobolev Spaces*, vol. 140 of Pure and Applied Mathematics (Amsterdam), Elsevier/Academic Press, Amsterdam, second ed., 2003.

[7] K. Astala and L. Päivärinta, *Calderón's inverse conductivity problem in the plane*, Annals of Mathematics, 163 (2006), pp. 265–299.

[8] R. C. Aster, B. Borchers, and C. H. Thurber, *Parameter Estimation and Inverse Problems*, Elsevier/Academic Press, Amsterdam, second ed., 2019.

[9] I. Babuska, B. A. Szabo, and I. N. Katz, *The p-version of the finite element method*, SIAM Journal on Numerical Analysis, 18 (1981), pp. 515–545.

[10] D. H. Baffet, Y. G. Gleichmann, and M. J. Grote, *Error estimates for aptive spectral decompositions*, Journal of Scientific Computing, 93 (2022).

[11] D. H. Baffet, M. J. Grote, and J. H. Tang, *Adaptive spectral decompositions for inverse medium problems*, Inverse Problems, 37 (2021), p. 025006.

[12] A. Bakushinskii, *Remarks on choosing a regularization parameter using the quasi-optimality and ratio criterion*, USSR Computational Mathematics and Mathematical Physics, 24 (1984), pp. 181–182.

[13] A. B. Bakushinskiĭ, *On a convergence problem of the iterative-regularized Gauss-Newton method*, Zh. Vychisl. Mat. i Mat. Fiz., 32 (1992), pp. 1503–1509.

[14] A. Bamberger, G. Chavent, and P. Lailly, *About the stability of the inverse problem in 1-d wave equations—application to the interpretation of seismic profiles*, Applied Mathematics and Optimization, 5 (1979), pp. 1–47.

[15] F. Bauer and M. A. Lukas, *Comparing parameter choice methods for regularization of ill-posed problems*, Math. Comput. Simulation, 81 (2011), pp. 1795–1841.

[16] H. H. Bauschke and P. L. Combettes, *Convex Analysis and Monotone Operator Theory in Hilbert Spaces*, Springer International Publishing, 2017.

[17] L. Beilina and M. V. Klibanov, *Approximate Global Convergence and Adaptivity for Coefficient Inverse Problems*, Springer US, 2012.

[18] D. P. Bertsekas, *Constrained Optimization and Lagrange Multiplier Mmethods*, Computer Science and Applied Mathematics, Academic Press, Inc. [Harcourt Brace Jovanovich, Publishers], New York-London, 1982.

[19] D. P. Bertsekas, *Nonlinear Programming*, Athena Scientific Optimization and Computation Series, Athena Scientific, Belmont, MA, third ed., 2016.

[20] K. Bredies, B. Kaltenbacher, and E. Resmerita, *The least error method for sparse solution reconstruction*, Inverse Problems, 32 (2016), pp. 094001, 18.

[21] M. Burger, G. Gilboa, M. Moeller, L. Eckardt, and D. Cremers, *Spectral decompositions using one-homogeneous functionals*, SIAM Journal on Imaging Sciences, 9 (2016), pp. 1374–1408.

[22] T. F. Chan and P. Mulet, *On the convergence of the lagged diffusivity fixed point method in total variation image restoration*, SIAM J. Numer. Anal., 36 (1999), pp. 354–367.

[23] M. Cheney, D. Isaacson, J. C. Newell, S. Simske, and J. Goble, *NOSER: An algorithm for solving the inverse conductivity problem*, International Journal of Imaging systems and technology, 2 (1990), pp. 66–75.

[24] G. Cohen, P. Joly, J. E. Roberts, and N. Tordjman, *Higher order triangular finite elements with mass lumping for the wave equation*, SIAM Journal on Numerical Analysis, 38 (2001), pp. 2047–2078.

[25] D. Colton, J. Coyle, and P. Monk, *Recent developments in inverse acoustic scattering theory*, SIAM Rev., 42 (2000), pp. 369–414.

[26] R. Courant, K. Friedrichs, and H. Lewy, *Über die partiellen Differenzengleichungen der mathematischen Physik*, Math. Ann., 100 (1928), pp. 32–74.

[27] M. de Buhan and M. Darbas, *Numerical resolution of an electromagnetic inverse medium problem at fixed frequency*, Computers & Mathematics with Applications, 74 (2017), pp. 3111–3128.

[28] M. de Buhan and M. Kray, *A new approach to solve the inverse scattering problem for waves: combining the TRAC and the adaptive inversion methods*, Inverse Problems, 29 (2013), p. 085009.

[29] M. de Buhan and A. Osses, *Logarithmic stability in determination of a 3d viscoelastic coefficient and a numerical example*, Inverse Problems, 26 (2010), p. 095006.

[30] R. S. Dembo, S. C. Eisenstat, and T. Steihaug, *Inexact Newton methods*, SIAM J. Numer. Anal., 19 (1982), pp. 400–408.

[31] J. Diaz and M. J. Grote, *Energy conserving explicit local time stepping for second-order wave equations*, SIAM J. Sci. Comput., 31 (2009), pp. 1985–2014.

[32] G. Dobmann, I. Altpeter, R. Becker, R. Kern, U. Laub, and W. Theiner, *Barkhausen noise measurements and related mesurements in ferromagnetic materials*, 1998.

[33] D. C. Dobson and F. Santosa, *Recovery of blocky images from noisy and blurred data*, SIAM J. Appl. Math., 56 (1996), pp. 1181–1198.

[34] D. L. Donoho, *Superresolution via sparsity constraints*, SIAM J. Math. Anal., 23 (1992), pp. 1309–1331.

[35] H. W. Engl, M. Hanke, and A. Neubauer, *Regularization of Inverse Problems*, vol. 375, Springer Science & Business Media, 1996.

[36] B. Engquist and A. Majda, *Absorbing boundary conditions for numerical simulation of waves*, Proceedings of the National Academy of Sciences, 74 (1977), pp. 1765–1766.

[37] B. Engquist, A.-K. Tornberg, and R. Tsai, *Discretization of Dirac delta functions in level set methods*, J. Comput. Phys., 207 (2005), pp. 28–51.

[38] L. Evans, *Partial Differential Equations*, American Mathematical Society, 2010.

[39] F. Faucher, O. Scherzer, and H. Barucq, *Eigenvector models for solving the seismic inverse problem for the Helmholtz equation*, Geophysical Journal International, (2020).

[40] B. G. Galerkin, *Series solution of some problems of elastic equilibrium of rods and plates*, Vestnik inzhenerov i tekhnikov, 19 (1915), pp. 897–908.

[41] G. Gilboa, M. Moeller, and M. Burger, *Nonlinear spectral analysis via one-homogeneous functionals: Overview and future prospects*, Journal of Mathematical Imaging and Vision, 56 (2016), pp. 300–319.

[42] D. Givoli, *A tutorial on the adjoint method for inverse problems*, Computer Methods in Applied Mechanics and Engineering, 380 (2021), p. 113810.

[43] Y. G. Gleichmann and M. J. Grote, *Adaptive spectral inversion for inverse medium problems*, Inverse Problems, (2023).

[44] M. Graff, M. J. Grote, F. Nataf, and F. Assous, *How to solve inverse scattering problems without knowing the source term: a three-step strategy*, Inverse Problems, 35 (2019), p. 104001.

[45] M. Grasmair, M. Haltmeier, and O. Scherzer, *Sparse regularization with l^q penalty term*, Inverse Problems, 24 (2008), pp. 055020, 13.

[46] A. Griewank, *Rates of convergence for secant methods on nonlinear problems in Hilbert space*, in Numerical analysis (Guanajuato, 1984), vol. 1230 of Lecture Notes in Math., Springer, Berlin, 1986, pp. 138–157.

[47] M. J. Grote and J. B. Keller, *Exact nonreflecting boundary conditions for the time dependent wave equation*, SIAM Journal on Applied Mathematics, 55 (1995), pp. 280–297.

[48] M. J. Grote, M. Kray, and U. Nahum, *Adaptive eigenspace method for inverse scattering problems in the frequency domain*, Inverse Problems, 33 (2017), p. 025006.

[49] M. J. Grote, S. Michel, and S. A. Sauter, *Stabilized leapfrog based local time-stepping method for the wave equation*, Math. Comp., 90 (2021), pp. 2603–2643.

[50] M. J. Grote and U. Nahum, *Adaptive eigenspace for multi-parameter inverse scattering problems*, Computers & Mathematics with Applications, 77 (2019), pp. 3264–3280.

[51] E. Haber, U. M. Ascher, and D. Oldenburg, *On optimization techniques for solving nonlinear inverse problems*, Inverse Problems, 16 (2000), pp. 1263–1280. Electromagnetic imaging and inversion of the Earth's subsurface.

[52] E. Haber, U. M. Ascher, and D. W. Oldenburg, *Inversion of 3d electromagnetic data in frequency and time domain using an inexact all-at-once approach*, GEOPHYSICS, 69 (2004), pp. 1216–1228.

[53] E. Haber, M. Chung, and F. Herrmann, *An effective method for parameter estimation with PDE constraints with multiple right-hand sides*, SIAM Journal on Optimization, 22 (2012), pp. 739–757.

[54] W. Hackbusch, *Elliptic Differential Equations*, Springer Berlin Heidelberg, 2017.

[55] J. S. Hadamard, *Sur les problèmes aux dérivées partielles et leur signification physique*, Princeton University Bulletin, (1902).

[56] E. Hairer, C. Lubich, and G. Wanner, *Geometric numerical integration*, vol. 31 of Springer Series in Computational Mathematics, Springer-Verlag, Berlin, 2002. Structure-preserving algorithms for ordinary differential equations.

[57] M. Hanke and P. C. Hansen, *Regularization methods for large-scale problems*, Surveys Math. Indust., 3 (1993), pp. 253–315.

[58] M. Hanke and T. Raus, *A general heuristic for choosing the regularization parameter in ill-posed problems*, SIAM J. Sci. Comput., 17 (1996), pp. 956–972.

[59] P. C. Hansen, *Analysis of discrete ill-posed problems by means of the L-curve*, SIAM Rev., 34 (1992), pp. 561–580.

[60] P. C. Hansen, *Rank-Deficient and Discrete Ill-Posed Problems*, SIAM Monographs on Mathematical Modeling and Computation, Society for Industrial and Applied Mathematics (SIAM), Philadelphia, PA, 1998.

[61] P. C. Hansen, *Discrete Inverse Problems*, vol. 7 of Fundamentals of Algorithms, Society for Industrial and Applied Mathematics (SIAM), Philadelphia, PA, 2010. Insight and algorithms.

[62] P. C. Hansen and D. P. O'Leary, *The use of the L-curve in the regularization of discrete ill-posed problems*, SIAM J. Sci. Comput., 14 (1993), pp. 1487–1503.

[63] K. Ito and B. Jin, *Inverse Problems: Tikhonov Theory and Algorithms*, Series On Applied Mathematics, World Scientific Publishing Company, 2014.

[64] K. Ito and K. Kunisch, *Lagrange Multiplier Approach to Variational Problems and Applications*, vol. 15 of Advances in Design and Control, Society for Industrial and Applied Mathematics (SIAM), Philadelphia, PA, 2008.

[65] B. Kaltenbacher, *Regularization by projection with a posteriori discretization level choice for linear and nonlinear ill-posed problems*, Inverse Problems, 16 (2000), pp. 1523–1539.

[66] B. Kaltenbacher, A. Neubauer, and O. Scherzer, *Iterative Regularization Methods for Nonlinear Ill-Posed Problems*, De Gruyter, 2008.

[67] B. Kaltenbacher and J. Offtermatt, *A refinement and coarsening indicator algorithm for finding sparse solutions of inverse problems*, Inverse Probl. Imaging, 5 (2011), pp. 391–406.

[68] B. Kaltenbacher and J. Offtermatt, *A convergence analysis of regularization by discretization in preimage space*, Math. Comput., 81 (2012), pp. 2049–2069.

[69] J. B. Keller, *Inverse problems*, The American Mathematical Monthly, 83 (1976), pp. 107–118.

[70] Y. L. Keung and J. Zou, *Numerical identifications of parameters in parabolic systems*, Inverse Problems, 14 (1998), pp. 83–100.

[71] A. Kirsch, *An Introduction to the Mathematical Theory of Inverse Problems*, vol. 120 of Applied Mathematical Sciences, Springer-Verlag, New York, 1996.

[72] L. Landweber, *An iteration formula for Fredholm integral equations of the first kind*, American Journal of Mathematics, 73 (1951), pp. 615–624.

[73] M. G. Larson and F. Bengzon, *The Finite Element Method: Theory, Implementation, and Applications*, vol. 10 of Texts in Computational Science and Engineering, Springer, Heidelberg, 2013.

[74] D. P. Laurie, *Algorithm 584: CUBTRI: Automatic cubature over a triangle*, ACM Transactions on Mathematical Software (TOMS), 8 (1982), pp. 210–218.

[75] O. V. Lepskij, *A problem of adaptive estimation in Gaussian white noise*, Teor. Veroyatnost. i Primenen., 35 (1990), pp. 459–470.

[76] K. Levenberg, *A method for the solution of certain non-linear problems in least squares*, Quart. Appl. Math., 2 (1944), pp. 164–168.

[77] C. D. Lines and S. N. Chandler-Wilde, *A time domain point source method for inverse scattering by rough surfaces*, Computing, 75 (2005), pp. 157–180.

[78] D. W. Marquardt, *An algorithm for least-squares estimation of nonlinear parameters*, J. Soc. Indust. Appl. Math., 11 (1963), pp. 431–441.

[79] G. A. Matzkanin, R. E. Beissner, and C. M. Teller, *The barkhausen effect and its applications to nondestructive evaluation*, 1979.

[80] V. Michel, *The two-dimensional inverse conductivity problem*, The Journal of Geometric Analysis, 30 (2020), pp. 2776–2842.

[81] P. Mojabi and J. Lovetri, *Microwave biomedical imaging using the multiplicative regularized gauss–newton inversion*, IEEE Antennas and Wireless Propagation Letters, 8 (2009), pp. 645–648.

[82] V. A. Morozov, *On the solution of functional equations by the method of regularization*, Soviet Math. Dokl., 7 (1966), pp. 414–417.

[83] V. A. Morozov, *Methods for Solving Incorrectly Posed Problems*, Springer-Verlag, New York, 1984. Translated from the Russian by A. B. Aries, Translation edited by Z. Nashed.

[84] W. A. Mulder, *Higher-order mass-lumped finite elements for the wave equation*, Journal of Computational Acoustics, 09 (2001), pp. 671–680.

[85] F. Natterer, *Regularisierung schlecht gestellter Probleme durch Projektionsverfahren*, Numerische Mathematik, 28 (1977), pp. 329–341.

[86] A. Neubauer, *Estimation of discontinuous solutions of ill-posed problems via adaptive grid regularization*, J. Inverse Ill-Posed Probl., 14 (2006), pp. 705–716.

[87] A. Neubauer, *Computation of discontinuous solutions of 2D linear ill-posed integral equations via adaptive grid regularization*, J. Inverse Ill-Posed Probl., 15 (2007), pp. 99–106.

[88] A. Neubauer, *Solution of ill-posed problems via adaptive grid regularization: convergence analysis*, Numer. Funct. Anal. Optim., 28 (2007), pp. 405–423.

[89] I. S. Newton, *Philosophiae Naturalis Principia Mathematica*, William Dawson & Sons, Ltd., London, undated.

[90] J. Nocedal and S. Wright, *Numerical Optimization*, Springer New York, 2006.

[91] J. M. Ortega and W. C. Rheinboldt, *Iterative Solution of Nonlinear Equations in Several Variables*, vol. 30 of Classics in Applied Mathematics, Society for Industrial and Applied Mathematics (SIAM), Philadelphia, PA, 2000. Reprint of the 1970 original.

[92] S. V. Pereverzev and S. Prössdorf, *On the characterization of self-regularization properties of a fully discrete projection method for Symm's integral equation*, J. Integral Equations Appl., 12 (2000), pp. 113–130.

[93] J. A. Pérez Benitez, T. Le Manh, and M. Alberteris, *Barkhausen noise for material characterization*, in Barkhausen Noise for Nondestructive Testing and Materials Characterization in Low-Carbon Steels, Woodhead Publishing Series in Electronic and Optical Materials, Woodhead Publishing, 2020, pp. 115–146.

[94] D. L. Phillips, *A technique for the numerical solution of certain integral equations of the first kind*, J. Assoc. Comput. Mach., 9 (1962), pp. 84–97.

[95] R. G. Pratt, C. Shin, and G. J. Hick, *Gauss Newton and full Newton methods in frequency-space seismic waveform inversion*, Geophysical Journal International, 133 (1998), pp. 341–362.

[96] R. G. Pratt, Z.-M. Song, P. Williamson, and M. Warner, *Two-dimensional velocity models from wide-angle seismic data by wavefield inversion*, Geophysical Journal International, 124 (1996), pp. 323–340.

[97] R. G. Pratt and M. H. Worthington, *Inverse theory applied to multi-source cross-hole tomography. part 1: Acoustic wave-equation method 1*, Geophysical prospecting, 38 (1990), pp. 287–310.

[98] J. Reddy, *An Introduction to the Finite Element Method*, Journal of Pressure Vessel Technology-transactions of The Asme, 111 (1989), pp. 348–349.

[99] M. Richter, *Inverse Problems – Basics, Theory and Applications in Geophysics*, Lecture Notes in Geosystems Mathematics and Computing, Birkhäuser/Springer, Cham, [2020]. Second edition [of 3615786].

[100] F. Riesz and B. Sz.-Nagy, *Functional Analysis*, Dover Books on Advanced Mathematics, Dover Publications, Inc., New York, 1990. Translated from the second French edition by Leo F. Boron, Reprint of the 1955 original.

[101] W. Ritz, *Über eine neue Methode zur Lösung gewisser Variationsprobleme der mathematischen Physik.*, crll, 1909 (1909), pp. 1–61.

[102] L. I. Rudin, S. Osher, and E. Fatemi, *Nonlinear total variation based noise removal algorithms*, Phys. D, 60 (1992), pp. 259–268. Experimental mathematics: computational issues in nonlinear science (Los Alamos, NM, 1991).

[103] E. W. Sachs, *Broyden's method in Hilbert space*, Math. Programming, 35 (1986), pp. 71–82.

[104] C. Sanders, M. Bonnet, and W. Aquino, *An adaptive eigenfunction basis strategy to reduce design dimension in topology optimization*, Internat. J. Numer. Methods Engrg., 122 (2021), pp. 7452–7481.

[105] O. Scherzer, *Handbook of Mathematical Methods in Imaging*, Springer New York, 2015.

[106] O. Scherzer, H. W. Engl, and K. Kunisch, *Optimal a posteriori parameter choice for Tikhonov regularization for solving nonlinear ill-posed problems*, SIAM Journal on Numerical Analysis, 30 (1993), pp. 1796–1838.

[107] O. Scherzer, M. Grasmair, H. Grossauer, M. Haltmeier, and F. Lenzen, *Variational Methods in Imaging*, vol. 167 of Applied Mathematical Sciences, Springer, New York, 2009.

[108] O. Scherzer and J. Weickert, *Relations between regularization and diffusion filtering*, J. Math. Imaging Vision, 12 (2000), pp. 43–63.

[109] T. Schuster, B. Kaltenbacher, B. Hofmann, and K. S. Kazimierski, *Regularization Methods in Banach Spaces*, DE GRUYTER, jul 2012.

[110] T. I. Seidman, *Nonconvergence results for the application of least-squares estimation to ill-posed problems*, J. Optim. Theory Appl., 30 (1980), pp. 535–547.

[111] N. Sloane, *A Handbook of Integer Sequences*, Elsevier, 1973.

[112] N.-Z. Sun, *Inverse Problems in Groundwater Modeling*, Springer Netherlands, 1999.

[113] J. H. Tang, *Solving Forward and Inverse Helmholtz Equations via Controllability Methods*, PhD thesis, Universität Basel, 2020.

[114] A. Tarantola, *Inversion of seismic reflection data in the acoustic approximation*, GEOPHYSICS, 49 (1984), pp. 1259–1266.

[115] A. Tarantola, *Inversion of travel times and seismic waveforms*, in Seismic Tomography, Springer Netherlands, 1987, pp. 135–157.

[116] A. N. Tikhonov, *On the regularization of ill-posed problems*, Dokl. Akad. Nauk SSSR, 153 (1963), pp. 49–52.

[117] A. N. Tikhonov, *On the solution of ill-posed problems and the method of regularization*, Dokl. Akad. Nauk SSSR, 151 (1963), pp. 501–504.

[118] A. N. Tikhonov, *Ill-Posed Problems in Natural Sciences*, De Gruyter, dec 1992.

[119] A. N. Tikhonov and V. Y. Arsenin, *Solutions of Ill-Posed Problems*, Wiley, 1977.

[120] A. N. Tikhonov and V. B. Glasko, *Use of the regularization method in non-linear problems*, USSR Computational Mathematics and Mathematical Physics, 5 (1965), pp. 93–107.

[121] G. M. Vainikko and U. A. Khyamarik, *Projection methods and self-regularization in ill-posed problems*, Izv. Vyssh. Uchebn. Zaved. Mat., (1985), pp. 3–17, 84.

[122] J. F. Van Doren, P. M. Van den Hof, J. D. Jansen, and O. H. Bosgra, *Parameter identification in large-scale models for oil and gas production*, IFAC Proceedings Volumes, 44 (2011), pp. 10857–10862. 18th IFAC World Congress.

[123] T. van Leeuwen and F. J. Herrmann, *3d frequency-domain seismic inversion with controlled sloppiness*, SIAM Journal on Scientific Computing, 36 (2014), pp. S192–S217.

[124] J. Virieux and S. Operto, *An overview of full-waveform inversion in exploration geophysics*, GEOPHYSICS, 74 (2009), pp. WCC1–WCC26.

[125] C. R. Vogel, *Computational Methods for Inverse Problems*, vol. 23 of Frontiers in Applied Mathematics, Society for Industrial and Applied Mathematics (SIAM), Philadelphia, PA, 2002. With a foreword by H. T. Banks.

[126] C. R. Vogel and M. E. Oman, *Iterative methods for total variation denoising*, SIAM J. Sci. Comput., 17 (1996), pp. 227–238. Special issue on iterative methods in numerical linear algebra (Breckenridge, CO, 1994).

[127] K. Wang, T. Matthews, F. Anis, C. Li, N. Duric, and M. A. Anastasio, *Breast ultrasound computed tomography using waveform inversion with source encoding*, in Medical Imaging 2015: Ultrasonic Imaging and Tomography, J. G. Bosch and N. Duric, eds., SPIE, mar 2015.

[128] D. Werner, *Funktionalanalysis*, Springer-Verlag, Berlin, extended ed., 2000.

[129] K. Yosida, *Functional Analysis*, Classics in Mathematics, Springer-Verlag, Berlin, 1995. Reprint of the sixth (1980) edition.